JOÃO MANOEL LOSADA MOREIRA

Space - Time Analysis of Reactivity Measurements

SPACE-TIME ANALYSIS OF REACTIVITY MEASUREMENTS

by

João Manoel Losada Moreira

A dissertation submitted in partial fulfillment
of the requirements for the degree of
Doctor of Philosophy
(Nuclear Engineering)
in The University of Michigan
1984

Doctoral Committee:

Professor John C. Lee, Chairman
Professor Wilfred Kaplan
Professor John S. King
Associate Professor William R. Martin

To My Parents

Maria Stela and Luiz Gonzaga

ACKNOWLEDGEMENTS

A sincere appreciation is expressed to the thesis advisor, Dr. John C. Lee, for his assistance and advice during the course of this research. Dr. Lee's understanding of nuclear reactor theory has been invaluable in my professional development.

I would like to gratefully acknowledge the efforts of Professors Wilfred Kaplan, John S. King, and William R. Martin for serving as members of the Doctoral Committee. I also would like to thank the staff members at the Institut für Reaktorentwicklung, Kernforschungsanlage Jülich, for all the hospitality offered during my stay in Jülich.

Financial support during this research, provided by the Comissão Nacional de Energia Nuclear, Brazil, was deeply appreciated.

Finally, a special gratitude is expressed to my friends for their support during all these long years.

TABLE OF CONTENTS

LIST OF TABLES

LIST OF FIGURES

CHAPTER I

INTRODUCTION

A major task in reactor theory is the verification of analytical methods used in safety and performance analysis against experimental observables. Measurements provide a quality control mechanism for assuring that the reactor is well represented by the analytical models, and also help to infer physical parameters associated with the steady state and dynamic behavior of the core. In the end, measurements can also help to reduce the uncertainties associated with the models describing the reactor and reduce conservatism in reactor design limits. In this dissertation we pay attention to the measurement of the core reactivity, one of the most important parameters that describe the state of a reactor[1]. Reactivity measurements are performed routinely during plant startups and under normal operating conditions.[2] The reactivity measurement system of a reactor, usually called a reactivity meter, includes both data collection and processing because the reactivity is not a direct observable but an inferred quantity[3].

There have been many methods proposed for the analysis of core behavior as a function of time. The detailed

numerical methods developed for the kinetics problems, in principle, can adequately represent the core behavior as a function of time, including thermal-hydraulic feedback effects[4-12]. These methods, however, can not be directly used in on-line reactivity measurements because they require a large amount of computer time and storage. In consequence, the techniques used for on-line reactivity measurements are usually much less sophisticated, often based on the point kinetics model through the inverse kinetics equation or the inhour equations[3,13]. More involved techniques for measuring the reactivity have been proposed and implemented, but they are not practical enough for routine measurement of reactivity during reactor operation.[14-21] Despite the considerable effort to account properly for the significant space- and time-dependent variations of the neutron flux, the delayed neutron precursor distributions, and other kinetics parameters measured at large multi-region cores,[1,14,15,22-24] this research area remains open to investigation.

The evaluation of measured reactivity effects due to thermal-hydraulic feedbacks has also been made with very simplified models, usually lumping the core in two regions: the fuel and the moderator or coolant regions.[25-29] Thus, the measurement techniques commonly used to infer the reactivity during transients lack in detail for representing complex phenomena such as those usually present in an operating power reactor.

Experiments such as rod-drop measurements, which are analyzed in this investigation, require careful consideration of the strong redistribution of the neutron flux during the transient. If not properly handled, it may incur large errors in the reactivity determination.[30] At power conditions, the problem becomes even more complex for the Doppler feedback effects start to act almost instantaneously throughout the core. In many cases it is almost impossible to separate, after a few seconds, the thermal-hydraulic feedback effect on the reactivity from that of the external perturbation, the rod motion itself. In this dissertation a new approach will be presented that can accurately account for the space-time effects, as well as the thermal-hydraulic feedback effects, on reactivity measurements.

The basic constraint in surveillance procedures is time. One is not often allowed to wait for hours in order to infer a desired parameter; actually one may even not be allowed to wait for several minutes. The desired framework of data processing for reactor operation or routine measurements is often the real time calculations. The raw data collected by the several sensors in the core and in the plant must be processed very quickly to yield information about the current status of the whole system. Thus, most of the detailed accurate methods used in reactor analysis are not directly applicable to surveillance systems. The consequence has been the use of a distinct set of techniques

each by the analyst and by the experimentalist to infer similar parameters[1,2].

Many proposed approaches for reactivity measurements in large reactors try to account for space-time effects based entirely on measured quantities.[1,24] Quantities like the amplitude function, power distribution, neutron flux, and adjoint neutron flux are approximated based on countrates from detectors placed in several locations in the core. Undoubtedly, from the standpoint of simplicity and of easy implementation in power plants, such approaches are interesting, but they certainly compromise in accuracy.

The approach taken in this investigation has been to utilize, as much as possible, the more accurate analytical methods used in reactor analysis, together with the data processing techniques already available to the experimentalists. This approach has been used for measuring feedback coefficients of reactivity; the difficulty in correctly measuring the temperature field in the reactor has led some experimentalists to estimate the temperature distribution theoretically in order to obtain the reactivity coefficients[28,29]. Thus, one has a blend of measurements and calculations for better inference of reactor parameters. We developed in this investigation an elaborate scheme to account for space-time effects on reactivity measurements, including thermal-hydraulic feedback, in the framework of

real time calculations, practical for on-site analysis of reactivity measurements.

The inverse kinetics formulation is used as the basis of the reactivity meter to yield reactivity as a function of time. The applicability of the method depends on the accurate determination of the amplitude function from the detector signal. In order to accomplish this, one needs to account for the time-dependent changes in the spatial distribution of the neutron flux at the detector location[1]. A model has been developed in the present investigation to perform efficiently such a space-time analysis in the framework of the inverse kinetics method[30]. This method has been compared against the FX2-TH code[9] for evaluation of its accuracy. It has also been applied to the analysis of the control rod worth measurements taken at the KAHTER facility[31], which is a zero-power high-temperature gas-cooled reactor test facility located at the Kernforschungsanlage Jülich (KFA)[32] in West Germany.

In the previous analysis of the KAHTER rod worth measurements[23,31] correction factors were obtained to convert the detector signals to the amplitude function. These correction factors were obtained with the assumption that the neutron flux reached an asymptotic spatial distribution following the rod movement and that this distribution could be obtained by means of a static eigenvalue calculation. In our investigation, a more

detailed accounting of the space-time evolution during and after the rod movement is made through the quasi-static method[3,33,34]. In the space-time kinetics methods reported by Doshi and Grossman[35], Luxat and Frescura[10], and Hauss and Kastenberg[36], approximate solutions to the shape function were suggested. In our study we have followed the basic idea used in Refs. 10 and 35, which involves a modal expansion technique coupled with some special treatment for local effects associated with the rod movement[37].

This type of local flux perturbation treatment would generally be applicable to our problem because the rod insertion perturbs substantially the neutron flux in its vicinity, with the perturbation in flux more gradual beyond a few mean free paths. Therefore, in this approach the global changes in neutron flux would be accounted for through a few-term modal expansion and the local changes through a localized treatment.

An accurate model for this localized treatment is important for efficient utilization of the modal expansion technique in the space-time analysis of the reactivity data. The local perturbation treatments reported so far[10,35] are rather crude. Doshi and Grossman[35] assumed a flux perturbation in the form of a step function limited exclusively to the region of perturbations in core parameters, and applied the scheme to transients related to sodium void in fast reactors. Lineberry[37] suggested a

variational procedure to generate an equation for the trial functions which could be obtained from diffusion theory calculations restricted to the region where the changes occurred. Luxat and Frescura[10] applied rather an ad-hoc form of the local perturbation terms in their one energy-group analysis. A multiplicative correction function in the form of an exponential decay centered in the perturbation was applied to the neutron flux in order to generate better kinetics parameters. It has been crucial in our study to develop a more general method of coupling local perturbation effects with the modal expansion technique. This investigation uses lambda modes[15,38-41] for a reference core configuration for both the forward and adjoint flux distributions, and a simple fixed-source diffusion theory calculation for the local function to estimate the time-dependent shape function[30]. This method provides a more accurate representation of the flux perturbations compared with the more ad-hoc treatments previously reported.

We begin in Chapter II with a derivation of the basic space-time kinetics equations emphasizing the inverse kinetics formulation, rather than the forward point kinetics equations, as is usually done in the literature. A discussion of several methods for obtaining the shape function is also presented. In Chapter III our proposed approach for space-time analysis of reactivity measurements, the modal-local method, is developed. The calculation of lambda modes through existing standard multi-group, multi-

dimensional neutron diffusion theory codes is also discussed, together with the numerical approaches involving the modal-local method.

In Chapter IV and V the results obtained with the modal-local method are presented. In Chapter IV, a general verification of the method, both for static and time-dependent problems, is presented through comparison with the CITATION code[42] and the FX2-TH code,[9] respectively. These calculations involve problems in two- and three-dimensional geometries in order to assess the ability of the proposed modal-local method to account for spatial redistribution of the neutron flux during transients. To evaluate the applicability of the modal-local method in the power reactor environment, a simplified one-dimensional model including both moderator and Doppler feedback effects is also considered in Chapter IV. In Chapter V, an application of the proposed modal-local method in analyzing experimental rod worth data is carried out. Both integral and differential rod worths were measured for the top-reflector control rods of the KAHTER facility,[30-32] through the rod-drop technique. A space-time analysis of the KAHTER rod worth data together with a discussion of the uncertainties involved in the experiments are also included in Chapter V. Finally, in Chapter VI we present a summary and conclusions of this research.

CHAPTER II

THE SPACE-TIME ANALYSIS

As mentioned in Chapter I it is necessary to account for space-time effects in the neutron flux distribution in order to determine the reactivity accurately from experimental data. To establish clearly how these space-time effects influence reactivity measurements we will discuss in this chapter the kinetics equations emphasizing the reactivity $\rho(t)$ rather than the amplitude function $n(t)$. The derivations will lead to the inverse kinetics equation with explicit definitions for the kinetics parameters[3], and a relationship between detector signals and the amplitude function[30].

There are several approaches possible for solving the time-dependent neutron balance equations. Usually they differ in the degree of sophistication with which the space-time effects are handled. In one extreme is the point kinetics equations which fully neglect any spatial effect[20,21], to be contrasted with the direct solution of the space, -time- and energy-dependent diffusion equation[4-8] in the other extreme. In this chapter will be discussed several approximations to the neutron balance equations,

with due consideration for their accuracy and usefulness for different types of problems. The approach proposed in this work for obtaining the shape function during rod worth measurements is a modal expansion technique coupled with a local treatment to account for the local effects of rod motion in the shape function. This formulation, called modal-local method, will be described in Chapter III.

A. The Kinetics Equations

The time-dependent diffusion equation with explicit consideration of the delayed neutrons is called here the kinetics equations. They have the following form:

$$\frac{1}{v}\frac{\partial\phi(\underline{r},E,t)}{\partial t} = (1-\beta)\chi_p(E)\frac{P(\underline{r},E,t)}{k_o}\phi(\underline{r},E,t) - L(\underline{r},E,t)\phi(\underline{r},E,t) + \sum_{i=1}^{6}\lambda_i\chi_{di}(E)c_i(\underline{r},t) \qquad (1a)$$

$$\frac{\partial c_i(\underline{r},t)}{\partial t} = -\lambda_i c_i(\underline{r},t) + \beta_i\frac{P(\underline{r},E,t)}{k_o}\phi(\underline{r},E,t), \qquad i=1,\ldots,6. \qquad (1b)$$

where

$\phi(\underline{r},E,t)$ = neutron flux distribution,

$c_i(\underline{r},t)$ = concentration of delayed neutron precursors for the i^{th} group,

$P(\underline{r},E,t)$ = total neutron production operator,

$L(\underline{r},E,t)$ = total neutron destruction operator,

k_o = initial eigenvalue of the system,

$\chi_p(E)$ and $\chi_{di}(E)$ = fission spectra for the prompt neutrons and i^{th} delayed group, respectively,

$\chi(E) = (1-\beta)\chi_p(E) + \sum_{i=1}^{6} \beta_i \chi_{di}(E)$ = total fission spectrum,

β_i = delayed neutron fraction for the i^{th} group,

$\beta = \sum_{i=1}^{6} \beta_i$ = total delayed neutron fraction,

λ_i = decay constant for the i^{th} group of delayed neutron precursors, and

v = neutron speed.

Eqs. (1) can be solved numerically and there are several computer codes that may be used for this purpose.[4-8] However, the limitation of the kinetics equations in this general form is its requirement of large computational time to simulate a transient. For actual reactor transients, which require an explicit two- or three-dimensional description of the core, these calculations become excessively expensive.

The kinetics equations can be written in a different form more suitable for approximations in view of the problems under consideration. To this end the neutron flux $\phi(\underline{r},E,t)$ is factorized, in the so called quasi-static approximation,[33] into two components: a slow time varying

shape function $\psi(\underline{r},E,t)$ and an amplitude function $n(t)$ which bears the most of the time dependence of the neutron flux[3]:

$$\phi(\underline{r},E,t) = \psi(\underline{r},E,t)\, n(t). \tag{2}$$

The amplitude function $n(t)$ can be interpreted as the magnitude of the neutron population in the core at a given time t. The shape function $\psi(\underline{r},E,t)$ does not change in magnitude but only in shape during a transient. For this reason its time dependence is not strong, and, therefore, it is more suitable for approximations. If this factorized form of the neutron flux is substituted in Eqs. (1) we obtain equations for the shape function:

$$\frac{1}{v}\frac{\partial\psi(\underline{r},E,t)}{\partial t} = [M_p(\underline{r},E,t)-L(\underline{r},E,t) - \frac{1}{v}\frac{\dot{n}}{n}]\psi(\underline{r},E,t) + \frac{1}{n(t)}\sum_{i=1}^{6}\lambda_i\,\chi_{di}(E)c_i(\underline{r},t) \tag{3a}$$

$$\frac{\partial c_i(\underline{r},t)}{\partial t} = -\lambda_i c_i(\underline{r},t) + \beta_i\frac{P(\underline{r},E,t)}{k_o}\psi(\underline{r},E,t)n(t) \qquad i=1,..6. \tag{3b}$$

with $M_p(\underline{r},E,t) = (1-\beta)\chi_p(E)\dfrac{P(\underline{r},E,t)}{k_o}$.

Eqs. (3) have to be solved together with a time-dependent equation for the amplitude function. Provided that $n(t)$ is known or estimated the shape function can then

be obtained using coarse time steps or approximately even from static calculations, since, by definition, $\psi(\underline{r},E,t)$ changes slowly in time.

The amplitude function equation is obtained by integrating Eqs. (1) over the space and energy variables with Eq. (2) substituted for $\phi(\underline{r},E,t)$. A weight function, usually the adjoint to the steady state neutron flux for some reference state, $\phi_o^\dagger(\underline{r},E)$, is included in the integrals in order to provide a definition for the reactivity free of first order errors. Because in doing the factorization of the neutron flux it is introduced one more degree of freedom in the system, a constraint should be imposed in either n(t) or $\psi(\underline{r},E,t)$. By imposing the constraint on the shape function that

$$<\phi_o^\dagger(\underline{r},E),\frac{1}{v}\psi(\underline{r},E,t)> = \text{constant} = C_o \ , \tag{4}$$

where the inner product means integration over energy and reactor volume, the well-known point kinetics equations are obtained:

$$\frac{dn(t)}{dt} = \frac{\rho(t)-\bar{\beta}(t)}{\Lambda(t)}\, n(t) + \sum_{i=1}^{6} \lambda_i c_i(t) \tag{5a}$$

$$\frac{dc_i(t)}{dt} = -\lambda_i c_i(t) + \frac{\bar{\beta}_i(t)}{\Lambda(t)}\, n(t), \quad i=1,\ldots,6. \tag{5b}$$

Here the kinetics parameters are defined as:

$$\rho(t) = \frac{\langle \phi_o^\dagger(\underline{r},E),\ [M(\underline{r},E,t) - L(\underline{r},E,t)]\psi(\underline{r},E,t)\rangle}{\langle \phi_o^\dagger(\underline{r},E),\ M(\underline{r},E,t)\psi(\underline{r},E,t)\rangle} \tag{5c}$$

= reactivity,

$$\bar{\beta}_i(t) = \frac{\langle \phi_o^\dagger(\underline{r},E),\ M_{di}(\underline{r},E,t)\psi(\underline{r},E,t)\rangle}{\langle \phi_o^\dagger(\underline{r},E),\ M(\underline{r},E,t)\psi(\underline{r},E,t)\rangle} \tag{5d}$$

= effective delayed neutron fraction for the i^{th} group of delayed neutrons,

$$\bar{\beta}(t) = \sum_{i=1}^{6} \bar{\beta}_i(t) \tag{5e}$$

= total effective delayed neutron fraction,

$$\Lambda(t) = \frac{\langle \phi_o^\dagger(\underline{r},E),\ \frac{1}{v}\ \psi(\underline{r},E,t)\rangle}{\langle \phi_o^\dagger(\underline{r},E),\ M(\underline{r},E,t)\psi(\underline{r},E,t)\rangle} \tag{5f}$$

= mean generation time,

with

$$M_{di}(\underline{r},E,t) = \beta_i \chi_{di}(E)\frac{P(\underline{r},E,t)}{k_o},$$

$$M(\underline{r},E,t) = M_p(\underline{r},E,t) + \sum_{i=1}^{6} M_{di}(\underline{r},E,t) = \chi(E)\frac{P(\underline{r},E,t)}{k_o}.$$

The utility of the point kinetics equations (5) depends on the accuracy of the kinetics parameters $\rho(t)$, $\Lambda(t)$, and $\bar{\beta}_i(t)$. If they are estimated correctly the point kinetics equations will yield accurate results. The principal difficulty, in general, is then the computation of the kinetics parameters. In fact, unless $\psi(\underline{r},E,t)$ or some accurate approximation to it can be found, Eqs. (5) can result in severe errors.

The simultaneous solution of the shape function equations (3) and the point kinetics equations (5) is equivalent to solving Eqs. (1). However, Eqs. (3) and (5) have the advantage of allowing approximate solutions for the shape function - the bulk of the calculation - which in the end is translated into substantial savings in computational effort. In the next section we will derive the inverse kinetics equation to be used for reactivity determination from experimental data.

B. The Inverse Kinetics Formulation

The inverse kinetics equation is widely used to infer instantaneous reactivity. A computational system with the specific purpose of yielding the reactivity as a function of time is often called a reactivity meter. This system

involves data collection and processing, and usually the inverse kinetics equation is used to convert the detector signals into the core reactivity. The inverse kinetics equation is readily obtained by writing Eq. (5a) for the reactivity $\rho(t)$, and substituting in the RHS the integrated form of the delayed neutron precursor equation (5b):

$$\rho(t) = \bar{\beta}(t) + \frac{\Lambda(t)\ \dot{n}(t)}{n(t)} - \frac{\Lambda(t)}{n(t)} \sum_{i=1}^{6} \lambda_i \int_{-\infty}^{t} dt' \frac{\bar{\beta}_i(t')\ n(t')}{\Lambda(t')} \exp[\lambda_i(t'-t)] \tag{6}$$

In a reactivity meter the inverse kinetics equation yields the reactivity based on countrates collected by detectors placed at different locations in the reactor. A detector signal $R(\underline{r}_o,t)$ cannot usually be taken as the amplitude function $n(t)$, because $R(\underline{r}_o,t)$ represents the evolution in time of the neutron flux at the detector location $\underline{r}_o$ which may differ from the amplitude function, an integral quantity of the reactor. A better understanding of the difference between the amplitude function and the detector signal can be found by expressing the latter formally in terms of the neutron flux:

$$R(\underline{r}_o,t) = \langle T(\underline{r},\underline{r}_o,E),\ \phi(\underline{r},E,t) \rangle \tag{7}$$

where $T(\underline{r},\underline{r}_o,E)$ is a weight function that essentially will determine the region viewed by the detector located at $\underline{r}_o$[43]. In principle, this weight function must be time dependent for the conditions of the detector and the core may change during the transient. In practice, however, for the small length of time involved in kinetics problems, a time-independent weight function has been found to be sufficient for most problems[23-32].

For an in-core neutron detector $T(\underline{r},\underline{r}_o,E)$ can be expressed as $\Sigma_d(E)\delta(\underline{r}-\underline{r}_o)$, and the detector signal is the neutron flux at the detector location $\underline{r}_o$ times some effective detector cross section $\Sigma_d(E)$:

$$R(\underline{r}_o,t) = \langle\Sigma_d(E),\ \phi(\underline{r}_o,E,t)\rangle_E, \tag{8}$$

where the inner product represents an energy integral.

For an ex-core detector the determination of $T(\underline{r},\underline{r}_o,E)$ requires some further consideration. This is because the neutron flux at the ex-core detector location depends mostly on high energy neutrons that penetrate the core and the reflector shield, with the resulting bias in the neutron flux for the forward direction. The air gaps that often exist between the ex-core detector and the core also make the diffusion theory approximation invalid in the region. Thus, it becomes necessary to obtain $T(\underline{r},\underline{r}_o,E)$ through transport theory calculations[43].

In any case, for both in-core and ex-core detectors, the relationship between the the amplitude function and the detector signal can be written as:

$$n(t) = \frac{R(\underline{r}_o,t)}{\langle T(\underline{r},\underline{r}_o,E),\ \psi(\underline{r},E,t)\rangle} \qquad (9)$$

where the neutron flux in Eq. (7) has been substituted by its factorized form introduced in Eq. (2). Eq. (9) shows that the amplitude function depends on both the detector countrates and the time behavior of the shape function. The factor $1/\langle T(\underline{r},\underline{r}_o,E),\psi(\underline{r},E,t)\rangle$ is the correction factor that should be applied to the detector signals to obtain the amplitude function. It is worth noting that if the transient under consideration does not perturb the shape of the neutron flux or shape function, there is no need for corrections, because the amplitude function will be directly proportional to the countrates. In this idealized case no matter where a detector is located it will yield the same reactivity as a function of time. However, in most cases and, especially in rod worth measurements, this does not happen, and the correction factors are necessary.

To demonstrate the importance of the correction factors, Yasinsky and Henry[34] obtained a ratio of the amplitude function to the detector signal for a bare slab reactor with a core height of 0.6 m, representing a typical light water reactor. The core consists of three regions

with a uniform material composition, with the center having a larger transverse buckling. The transient consists of a step increase, followed by a linear decrease to the initial value, in the fission cross section of the first region. As shown in Fig. 2.1, depending on the detector location, the signal R(t) can be greater or smaller than the amplitude function, and the ratio n(t)/R(t) changes during the transient. It should be noticed that, even for a small core like the one considered here, the magnitude of the correction is as large as 40%.

The analysis of rod worth data through the inverse kinetics formulation thus requires the solution of the shape function equations (3) during the transient to obtain the necessary correction factors for the detector signals. For on-site analysis in real time with a reactivity meter, the shape function must be obtained in a fast and accurate way. In the next section we discuss several approaches to obtain the shape function during a transient.

C. Methods for the Shape Function Calculation

In this section consideration will be given to the estimation of the shape function $\psi(\underline{r},E,t)$ during a transient. It was mentioned in Sect. A that the point kinetics or the inverse kinetics equations are accurate only if the kinetics parameters are accurately obtained, and, to achieve that, it is necessary to have the shape function as

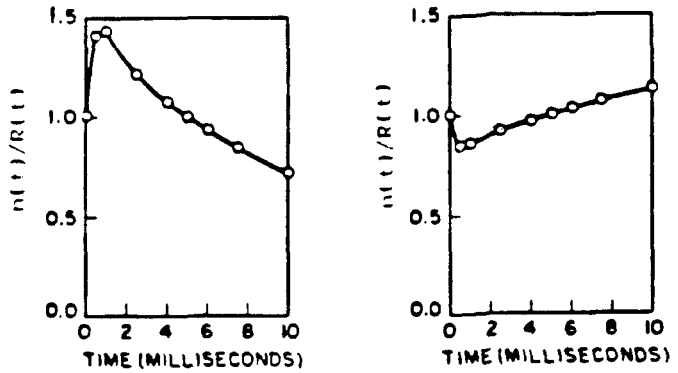

Figure 2.1 Ratio of amplitude function to detector signals

a function of time. The shape function can be approximated in several ways depending on the type of problem in question.

The aim of all approximations is the reduction of shape function calculations to a minimum because it is the most expensive part of the space-time kinetics solution. The idea has been invariably to calculate the shape function infrequently during a transient, while the point kinetics equations are solved in fine time steps more frequently. Over the years several methods have been developed to account for, with a varying degree of complexity, the neutron flux redistribution during transients[33,34]. In this section will be discussed some of these methods in a manner suggested by Ott and Meneley[33], with emphasis on the approximations and their physical significance.

We start by analyzing the conditions under which Eqs. (3) can be simplified. In order to do that we rewrite them in a different form to show more clearly the approximations involved:

$$[M_p - L]\psi(\underline{r},E,t) = \frac{1}{v}\left[\frac{\partial\psi}{\partial t} + \frac{\dot{n}}{n}\psi(\underline{r},E,t)\right]$$

$$- \frac{1}{n(t)}\sum_{i=1}^{6}\int_{-\infty}^{t} M_{di}(\underline{r},E,t')n(t')\,\psi(\underline{r},E,t')e^{-\lambda_i(t-t')}dt' \quad (10)$$

where Eq. (3b) has been integrated and substituted into Eq. (3a).

The first approximation called the quasi-static method[9,33] retains all the terms in the RHS of Eq. (10). The time derivative of the shape function is, however, replaced by a backward difference form of first order:

$$\frac{\partial \psi(\underline{r},E,t)}{\partial t} \simeq \frac{\psi(\underline{r},E,t) - \psi(\underline{r},E,t-\Delta t)}{\Delta t} \qquad (11)$$

where $t-\Delta t$ is the time of the previous shape function calculation. The term $\frac{\dot{n}}{n}$ is obtained from the last point kinetics calculation performed in small time steps, and the feedback effects are accounted for through temperature effects on operators M_p and L. The delayed neutron source term is integrated over the time step Δt assuming a linearly extrapolated shape function $\psi(\underline{r},E,t)$ based on its values at the previous time steps, with the amplitude function obtained from the point kinetics calculation. In the quasi-static approximation a time step for the shape function calculation can contain several smaller time-steps for the point kinetics calculation, and according to the severity of the transient the shape function time-step can also be shortened or increased. In Fig. 2.2 is shown the relation between the shape function time-step and the point kinetics time steps in the quasi-static approximation. After the shape function is computed, a new delayed neutron source can be estimated and the shape function calculated again, in order to minimize error accumulation.

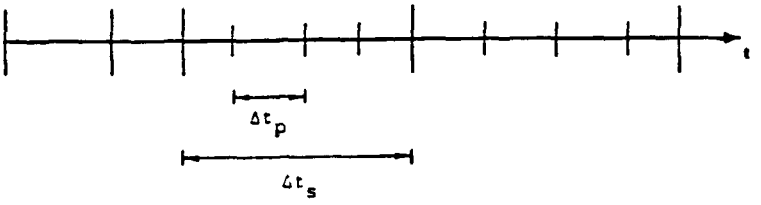

Δt_p = time step for point kinetics calculation

Δt_s = time step for shape function calculation

Figure 2.2 Time steps for the quasi-static method.

The next approximation is the neglect of the time derivative involving the shape function, usually possible when the redistribution of the neutron flux is very slow during a transient. The neglect of the time derivative term, however, does not significantly decrease the computation effort when compared with the quasi-static approximation.

The next approximation is the adiabatic approach. In this approximation, besides neglecting the time derivatives of both the amplitude and the shape function, one neglects the distinction between the delayed and prompt neutrons. Thus, one neglects the time retardation effects of the delayed neutrons in the shape function and assumes that the neutron flux adapts to the new core conditions instantaneously or adiabatically. The equation for the shape function becomes:

$$[\, M - L \,]\psi(\underline{r},E,t) = 0 \ . \qquad (12)$$

This approach thus neglects to a large extent the coupling between the shape function and amplitude function equations, but still can include the feedback coupling through explicit accounting of temperature effects on operators M and L.

One step further in the approximation is the complete decoupling of the shape and amplitude function equations, that is, the coupling via feedback is also neglected. The

time-dependent shape function can then readily be calculated a priori by using Eq. (12) for several intermediate states of the transient. The procedure would then be to use these shape functions to calculate the kinetic parameters as a function of time, and with them, to solve the point kinetics equations[23,34,45]. This approach has been used extensively as it generates good results provided one uses the correct shape functions. Experience and physical insight to the problem in question will determine the success of the method. The major problem with this approach is that it does not usually allow for adequate thermal-hydraulic feedback treatment, since the shape functions are determined often prior to the transient analysis.

The last approximation to be discussed is the widely used point model[3]. The shape function is assumed to remain constant during the transient and, therefore, no spatial effects can be accounted for in this model. The utility of the point model is very limited because of its requirement of an idealized situation, but it is nonetheless in use because of its simplicity.

The advantage of all the above approximations, compared with a direct numerical solution of the time-dependent diffusion equation, is that the shape function is determined infrequently. In a problem in which the amplitude function changes by several orders of magnitude, calculation of the shape function may be required only a few times. On the

other hand, due to the large variation, the amplitude function may have to be determined using the point kinetics equations for many small time steps. Since computations of the shape function are much more time-consuming it is a great advantage to be able to limit the number of the shape function calculations to a minimum. In contrast a direct solution of the time-dependent diffusion equation would require a time step as small as that for the point kinetics equations themselves.[4-8]

To demonstrate the accuracy of the several approximations mentioned in the previous paragraphs, we review a series of calculations done by Ott and Meneley[33]. They considered a large core represented by a homogeneous slab, 2.4 m in thickness, together with a transverse buckling to account for radial leakage. The core is divided into three regions so that the middle region with the largest buckling forces the flux to peak at the outer regions. The transient is induced by a ramp increase in the fission rate in one of the outer regions leveling off at t = 11 ms. As a consequence, the initially symmetric shape function becomes substantially tilted. The reactivities obtained by using the definition given in Eq. (5c) for the point model, adiabatic approximation, quasi-static with and without time derivative of the shape function, and the direct solution are shown in Fig. 2.3. It is seen that the reactivities obtained with both the point model and the adiabatic approach level off at the end of the ramp. The

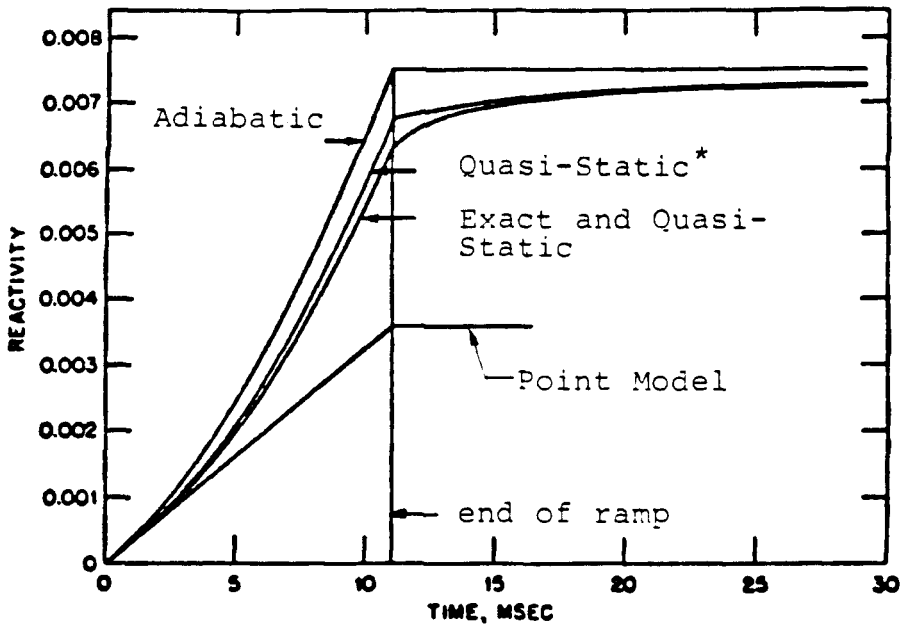

* quasi-static method without shape function time derivative

Figure 2.3 Reactivity as function of time for several approximate treatments for the shape function.

direct solution of the time-dependent diffusion equation and quasi-static approximation approach the adiabatic result gradually only after the delayed neutron precursors have adjusted to the new flux shape. The neglect of the neutron flux redistribution in the point model is seen to be an unacceptable approximation in this transient.

The neglect of the time derivative of the shape function can also create problems as is shown in Fig. 2.3. The assumption of instantaneous flux shape adaptation can only be valid for reactors which have a small mean generation time like the fast breeder reactors. For thermal reactors with a larger mean generation time it is necessary to have a method which accounts better for slow flux shape adaptation. Of all these methods, the quasi-static approach with shape function time-derivative included seems to be the most applicable for the problem of rod worth analysis. It is general, and can be made more accurate by tightening the time steps.

D. Thermal Hydraulic Feedback

There are basically two mechanisms by which flux distributions in a reactor core can be changed: The first is through any external change introduced in the reactor, e.g., a rise in inlet coolant temperature or insertion of a control rod, and the second, through the inherent response of the reactor due to perturbation in the temperature field

in the core. This latter response may be manifested altering the rate of neutron absorption in the core, the rate of moderation of neutrons to lower energies, or the total fission rate in the core or the total power output. These effects can be very detailed as is easily seen by writing the destruction and production operators also as a function of temperature:

$$P = P(\underline{r},E,t,T) \tag{13a}$$

$$L = L(\underline{r},E,t,T) \tag{13b}$$

Temperature feedback effects arise from several different mechanisms, and we need an accurate estimation of the temperature in reactor components. The most important mechanisms are basically those affecting the fuel, moderator, and coolant.

If temperature rises the fuel expands, reducing the density and affecting the cross sections appearing in the neutron diffusion equation. The most important effect from a fuel temperature rise, however, is the Doppler broadening of resonance cross sections. The magnitude and the resultant effect on reactivity will depend on the core configuration. In most reactors the effect is to increase neutron absorption in the non-fissile isotopes in the fuel, such as ^{238}U, thus tending to decrease the reactivity. In this case the reactor is said to have a negative Doppler

coefficient of reactivity. As the isotopic composition of the fuel changes with burnup of ^{235}U and production of plutonium, it is possible that Doppler broadening may even contribute positively to reactivity. Since the fuel is by and large the fastest feedback mecanism in a reactor, it is important for safety reasons that the fuel coefficient of reactivity remains negative throughout the reactor life.

The important aspect of the Doppler broadening in reactivity measurements is that it influences the measurement almost instantaneously. For instance, with a quick control rod withdrawal in a step fashion, the positive reactivity causes the power to rise. The fuel temperature increases rapidly following the power rise because there is not enough time for the heat generated to be transported across the fuel and deposited in the coolant. Therefore, almost instantaneously, the Doppler broadening effect on reactivity can be seen. In Fig. 2.4 is shown a plot of reactivity versus fuel temperature from measurements performed by A. R. R. Telford in a gas cooled reactor[27]. It clearly shows the Doppler feedback effect decreasing the reactivity as the fuel temperature rises. It is important to notice that at power conditions it is impossible to measure rod worth without accounting for the Doppler feedback effect. If one waits a little while longer, one will be measuring the combined effect of the control rod and the Doppler feedback[24-28].

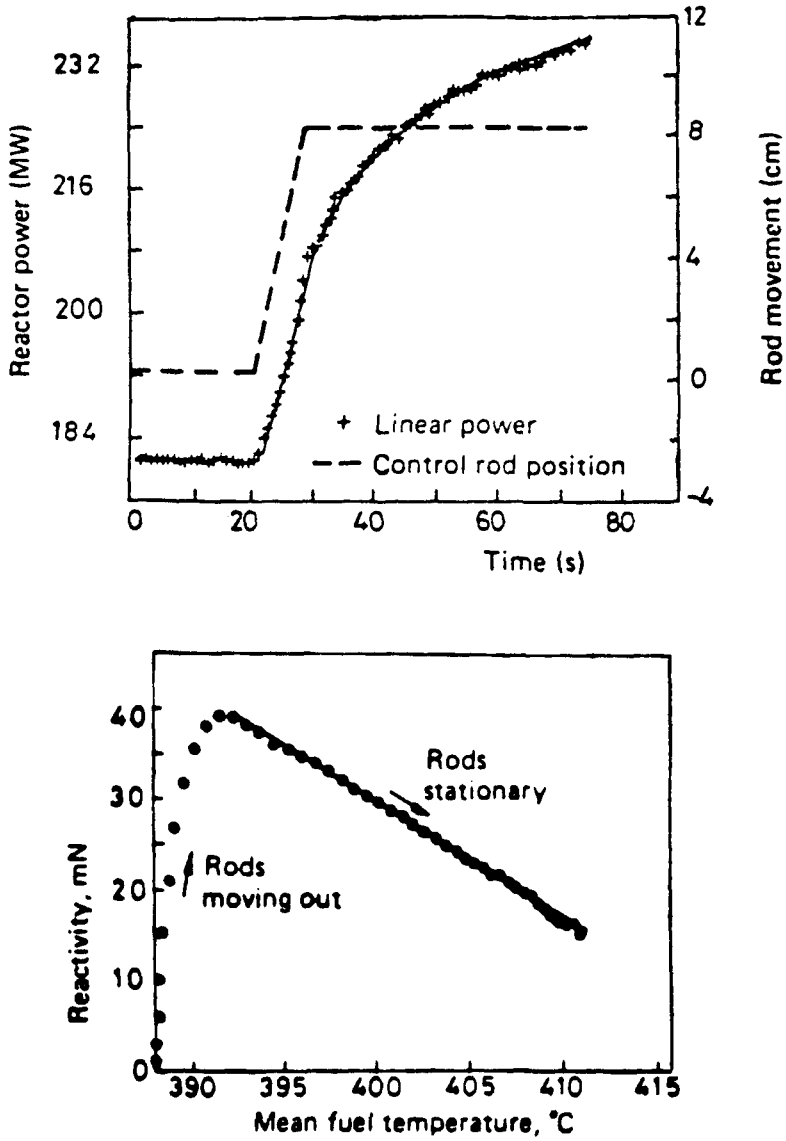

Figure 2.4 Doppler feedback effect on reactivity measurements.

When the temperature increases in the moderator or in the coolant, there also is thermal expansion which decreases the cross sections, most importantly the scattering cross section, responsible for neutron moderation. Thus, an increase in moderator temperature makes the neutron spectrum harder in the core, that is, less neutrons are moderated to the thermal energies. The effect on reactivity or on the neutron balance will depend on the type of reactor being analyzed. In thermal reactors where most of the fissions are caused by thermal neutrons the effect will be to decrease reactivity while for fast reactors the effect might very well be to increase reactivity. Fortunately the moderator temperature feedback is characterized by a somewhat longer time constant than that for the fuel, since the heat has to pass outwards through the fuel, gap, and cladding into the moderator. In some reactors the time constant for the moderator can be an order of magnitude larger than the fuel time constant, making it possible to isolate the moderator feedback effects from the fuel feedback effects. In fact, to obtain the results shown in Fig. 2.4, Telford made the transient sufficiently fast so that he could essentially maintain constant moderator temperatures.[27]

One important note related to thermal-hydraulic feedback is that by design they are required to be negative, that is, the net effect of the feedback should go against the forces that generate them. For instance, the feedback

effect due to a power increase should bring the power down, as is shown in Fig. 2.4. Hence, the presence of negative feedback will have an inhibiting effect on spatial redistribution of the neutron flux in the core, which makes the transient less stringent and more suitable for approximate treatment of the shape function. This does not imply that correct reactivity determinations can be achieved with greater ease. At zero power, if one waits for the shape function to attain an asymptotic behavior, there will be no need for correction factors; the count rates can be taken as the amplitude function directly, and period measurements can yield the required reactivity through the inhour equation[3]. The time required for the neutron flux to reach the asymptotic behavior is of the order of the longest lived delayed neutron precursor half life, about a minute or or more. In the presence of thermal-hydraulic feedback one does not have the time to wait for an asymptotic behavior of the shape function. Almost instantaneously after the rod motion has ceased, the feedback effects will replace spatial effects as the major influence on reactivity determination, irrevocably disrupting the ability to observe the pure reactivity effect of the rod motion. Hence, an ever greater importance is placed on accuracy in the immediate determination of reactivity.

To account for these thermal-hydraulic feedback effects it is necessary, in the first place, to determine the temperature field $T(\underline{r},t)$ in the reactor. Second, a

functional relationship must be found between the temperature and the several reactor parameters present in the destruction and production operators, the diffusion coefficient $D(\underline{r},E,t,T)$, absorption cross section $\Sigma_a(\underline{r},E,t,T)$, scattering cross section $\Sigma_s(\underline{r},E,t,T)$, and fission cross section $\nu\Sigma_f(\underline{r},E,t,T)$. The degree of sophistication needed to determine the temperature $T(\underline{r},t)$, and the operators $P(\underline{r},E,t,T)$ and $L(\underline{r},E,t,T)$ will depend on the specific problem being analyzed.

In the power reactor environment, the usual procedure to measure the reactivity, due to some perturbation in the core, is to make first the reactor critical and then to introduce the perturbation. The reactor can be made critical by any control means such as variation of boron concentration in the coolant, inlet coolant temperature, or motion of the control rods. In the case of differential rod worth measurement, the perturbation is the slight motion of the control rods. During and after the rod motion, general data such as rod position, detector countrates, and inlet and outlet temperatures must be recorded. Before the power output varies about 10 %, the reactor is again made critical by either returning the control rod to its original position or by other control means.

From the data collected during the transient one can perform an inverse kinetics analysis to obtain the net reactivity due to the control rod motion and the thermal

hydraulic feedback. The control rod reactivity or the feedback reactivity component has to be found by means of some theoretical model. The difference between the net reactivity obtained from the inverse kinetics analysis and the theoretically estimated feedback reactivity will yield the other component, the control rod reactivity.

For differential rod worth this procedure is repeated for several rod positions in the core at a given power level. A curve of differential rod worth as a function of rod position may then be constructed, that is, $\frac{\partial \rho}{\partial z}$ vs. z, the rod tip position. The total reactivity worth of the control rod, the integral rod worth, is obtained[2] by integrating $\frac{\partial \rho}{\partial z}$ over the core height H,

$$\text{integral rod worth} = \int_0^H \frac{\partial \rho}{\partial z}\, dz.$$

It is important to note here that it is impossible to directly measure the temperature field everywhere in the core, e.g., the local changes in the temperature distribution which will affect the core parameters. Thus, it is always necessary to rely on theoretical models to assess the temperature distribution in the core and also its influence on the reactor parameters. In any case the set of equations representing the thermal hydraulic model chosen must be solved simultaneously with Eqs. (1) or Eqs. (3) and Eq. (6), which give the neutronic behavior. Indeed, the

inclusion of thermal hydraulic feedback makes the difficult space-time analysis a formidable problem.

E. Further Remarks on the Space-Time Analysis

As discussed in this chapter, it is, in general, necessary to account for the neutron flux redistribution in the core during a transient involving strong flux tilting. The assumption of an unperturbed shape function throughout the transient can cause large errors in the estimation of reactivity. For rod worth analysis such as rod-drop experiments the neutron flux might be substantially tilted, making it necessary to have an accurate estimation of the shape function as a function of time.

Analysis of rod worth data through the inverse kinetics equation requires correction factors for the detector signals. To obtain these corrections factors it is necessary to determine the shape function as a function of time at the detector location. The inverse kinetics equation is known to be very sensitive to errors in the amplitude function[30], and, therefore, the use of detector signals in the reactivity meter can only be done with the help of accurate correction factors. Of all the methods presented for estimation of the shape function, the quasi-static approach seems to be the most applicable for the reactivity meter because of its greater accuracy and generality. The presence of thermal-hydraulic feedback at

power condition does not change the whole problem in philosophy, but increases its difficulty. Almost instantaneously after the rod motion has ceased, the feedback effects replace the spatial effects as the major cause for reactivity change, disrupting the ability to observe the pure reactivity effect of the rod motion. Hence, an immediate determination of reactivity is even more important.

In the next chapter an implementation of the quasi-static method in a reactivity meter is presented. The proposed modal-local method will allow real time calculations of the shape function.

CHAPTER III

THE MODAL-LOCAL METHOD

The utility of any approach to estimate the shape function in a reactivity meter depends, of course, on its accuracy and on its required calculational time. The reactivity meter should be operated on real time, that is, generate the results in a few seconds, and should require minimum storage, for implementation in micro-processors usually available in the reactor control room. With the advent of more general and powerful micro- and mini-computers it is no longer necessary to restrict the analysis of on-site measurements to analog processors[47], given that today's micro-computers have compilers for high-level languages such as FORTRAN and Pascal. In this chapter the proposed modal-local method is developed for estimating the shape function in a fast and accurate way. This method satisfies the conditions necessary for a reactivity meter by implementing a modal expansion of the shape function coupled with a local treatment for the finer effects caused by the rod motion[10,30,35,37]. In this method it is possible with few modes to obtain both accuracy and calculational speed in describing perturbed configurations of the core.

In Sects. A and B the modal-local method is developed in a general form for the time-dependent and steady state neutron diffusion equations, and in Sect. C is presented the approach used to obtain higher lambda modes. The numerical methods utilized in the proposed modal-local method for calculating the shape function and the reactivity as a function of time are presented in Sect. D.

A. The Coupled Modal-Local Method

Of the common methods known for estimating perturbed flux distribution the most suitable one for real-time application seems to be the modal expansion technique coupled with some special treatment for local perturbation effects.[10,30,35,37] The principal difficulty in the modal analysis has been that, in general, it requires very many modes to achieve a desired accuracy, and as the number of modes increases, the calculation becomes slower and more troublesome. To avoid such problems the modal expansion technique has been used with the expediency of physical insight in the choice of the modes[34]. Others obtain the intermediate states based on linear combination of the limiting states.[36] The inclusion of a local term is intended to ameliorate this problem for it describes the finer details of the neutron flux distribution, which would require many modes for an accurate representation. Thus, the philosophy behind the modal expansion technique coupled with some local treatment is that the substantial flux

perturbation in the vicinity of variations in reactor parameters be represented through a local function, while the overall smooth perturbations in the flux be represented in terms of a few-term modal expansion.

The incorporation of the local term in the expansion aims basically to reduce the number of modes necessary to achieve a prescribed accuracy. Therefore the local term should primarily have components of higher modes so that it is possible to keep only a few modes in the modal expansion:

$$\psi = a_o\phi_o + a_1\phi_1 + a_1\phi_2 + \ldots + \qquad \text{(modal term)}$$

$$\ldots + a_n\phi_n + a_{n+1}\phi_{n+1} + \ldots + \qquad \text{(local term)}$$

The lower harmonic modes in the modal term would then take care of the more smooth and gradual changes in the neutron flux, while the local term, made up mostly of higher harmonic modes, would represent the finer details of localized changes in the neutron flux. Thus, in our local treatment, the shape function is split into two terms, the modal function $h(\underline{r},E,t)$ and the local function $f(\underline{r},E,t)$:

$$\psi(\underline{r},E,t) = h(\underline{r},E,t) + f(\underline{r},E,t) \qquad (1)$$

The governing equation for the local function $f(\underline{r},E,t)$ should carry information on the local changes in the core;

it should include the variations in the production and destruction operators which characterize the perturbed state. For the modal function $h(\underline{r},E,t)$, its governing equation should account for the multiplicative effects which tend to propagate the localized changes throughout the core; it should have the reference production operator. In the modal-local method the functions f and h satisfy:

$$\frac{1}{v}\frac{\partial f(\underline{r},E,t)}{\partial t} + L_o f(\underline{r},E,t) = [\delta M_p - \delta L]_{ext}\psi(\underline{r},E,t) \qquad (2a)$$

$$\frac{1}{v}\frac{\partial h(\underline{r},E,t)}{\partial t} = [M_{po} - L_o - \frac{1}{v}\frac{\dot{n}}{n}]\, h(\underline{r},E,t)$$

$$+ [M_{po} - \frac{1}{v}\frac{\dot{n}}{n}]\, f(\underline{r},E,t) + \frac{1}{n(t)}\sum_{i=1}^{6}\lambda_i \chi_{di}(E)c_i(\underline{r},t) \qquad (2b)$$

$$+ [\delta M_p - \delta L]_{feed}\psi(\underline{r},E,t)$$

$$\frac{\partial c_i(\underline{r},t)}{\partial t} = -\lambda_i c_i(\underline{r},t)$$

$$+ \beta_i \frac{P(\underline{r},E,t)}{k_o}[h(\underline{r},E,t) + f(\underline{r},E,t)]n(t) \qquad (2c)$$

where the perturbed operators have been written as:

$$L(\underline{r},E,t) = L_o(\underline{r},E) + \delta L(\underline{r},E,t),$$

$$M_p(\underline{r},E,t) = M_{po}(\underline{r},E) + \delta M_p(\underline{r},E,t),$$

Here, the subscripts o, ext, and feed indicate reference state, external perturbation, and feedback perturbation, respectively.

The equation for $f(\underline{r},E,t)$ carries information on the local changes, as it has in the source term on the RHS variations in the production and destruction operators due to external perturbations, which in the case of control rod motion can be localized. The term $L_o f(\underline{r},E,t)$ transmits the effects of the local changes throughout the reactor. Eq. (2b) has only operators of the reference state and is driven by the local function f and the feedback perturbation term, which is more distributed over the core. Since it has the production operator $M_{po}(\underline{r},E)$ this equation accounts for multiplicative effects or global variations in the shape function due to local flux perturbations.

The inclusion of the feedback term in Eq. (2b) for $h(\underline{r},E,t)$ is justified by noting two points: First, in nuclear reactors the thermal-hydraulic feedback effects tend to decrease the perturbation in the neutron flux since they work against the mechanisms driving the transient. Second, the feedback effects are present in the core wherever a change in temperature occurs, as opposed to the external perturbation which can be very localized as in the case of control rod motion.

In order to obtain solutions for Eqs. (2a) and (2b) we introduce some approximations. First, we neglect the time

derivative term in Eq. (2a). This is equivalent to adiabatically representing the local variations through f, while the gradual evolution of the shape function is accounted for in the global function h in a fully time-dependent fashion. Second, the second-order terms in Eq. (2a) are neglected to yield:

$$L_o f(\underline{r},E,t) = [\delta M_p(\underline{r},E,t)-\delta L(\underline{r},E,t)]_{ext}\psi_o(\underline{r},E) \qquad (3)$$

The practical purpose of this approximation is readily noticed. The local function given by Eq. (3) can be readily obtained from standard diffusion theory codes through a fixed source calculation, while Eq. (2a) cannot. Physically, the local changes in the neutron flux occur in the vicinity of the external perturbation, which thus can be attained almost instantaneously.

The time-dependent shape function can now be calculated by solving Eq. (3) and Eq. (2b) coupled with Eq. (2c). Given the solution for $f(\underline{r},E,t)$, we propose to solve Eqs. (2b) and (2c) by expanding $h(\underline{r},E,t)$ in terms of a few lambda modes[30]:

$$h(\underline{r},E,t) = \sum_{n=0}^{N} a_n(t)\phi_n(\underline{r},E) \qquad (4)$$

where ϕ_n are the lambda modes for some reference state.

To obtain the equations for the expansion coefficients $a_n(t)$, $n=1,\ldots,N$, we substitute Eq. (4) in Eq. (2b), premultiply the whole equation by the adjoint $\phi_m^\dagger$ to the lambda modes and integrate over energy and reactor volume. In order to eliminate the cross-terms in the equations we note the following:

$$\langle \phi_m^\dagger, (M_{po}-L_o)\phi_n \rangle \ll \langle \phi_m^\dagger, (M_{po}-L_o)\phi_m \rangle, \quad m \neq n, \text{ and}$$

$$\langle \phi_m^\dagger, \frac{1}{v}\phi_n \rangle \ll \langle \phi_m^\dagger, \frac{1}{v}\phi_m \rangle, \quad m \neq n.$$

The first approximation can be understood readily, since M_{po} differs from M_o only slightly, and hence

$$\langle \phi_m^\dagger, (M_{po}-L_o)\phi_m \rangle \simeq 1 - \frac{k_o}{k_m},$$

while

$$\langle \phi_m^\dagger, (M_{po}-L_o)\phi_n \rangle \simeq (1 - \frac{k_o}{k_m})\delta_{mn}.$$

The second approximation will hold if the production operator M_o is spatially uniform, which is approximately the case in many reactor configurations. Moreover, this integral is small compared to others present in this

formulation. We then obtain for the modal expansion coefficients:

$$\langle \phi_m^\dagger, \frac{1}{v}\phi_m \rangle \dot{a}_m(t) = \langle \phi_m^\dagger, (M_{po} - L_o)\phi_m \rangle a_m(t)$$

$$- \frac{\dot{n}(t)}{n(t)} \langle \phi_m^\dagger, \frac{1}{v}\phi_m \rangle a_m(t) + \langle \phi_m^\dagger, M_{po} f \rangle \qquad (5)$$

$$- \frac{\dot{n}(t)}{n(t)} \langle \phi_m^\dagger, \frac{1}{v} f \rangle + \sum_{i=1}^{6} \lambda_i \langle \phi_m^\dagger, \chi_{di} \frac{c_i}{n(t)} \rangle$$

$$+ \langle \phi_m^\dagger, [\delta M_p - \delta L]_{feed} \psi \rangle$$

Eq. (5) can be written in a form that resembles the point kinetics equations by noting that:

$$\langle \phi_m^\dagger, (M_{po} - L_o)\phi_m \rangle = \langle \phi_m^\dagger, (M_o - L_o)\phi_m \rangle - \sum_{i=1}^{6} \langle \phi_m^\dagger, M_{odi}\phi_m \rangle$$

$$= \left(\frac{k_m - k_o}{k_m}\right) \langle \phi_m^\dagger, M_o \phi_m \rangle - \sum_{i=1}^{6} \langle \phi_m^\dagger, M_{odi}\phi_m \rangle .$$

Substituting the above expression into Eq. (5) we obtain:

$$\langle \phi_m^\dagger, \frac{1}{v}\phi_m \rangle \dot{a}_m(t) = \left(\frac{k_m - k_o}{k_m}\right) \langle \phi_m^\dagger, M_o \phi_m \rangle a_m(t)$$

$$- \sum_{i=1}^{6} \langle \phi_m^\dagger, M_{odi}\phi_m \rangle a_m(t) - \frac{\dot{n}(t)}{n(t)} \langle \phi_m^\dagger, \frac{1}{v}\phi_m \rangle a_m(t) \qquad (6)$$

$$+ \langle \phi_m^\dagger, M_{po} f \rangle \quad - \quad \frac{\dot{n}(t)}{n(t)} \langle \phi_m^\dagger, \frac{1}{v} f \rangle$$

$$+ \langle \phi_m^\dagger, [\delta M_p - \delta L]_{feed} \psi \rangle \quad + \quad \sum_{i=1}^{6} \lambda_i \langle \phi_m^\dagger, \chi_{di} \frac{c_i}{n(t)} \rangle$$

Eq. (2c) for the delayed neutron precursors is also expanded in terms of lambda modes, but first we rewrite the time derivative term as:

$$\frac{1}{n(t)} \frac{\partial c_i(\underline{r},t)}{\partial t} = \frac{\partial}{\partial t} \left[\frac{c_i(\underline{r},t)}{n(t)}\right] + \frac{\dot{n}(t)}{n(t)} \frac{c_i(\underline{r},t)}{n(t)}$$

We then premultiply Eq. (2c) by $\phi_m^\dagger(\underline{r},E)\chi_{di}(E)/n(t)$ and integrate over energy and volume of the reactor. To eliminate cross-terms we assume that the differences in the total and delayed neutron fission spectra are small such that:

$$\langle \phi_m^\dagger, M_{di} \phi_n \rangle \ll \langle \phi_m^\dagger, M_{di} \phi_m \rangle, \quad m,n=1,\ldots,N.$$

The second order terms are also neglected, similar to our earlier derivations:

$$M_{di}\phi_m \simeq M_{odi}\phi_m \ , \quad m=1,\ldots,N, \text{ and}$$
$$M_{di} f \simeq M_{odi} f \ , \quad m=1,\ldots,N.$$

Then we obtain for delayed neutron precursors:

$$\frac{d}{dt}\langle\phi_m^\dagger, \chi_{di}\frac{c_i}{n}\rangle = -(\lambda_i + \frac{\dot{n}}{n})\langle\phi_m^\dagger, \chi_{di}\frac{c_i}{n}\rangle$$

$$+ a_m(t)\langle\phi_m^\dagger, M_{odi}\phi_m\rangle + \langle\phi_m^\dagger, M_{odi}f\rangle, \quad i=1,\ldots,6. \tag{7}$$

The solution of Eqs. (6) and (7) provides the coefficients $a_m(t)$ for the modal function $h(\underline{r},E,t)$.

In order to simplify the notation we introduce the following definitions:

$$\Lambda_m = \langle\phi_m^\dagger, \frac{1}{v}\phi_m\rangle,$$

$$\rho_m = \frac{k_m - k_o}{k_m}$$

$$s(t) = \frac{\dot{n}(t)}{n(t)},$$

$$\beta_{im} = \langle\phi_m^\dagger, M_{odi}\phi_m\rangle, \qquad \beta_m = \sum_{i=1}^{6}\beta_{im},$$

$$g_{im}(t) = \frac{1}{\Lambda_m}\langle\phi_m^\dagger, \chi_{di}\frac{c_i}{n(t)}\rangle,$$

$$f_{pm}(t) = \frac{1}{\Lambda_m}\langle\phi_m^\dagger, M_{po}f\rangle,$$

$$f_m(t) = \frac{1}{\Lambda_m}\langle\phi_m^\dagger, \frac{1}{v}f\rangle,$$

$$f_{dim}(t) = \frac{1}{\Lambda_m} <\phi_m^\dagger, M_{odi} f>,$$

$$\xi_m(t) = \frac{1}{\Lambda_m} <\phi_m^\dagger, [\delta M_p - \delta L]_{feed} \psi>,$$

$$m=1,\ldots,N \text{ and } i=1,\ldots,6.$$

Then Eqs. (6) and (7) become:

$$\dot{a}_m(t) = [\frac{\rho_m - \beta_m}{\Lambda_m} - s(t)]\, a_m(t) + f_{pm}(t) - s(t) f_m(t) + \xi_m(t) + \sum_{i=1}^{6} \lambda_i\, g_{im}(t) \tag{8a}$$

$$\dot{g}_{im}(t) = -[\lambda_i + s(t)]\, g_{im}(t) + \frac{\beta_{im}}{\Lambda_m} a_m(t) + f_{dim}(t), \tag{8b}$$

$$m=1,\ldots,N \text{ and } i=1,\ldots,6.$$

As is the case with any modal analysis, the coefficient $a_o(t)$ cannot be obtained through Eqs. (8). It should rather be calculated so that the shape function $\psi(\underline{r},E,t)$ satisfy the normalization condition of Eq. (4) from Chapter II. Substituting ψ by Eq. (1) in Eq. (4) of Chapter II, we obtain for $a_o(t)$:

$$a_o(t) = \frac{C_o - \sum_{m=1}^{N} a_m(t) <\phi_o^\dagger, \frac{1}{v}\phi_m> - <\phi_o^\dagger, \frac{1}{v} f>}{<\phi_o^\dagger, \frac{1}{v}\phi_o>} \tag{8c}$$

The set of Eqs. (8) coupled with Eq. (3) provide a general method for solving a space-time problem with or without feedback considerations. Although many integrals are required to evaluate the parameters appearing in Eqs. (8), most of the integrals can be calculated a priori and hence the present method can be applied to efficient space-time reactivity calculations. The integrals $\xi_m(t)$ have to be evaluated as a function of time, with explicit accounting for thermal hydraulic feedback. The unknown shape function at time t present in $\xi_m(t)$ is approximated by its estimate at a time immediately before. In the case of no feedback $\xi_m(t)$ are all zero and all other integrals can be evaluated prior to the time-dependent calculations involving Eqs. (8).

For obtaining $\xi_m(t)$ a model should be developed to determine the temperature distribution across the core as a function of time, as well as cross section dependence on temperature. The single channel model which yields fuel and coolant temperature for an average coolant channel of the core is considered here as our sample feedback case limited to a one-dimensional calculation. The channel consists of a fuel rod and the surrounding coolant which flows in the upward direction. The heat conduction in the axial direction in the fuel is neglected because the temperature gradient in this direction is small. Thus, we assume the

heat produced in the fuel rod is transported radially to the coolant which is heated up as it flows along the channel.[4,9,45] The fuel and coolant temperatures are found to satisfy the following equations:

$$\rho_f C_f \frac{\partial T_f(z,t)}{\partial t} + \frac{MU}{A_f}[T_f(z,t)-T_c(z,t)] = Q(z,t) \qquad (9a)$$

$$\rho_c C_c A_c \frac{\partial T_c(z,t)}{\partial t} + GC_c \frac{\partial T_c(z,t)}{\partial z} = \qquad (9b)$$

$$\frac{MU}{A_c}[T_f(z,t)-T_c(z,t)]$$

where ρ is density, C is the heat capacity, G is the mass velocity, Q is the heat generation per unit volume in the fuel rod, A_f is the fuel cross sectional area in the channel, A_c is the coolant cross sectional area in the channel, M is the wetted perimeter, and U is the effective heat transfer coefficient from fuel to the coolant. The subscripts f and c indicate fuel and coolant, respectively.

For solving Eqs. (9) we propose that the fuel and coolant temperatures be expanded in terms of the lambda modes along the thermal hydraulic channel in the following manner:

$$T_f(z,t) = \sum_{n=o}^{N} e_n(t)\theta_n(z) + T_c(z,t)$$

$$T_c(z,t) = \sum_{n=o}^{N} u_n(t)\mu_n(z)$$

where

$$\theta_n(z) = P_o(z,E)\phi_n(z,E),$$

$$\mu_n(z) = \int_o^z \theta_n(z')dz'.$$

The function θ_n can be seen as the power distribution produced by the mode ϕ_n along the axial direction.

A set of equations for the expansion coefficients $e_n(t)$ and $u_n(t)$ is found by substituting the expansions of T_f and T_c into Eqs. (9), pre-multiplying by $\theta_m^\dagger$ and integrating over the channel volume:

$$\sum_{n=o}^{N} [\ A_{mn}\dot{u}_n(t) + B_{mn}u_n(t)\ ] = \sum_{n=o}^{N} C_{mn}e_n(t) \qquad (10a)$$

$$\sum_{n=o}^{N} [\ E_{mn}\dot{u}_n(t) + F_{mn}\dot{e}_n(t) + D_{mn}e_n(t)\ ] = Q_m(t) \qquad (10b)$$

$$m,n=1,\ldots,N,$$

where $A_{mm} = \langle \theta_m^\dagger, \rho_c C_c \mu_n \rangle$,

$$B_{mn} = \langle \theta_m^\dagger, GC_c\theta_n \rangle,$$

$$C_{mn} = \langle \theta_m^\dagger, \frac{MU}{A_c}\theta_n \rangle,$$

$$D_{mn} = \langle \theta_m^{\dagger}, \frac{MU}{A_f} \theta_n \rangle,$$

$$E_{mn} = \langle \theta_m^{\dagger}, \rho_f C_f \mu_n \rangle,$$

$$F_{mn} = \langle \theta_m^{\dagger}, \rho_f C_f \theta_n \rangle, \text{ and}$$

$$Q_m = \langle \theta_m^{\dagger}, Q \rangle.$$

The inner products involve only the channel volume.

For feedback representation we will consider only first order variation of the cross sections with temperature but the cross sections can in general be a nonlinear function of the temperature. Thus:

$$\xi_m(t) = \sum_{n=o}^{N} \{[e_n(t)-e_n(0)]\zeta_{mn} + [u_n(t)-u_n(0)]\kappa_{mn} + [u_n(t)-u_n(0)]\tau_{mn}\} \tag{11}$$

where $$\zeta_{mn} = \langle \phi_m^{\dagger}, \left[\frac{\partial(M_p-L)}{\partial T_f} \theta_n\right] \psi \rangle,$$

$$\kappa_{mn} = \langle \phi_m^{\dagger}, \left[\frac{\partial(M_p-L)}{\partial T_f} \mu_n\right] \psi \rangle, \text{ and}$$

$$\tau_{mn} = \langle \phi_m^{\dagger}, \left[\frac{\partial(M_p-L)}{\partial T_c} \mu_n\right] \psi \rangle.$$

In the case of feedback reactivity measurements the several components of the reactivity cannot be obtained from the inverse kinetics equation. The inverse kinetics equation provides only the net reactivity as a function of time. The components can be obtained through Eq. (5c) of Chapter II by considering only the external or the feedback perturbation in the numerator. Thus, the external reactivity component ρ_{ext} and the feedback reactivity component ρ_{feed} will be given by:

$$\rho_{ext}(t) = \frac{\langle \phi_o^\dagger, [\delta M - \delta L]_{ext} \psi \rangle}{\langle \phi_o^\dagger, M\psi \rangle} \tag{12a}$$

$$\rho_{feed}(t) = \frac{\langle \phi_o^\dagger, [\delta M - \delta L]_{feed} \psi \rangle}{\langle \phi_o^\dagger, M\psi \rangle} \tag{12b}$$

where $\psi(\underline{r},E,t)$ is the modal-local estimate of the shape function.

In many cases, one of the reactivity components is known very accurately based on other measurements or calculations. In this case the unknown component can be obtained from the difference between the net reactivity and the known component. This procedure is extensively used in practice to determine either differential rod worths, boron worths, or reactivity coefficients.

The input parameters necessary for implementing the modal-local method as a reactivity meter are then the integrals Λ_m, β_{im}, $f_{pm}(t)$, $f_m(t)$, $f_{dim}(t)$, ζ_{mn}, κ_{mn}, and τ_{mn}, the eigenvalue relations ρ_m, values of the lambda modes and local function at the detector locations, decay constants for delayed precursors, and detector signals measured during the transient. Once these data are available the modal-local method can predict in real time the reactivity worth of control rods. In the next section we present why the local function $f(\underline{r},E,t)$ obtained from Eq. (3) is expected to bear mostly the local changes in the shape function.

B. The Local Function

In order to emphasize the specific characteristics of both $h(\underline{r},E,t)$ and $f(\underline{r},E,t)$ we consider the well known problem of obtaining the perturbed flux distribution in the reactor based on a set of modes of some reference configurations[40,41,48,49]. Consider that the reference core configuration can be described by the production operator $M_o(\underline{r},E)$, the destruction operator $L_o(\underline{r},E)$, the neutron flux distribution $\phi_o(\underline{r},E)$, and the effective multiplication factor k_o, already incorporated as an eigenvalue in the production operator. Then the steady state neutron diffusion equation describing the core is:

$$L_o(\underline{r},E)\phi_o(\underline{r},E) = M_o(\underline{r},E)\phi_o(\underline{r},E) \qquad (13)$$

The perturbed core configuration, which can be arrived at by changes in either the production or destruction operators such as control rod motion or coolant density changes due to a temperature rise is described by:

$$\begin{aligned} L(\underline{r},E) &= L_o(\underline{r},E) + \delta L(\underline{r},E) \\ M(\underline{r},E) &= M_o(\underline{r},E) + \delta M(\underline{r},E) \\ \phi(\underline{r},E) &= \phi_o(\underline{r},E) + \delta\phi(\underline{r},E) \end{aligned} \tag{14}$$

so that:

$$L(\underline{r},E)\phi(\underline{r},E) = M(\underline{r},E)\phi(\underline{r},E). \tag{15}$$

This can be rewritten using the above definitions as:

$$[L_o(\underline{r},E)-M_o(\underline{r},E)]\phi(\underline{r},E) = [\delta M(\underline{r},E)-\delta L(\underline{r},E)]\ \phi_o(\underline{r},E) \tag{16}$$

where the second-order term $[\delta M-\delta L]\delta\phi$ were assumed to be small[40,41,48,49] and are neglected. Higher order approximations to Eq. (15) can be derived[50,51], but we will limit our discussion here to the first order approximation, Eq. (16), without any loss of generality.

In any modal expansion technique the perturbed flux ϕ in Eq. (16) is expanded in terms of modes from some known reference state of the reactor. We will consider here for

our modal expansion the lambda modes from the steady state neutron diffusion equation, Eq. (13):

$$\phi(\underline{r},E) = \sum_{n=o}^{\infty} c_n \phi_n(\underline{r},E) \tag{17}$$

Substituting Eq. (17) into Eq. (16), premultiplying the equation by $\phi_m^\dagger$ and integrating over energy and volume, one obtains:

$$\sum_{n=o}^{\infty} c_m \langle \phi_m^\dagger, M_o \phi_n \rangle \left(\frac{k_o - k_n}{k_n}\right) = \langle \phi_m^\dagger, [\delta M - \delta L]\phi_o \rangle$$

Using the orthonormality condition, we obtain:

$$c_m = \frac{\langle \phi_m^\dagger, [\delta M - \delta L]\phi_o \rangle}{\frac{k_o - k_m}{k_m}} . \tag{18}$$

Eq. (18) is not defined for m=0, the fundamental mode, because the denominator becomes zero[49]. It is only used to obtain the coefficients a_m for the higher modes. The fundamental component of the perturbed flux is usually found by adjusting it such that a required normalization is met. In static problems usually the power distribution is normalized, while in time-dependent problems, the shape

function normalization given in Eq. (4) of Chapter II is preferable.

In this static problem the modal-local method becomes:

$$\phi(\underline{r},E) = h(\underline{r},E) + f(\underline{r},E) \tag{19}$$

with the following governing equations:

$$L_o f(\underline{r},E) = [\delta M - \delta L]\phi_o(\underline{r},E) \tag{20a}$$

$$[L_o - M_o]h(\underline{r},E) = \cancel{\delta M_o} f(\underline{r},E) \tag{20b}$$

We want to verify if $f(\underline{r},E)$ bears the local changes in the shape function and $h(\underline{r},E)$ bears the global changes in the shape function. We expand them in terms of lambda modes and compare the expansion coefficients with those of Eq. (18) from the expansion of $\phi(\underline{r},E)$ itself. In the expansions

$$f(\underline{r},E) = \sum_{n=o}^{\infty} b_n \phi_n \tag{21a}$$

$$h(\underline{r},E) = \sum_{n=o}^{\infty} a_n \phi_n \tag{21b}$$

the coefficients b_m for the local function are given by:

$$b_m = \frac{\langle \phi_m^\dagger, [\delta M - \delta L]\phi_o \rangle}{\frac{k_o}{k_m}}$$

The relationship between the coefficients b_m for the local function, a_m for the modal function, and c_m for the total perturbed flux is:

$$c_m = a_m + b_m \tag{22}$$

Combining the above expression with the ones defining b_m and c_m we obtain:

$$b_m = \frac{k_o - k_m}{k_o} c_m \tag{23a}$$

$$a_m = \frac{k_m}{k_o} c_m \tag{23b}$$

If the eigenfunctions are ordered such that the eigenvalues k_m go from the largest to the smallest, b_m will account for a greater fraction of c_m for the harmonic modes with smaller eigenvalues, and a_m a greater fraction of c_m for the harmonic modes with greater eigenvalues. Thus, the split of the perturbed neutron flux into two components, as suggested in Eqs. (19) and (20), leads to a modal function $h(\underline{r},E)$ responding to global flux tilts in the core characterized mostly by the lower harmonic modes, and to a local function $f(\underline{r},E)$ responding to the localized change in the neutron flux characterized mostly by the higher harmonic modes.

This shows that in the modal-local method the number of modes can be reduced without compromising the accuracy.

We have seen that the modal-local method can be implemented for time dependent analysis of reactor problems and have presented the set of equations governing the shape function $\psi(\underline{r},E,t)$. In all the analysis we have assumed that the lambda modes for some reference configuration of the rector were available. The calculation of the lambda modes is not a simple task but can be carried out with some modifications in standard multi-dimensional, multi-group diffusion theory codes. In the Appendix we discuss in detail the problems involved with calculation of the lambda modes and the actual approach used in this investigation for obtaining the lambda modes. In the next section we consider the numerical approaches used for the implementation of the modal-local method as a reactivity meter.

C. Numerical Methods for the Modal-Local Method

The theory of the modal-local method has been presented in the previous sections. The actual implementation of the modal-local equations (3) and (8), together with the inverse kinetics equation, in a computer program that can be used as a reactivity meter is presented here. This includes the numerical scheme for solution of the inverse kinetics equation, and the quasi-static approximation in the modal-local method for estimating the shape function $\psi(\underline{r},E,t)$.

The treatment of the local function as a function of time is discussed, as well as the solution of the coupled differential equations for the modal expansion coefficients.

1. Numerical Solution of the Inverse Kinetics Equations

The inverse kinetics equation is somewhat easier to be implemented numerically than the forward point kinetics equation, because the reactivity usually varies slightly during the transient. Therefore, problems with numerical stability are much less stringent in the inverse case than with the forward kinetics equation in which the amplitude function may scan several orders of magnitude. Our numerical approach for the inverse kinetics equation follows closely the algorithm of the IVKDT1 code[46] currently in use at the KFA. This algorithm will be described briefly in this section.

The known quantities in the inverse kinetics equation are the kinetics parameters $\Lambda(t)$, $\bar{\beta}_i(t)$, $\bar{\beta}(t)$, and the amplitude function n(t) obtained from detector count rates accumulated during fixed time intervals. Since the kinetics parameters change very little they are assumed constant over each time step. The amplitude function may change very rapidly during a transient, and, therefore, requires some special treatment for a correct estimation of the time derivative term and more importantly, the convolution integral involving the delayed neutrons. When dealing with

detector signals one will always find some noise or fluctuation in the data which may require some type of data smoothing. Basically, our numerical scheme uses a quadratic fit for the amplitude function n(t) over three consecutive time intervals of length Δt_k centered around $t = t_k$:

$$n(t) = a + bt + ct^2, \tag{30}$$

for $t_{k-1}-\Delta t_{k-1}/2 < t < t_{k+1}+\Delta t_{k+1}/2$. In Fig. 3.1 is found a sketch of this interpolation scheme. The coefficients a, b, and c are obtained by equating the integrals:

$$\int_{\Delta t_m} n(t)dt = n(t_m)\Delta t_m, \quad \text{for } m = k-1,\ k,\ k+1. \tag{31}$$

where n(t) is given by Eq. (30), and $n(t_m)$ is obtained from the detector signals.

This set of three equations can be readily solved for the three unknown coefficients a, b, and c. Once the time dependence of the amplitude function is established over the time intervals, the time derivative term and the convolution integral can be estimated. For this purpose the inverse kinetics equation (6) from Chapter II is rewritten in the following form for $t = t_k$:

$$\rho(t_k) = \rho_p(t_k) + \rho_d(t_k) \tag{32a}$$

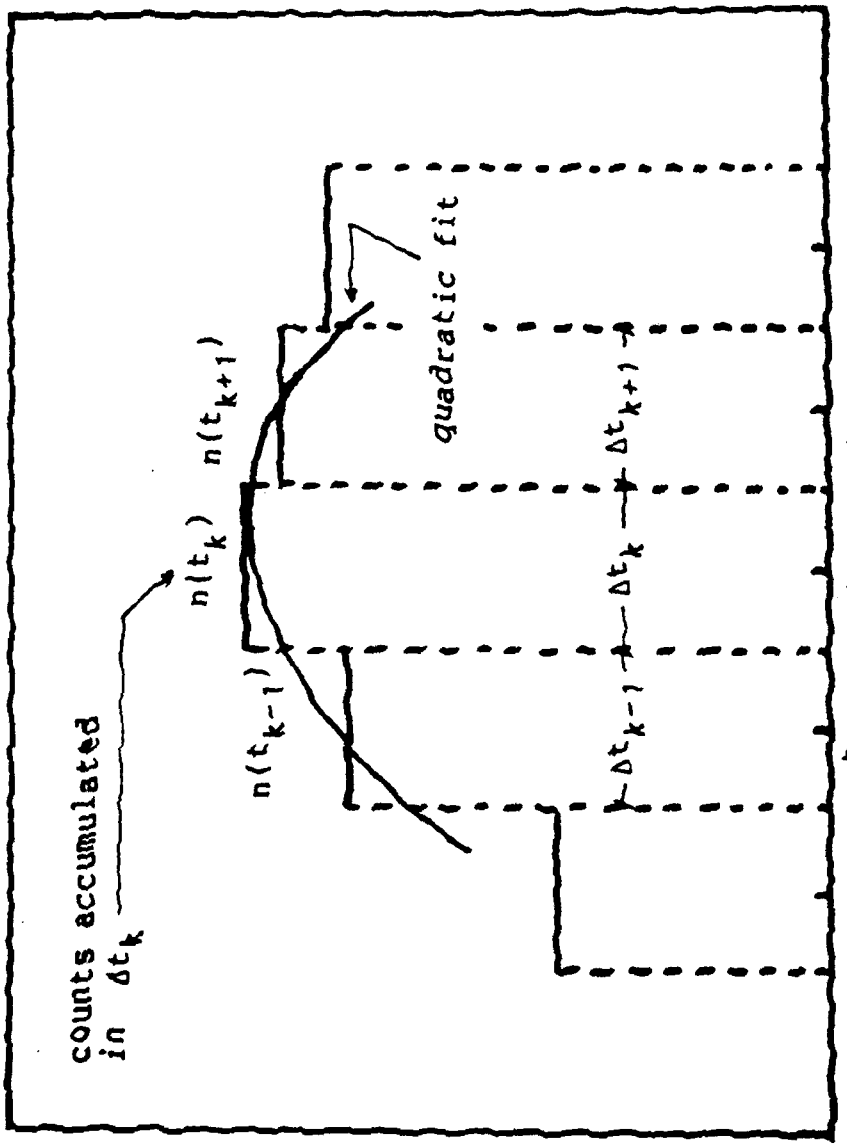

Figure 3.1 Sketch of the integration scheme for *inverse kinetics equation.*

where:

$$\rho_p(t_k) = \bar{\beta}(t_k) + \frac{\Lambda(t_k)\dot{n}(t_k)}{n(t_k)}, \quad \text{and,} \tag{32b}$$

$$\rho_d(t_k) = -\frac{\Lambda(t_k)}{n(t_k)} \cdot \sum_{i=1}^{6} \lambda_i \int_{-\infty}^{t_k} dt' \frac{\bar{\beta}_i(t')n(t')}{\Lambda(t')} \exp[\lambda_i(t'-t_k)] \tag{32c}$$

The time derivative $\dot{n}(t_k)$ in the prompt reactivity term is $b + 2ct_k$. For the delayed reactivity term a recurrence formula can be found based on the previous time steps. Dividing the convolution integral into two integrals with limits from $-\infty$ to t_{k-1} and from t_{k-1} to t_k, respectively, one arrives at:

$$\rho_d(t_k) = -\frac{\Lambda(t_k)}{n(t_k)} \left(\rho_d(t_{k-1}) \frac{n(t_{k-1})}{\Lambda(t_{k-1})} \exp[\lambda_i(t_{k-1}-t_k)] - \sum_{i=1}^{6} \lambda_i \int_{t_{k-1}}^{t_k} dt' \frac{\bar{\beta}_i(t')n(t')}{\Lambda(t')} \exp[\lambda_i(t'-t_k)] \right) \tag{33}$$

The convolution integral in the current time step between t_{k-1} and t_k can be readily solved by substituting Eq. (30) in Eq. (33) and assuming $\bar{\beta}_i(t')$ and $\Lambda(t')$ constant over the

time step. This procedure is repeated until the whole transient is covered.

This algorithm has been implemented in the INVK code and its accuracy tested against direct point kinetics results[57]. It will be shown in chapter IV that this algorithm is very accurate, even for strong reactivity insertion in the core such as in rod-drop transients. In the next section we will discuss the implementation of the quasi-static approach for the modal-local method in order to obtain the correction factors needed to convert the detector signals to the amplitude function.

2. The Quasi-Static Approach for the Modal-Local Method

In the quasi-static approach the time steps for the shape function calculation can be much larger than the time step for the forward point kinetics equations or, in our problem, the inverse kinetics equation. The most time-consuming part of the calculation in the modal-local approach is the calculation of the local function $f(\underline{r},E,t)$. It is performed in larger time steps called the local-function time steps. The equations for the modal coefficients and the inverse kinetics are solved in the small time steps. Since the source term of Eq. (3) is known a priori, $f(\underline{r},E,t)$ is precalculated for several intermediate states of the transient under study. Consistent with the quasi-static method, the local function is then linearly

interpolated over the smaller time steps where the equations for the modal coefficients and the inverse kinetics are solved. The time steps used in the modal-local method are shown in Fig. 3.2.

The feedback integral $\xi_m(t)$ in Eq. (8a) is evaluated in the small time steps, Δt_p, together with the modal coefficients. The calculation is repeated in each small time step until some convergence criterion is met, which usually occurs in 1 or 2 iterations. In the evaluation of $\xi_m(t)$ we use the shape function of the previous small time step $\psi(\underline{r},E,t-\Delta t_p)$, a procedure more accurate than the first order approximation for the shape function.

For the solution of the modal-local Eqs. (8) and the thermal hydraulic Eqs. (10), we use an explicit time differencing scheme consistent with the quasi-static approach. Thus, every term on the RHS of Eqs. (8) and (10) is evaluated in the previous time step. The time derivatives at a time t_k are approximated by:

$$\frac{dr_m(t_k)}{dt} \simeq \frac{r_m(t_k) - r_m(t_{k-1})}{\Delta t}$$

where $r_m = a_m$, g_{im}, e_m, u_m, and $\Delta t = t_k - t_{k-1}$. The set of coupled differential equations become a set of algebraic equations for the coefficients $a_m(t_k)$, $g_{im}(t_k)$, $e_m(t_k)$ and $u_m(t_k)$ which are solved by the Gauss elimination method.

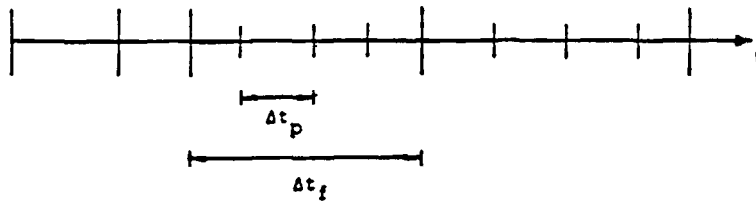

Δt_p = time step for the calculation of the modal coefficients and the inverse kinetics equation.

Δt_f = time steps for the calculation of the local function and feedback integrals.

Figure 3.2 Time steps for the Modal-Local Method.

The inverse kinetics equation is solved in the same time step after the appropriate correction factors have been obtained for the detector signals. For this, only the values of the lambda modes and the local functions in the detector locations are required. In Fig. 3.3 is illustrated a brief flow chart of the modal-local method applied to a reactivity meter.

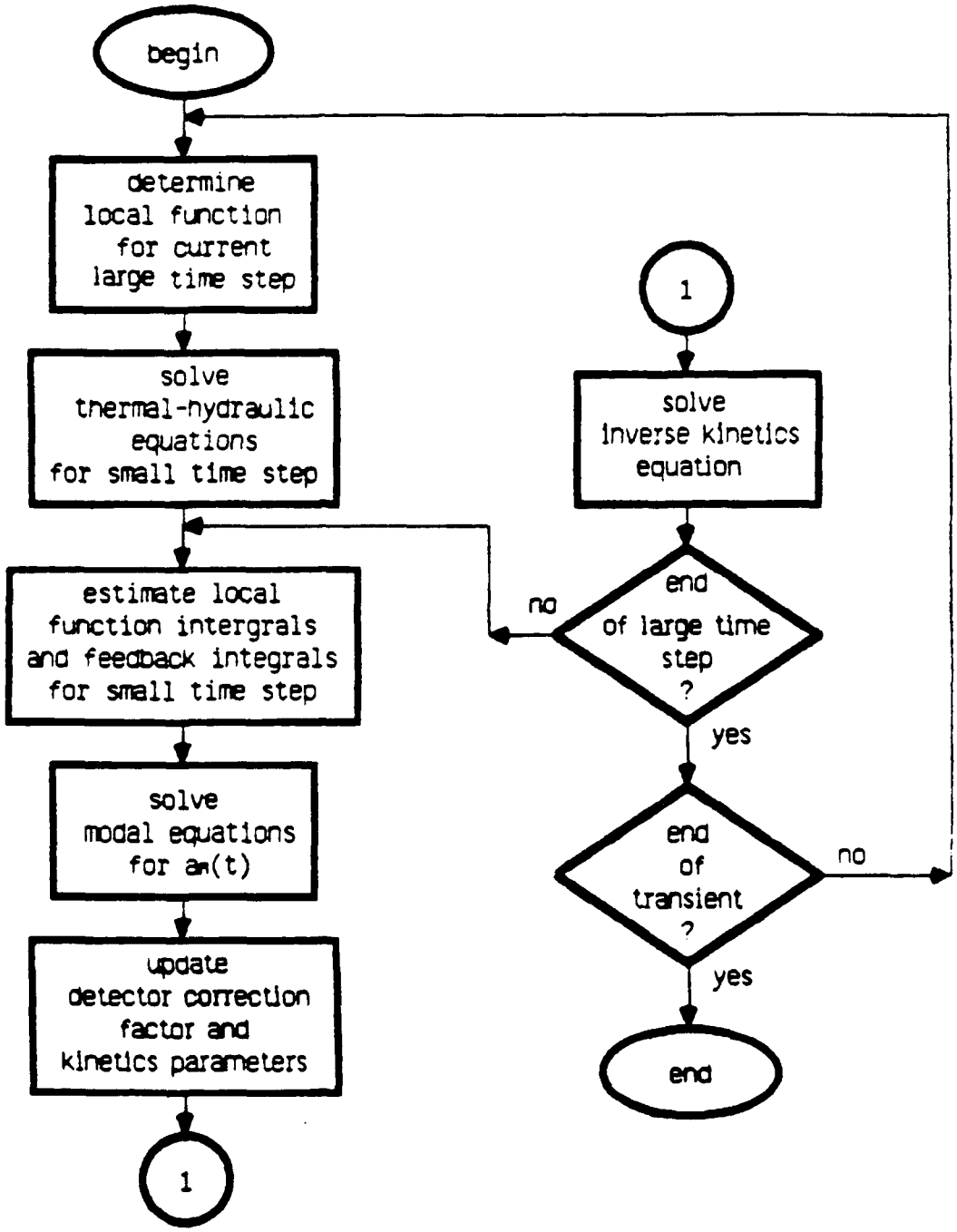

Figure 3.3 Flow chart for the modal-local method implemented as a reactivity meter.

CHAPTER IV

ACCURACY OF THE MODAL-LOCAL METHOD

In this chapter attention will be given to the overall accuracy of the coupled modal-local method implemented as a reactivity meter. Testing the performance of a new method is a difficult problem, but it has little value until its accuracy has been assessed. Comparison of results with other known methods or applicable experimental data are the obvious approaches to use. In this investigation the CITATION code[42], and the FX2-TH code[9] are taken as the references for static and time-dependent problems, respectively, against which the modal-local method presented in Chapter III is tested. The CITATION code is a multi-group, three-dimensional diffusion theory code, and the FX2-TH code solves the multi-group, two-dimensional time-dependent diffusion equation based on the quasi-static method. Both CITATION and FX2-TH codes are accurate in the sense of finite-difference diffusion theory calculations. The quasi-static method considered in the FX2-TH code is accurate if proper time steps are considered for the calculation of the shape function. Thus, these two codes can provide a means of verification of the modal-local method.

We start with a quantification of how well the modal-local treatment can predict strong perturbations in neutron flux such as those caused by a control rod motion in the core. We consider the full withdrawal of the top-reflector bank of control rods in the KAHTER facility[31], and obtain its unrodded configuration having the rodded configuration as a reference state. Direct comparison of the modal-local and the CITATION results is then made. For time-dependent problems, the rod-drop experiments performed at the KAHTER facility,[30-32] are simulated with the FX2-TH code. With the FX2-TH thermal flux at selected positions in the core taken as detector signals, the modal-local method is then used to generate the correction factors needed in an inverse analysis to obtain the reactivity. Comparisons are made between the FX2-TH results and the modal-local method. Finally, a thermal-hydraulic feedback problem is considered for assessing the feasibility of the modal-local method in the power reactor environment. A control rod movement is simulated with the FX2-TH code in a one-dimensional description of a power reactor. The modal-local method is used to simulate the same transient and its results are compared with those from the FX2-TH code. In this way the accuracy of the modal-local method is verified and quantified in static and time-dependent problems.

We begin in Sect. A with a brief description of the KAHTER facility. In Sect. B are presented the two- and three-dimensional lambda modes obtained for the KAHTER

facility which are needed in the modal-local formulation. The comparison calculations for static problems are presented in Sect. C. The overall test calculations for time-dependent problems begin in with the accuracy verification of the inverse kinetics algorithm in Sect. D. It is followed by a simulation in Sect. E of the rod-drop experiment and a control rod calibration in a power reactor in Sect. F.

A. Brief Description of the KAHTER Facility

The critical facility KAHTER[32] has been established in the Institut für Reacktorentwicklung at the Kernforschungsanlage Jülich as a mock-up for general testing of high-temperature gas-cooled pebble-bed reactors with a nominal power of 49.1 Watts. The core has a diameter of 2.16 m, and a height of 3.0 m. As shown schematically in Fig. 4.1, the core is surrounded by a radial graphite reflector 0.4 m thick, and a 0.6 m thick graphite reflector at the bottom. The KAHTER-OTTO 5/5 configuration also has a 0.5 m thick graphite reflector at the top. The control elements, all made of B_4C, include 8 absorber rods symmetrically located in the radial reflector, 8 absorber rods symmetrically located in the top reflector, and one central absorber rod. For the purpose of flux measurements, there are several axial and radial channels through which detectors can scan almost the entire core.

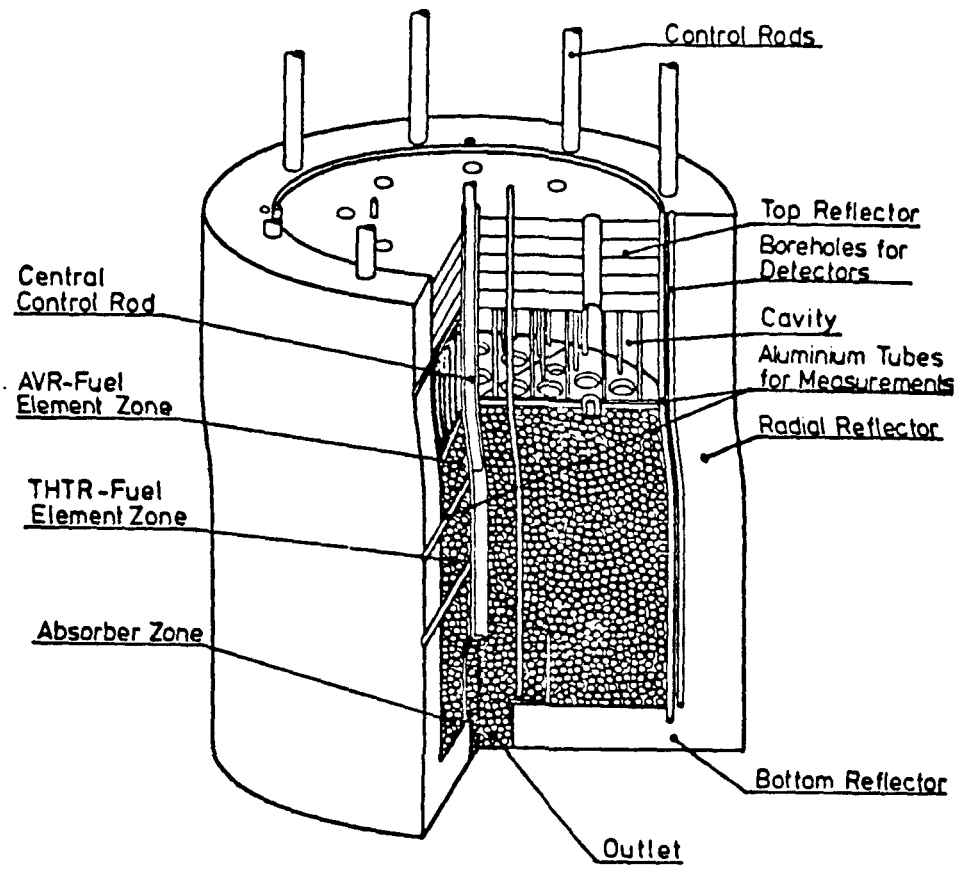

Figure 4.1 Overall layout of the KAHTER facility.

The fuel elements in the form of spherical pebbles have a diameter of 0.06 m and are randomly distributed in the core. The inner zone of these pebbles contains a mixture of particles of uranium and thorium coated with graphite, and the outer shell consists of pure graphite. In the OTTO (Once Through Then Out) fuel cycle the fuel elements are continuously dropped into the core from the top and discharged at the bottom so that they move slowly down with radially varying speeds.

B. Lambda Modes for the KAHTER Facility

The method outlined in the Appendix was implemented to obtain lambda modes in three diffusion theory codes during the course of this research: the one-dimensional two-group ONED code[55], the two-dimensional multigroup 2DBUM code[54], and the CITATION code. During the developmental phase of the work the ONED code was extensively used for its simplicity and low cost. The 2DBUM code was used to generate lambda modes in order to verify the accuracy of the modal-local method in a direct comparison with the FX2-TH code. For the actual analysis of the KAHTER rod worth data, presented in the next chapter, three-dimensional lambda modes were calculated with the CITATION code. A three-dimensional description of the core was necessary to provide the correction factors for the detector signals in the inverse kinetics analysis.

In Sect. 1 we present the lambda modes for the KAHTER facility obtained with a modified version of the CITATION code in a six energy group, (r-θ-z) three-dimensional representation. In Sect. 2, the two-dimensional (r-z) lambda modes for the KAHTER facility obtained with the 2DBUM code are presented. The cross sections used in the 2DBUM calculations have been condensed from 6 energy groups to 2 energy groups and homogenized in the azimuthal direction. The steps taken for obtaining the two-group set of cross sections are also given in Sect. 2.

1. Three-Dimensional Lambda Modes for the KAHTER Facility

We used a modified version of the CITATION code to obtain both the forward and adjoint lambda modes for the KAHTER-OTTO 5/5 configuration. Taking advantage of the azimuthal symmetry in the KAHTER configuration we used a three-dimensional model[32] (r-θ-z geometry) with 6 energy groups, 27 radial meshes, 6 azimuthal angular meshes, and 41 axial meshes. In Fig. 4.2 is illustrated the mesh and material layout used to model the KAHTER configuration. Zone 44 corresponds to the top-reflector control rods which can be inserted 0.97 m down to the core-void interface. Zones 41 and 43 correspond to the radial-reflector control rods and the central absorber rod, respectively. Zones 29 and 30 represent the cavity or void region between the top-reflector and the core. Zones 33, 34, 37 and 38 represent the top-reflector, and zones 3, 4, 7, 8, 11, 12, 15, 16, 19,

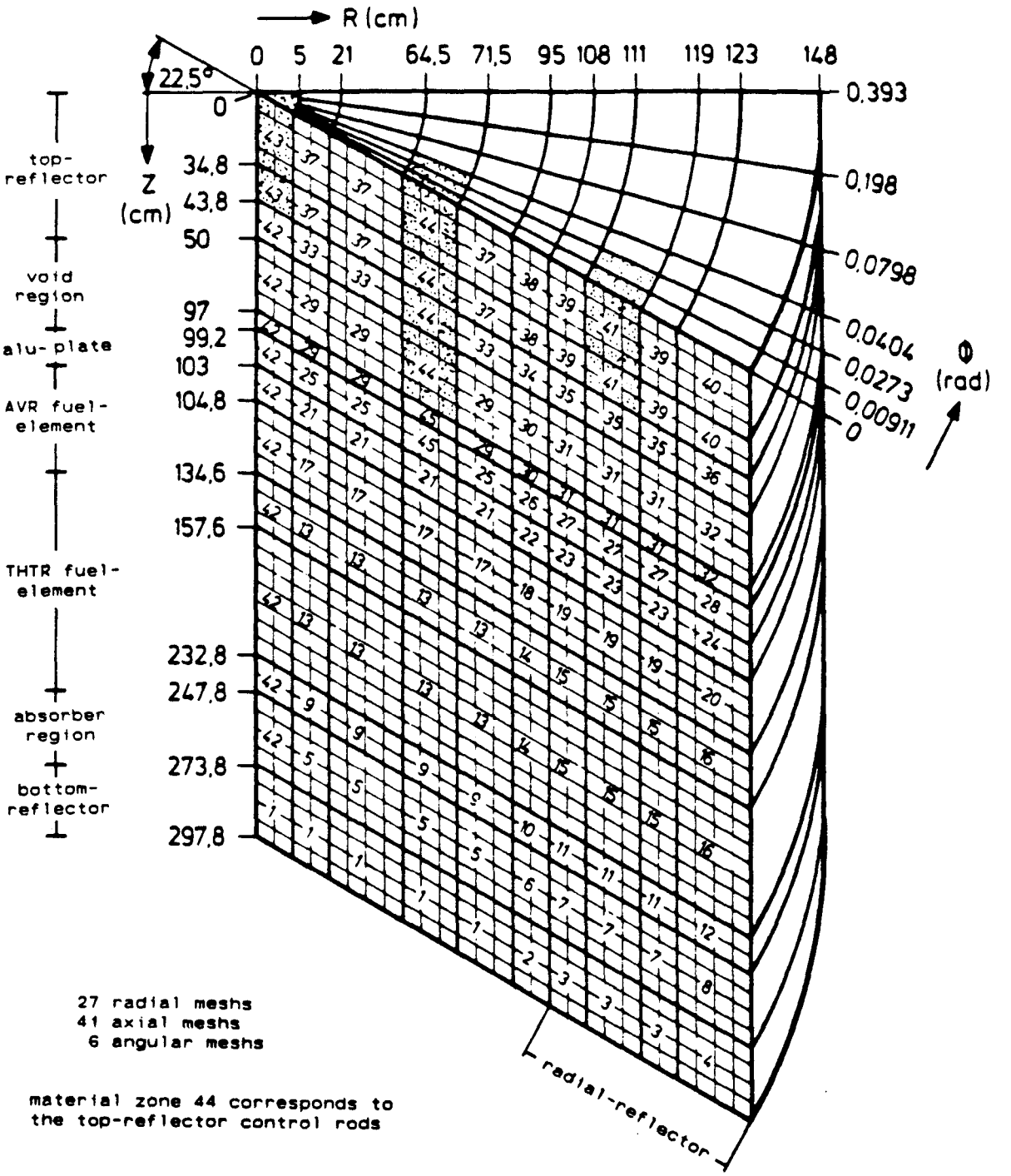

Figure 4.2 Mesh and material zone layout for the KAHTER facility.

20, 23, 24, 27, 28, 31, 32, 35, 36, 39 and 40 represent the radial-reflector region. The core is composed of two types of fuel elements, the AVR fuel elements in zones 17, 18, 21 and 22, and the THTR fuel elements in zones 9, 10, 13 and 14. The absorber region at the bottom of the core corresponds to zones 5 and 6, while zones 1 and 2 correspond to the bottom-reflector region.

Calculation of the lambda modes has been limited to the fundamental and the first harmonic modes, due to oscillatory behaviors encountered in the source iterations for higher harmonics. The fundamental and first harmonic modes for the first (fast) and for the sixth (thermal) groups are presented in Figs. 4.3 through 4.6. The modal distributions shown here and all the flux distributions presented in the rest of this section are for a (r-z) plane at the first angular mesh. Fig. 4.3 shows the fast and thermal profiles for the fundamental forward mode, and Fig. 4.4 shows the fast and thermal profiles for the first forward harmonic. Similar profiles for the fundamental and first adjoint harmonics are presented in Fig. 4.5 and 4.6. Figs. 4.4 and 4.6 indicate that the first harmonic modes possess primarily the characteristics of an axial first harmonic shape, since they are positive in the top and negative at the bottom of the core.

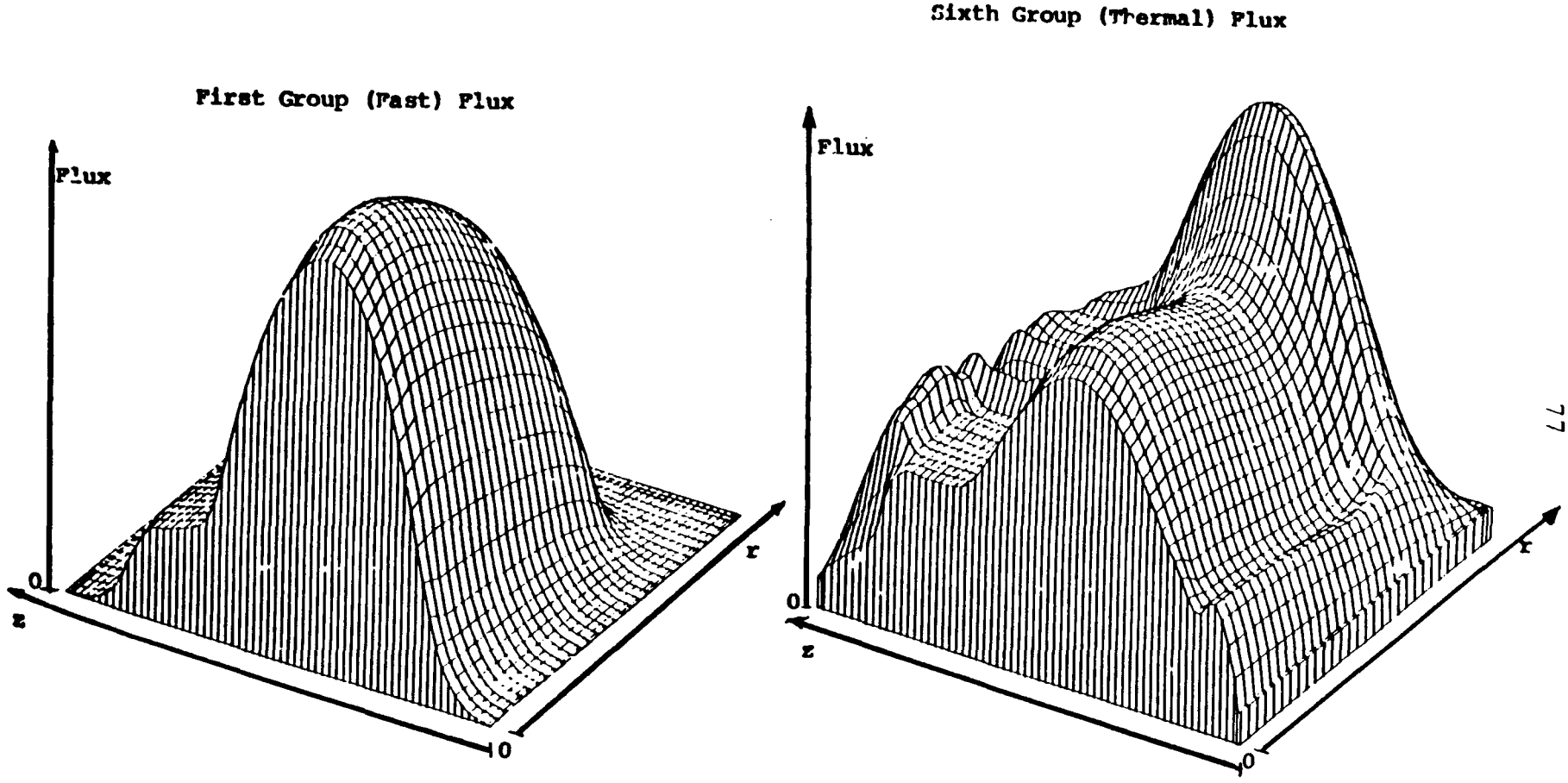

Figure 4.3 Fundamental forward mode for the KAHTER, rodded configuration, three-dimensional calculation.

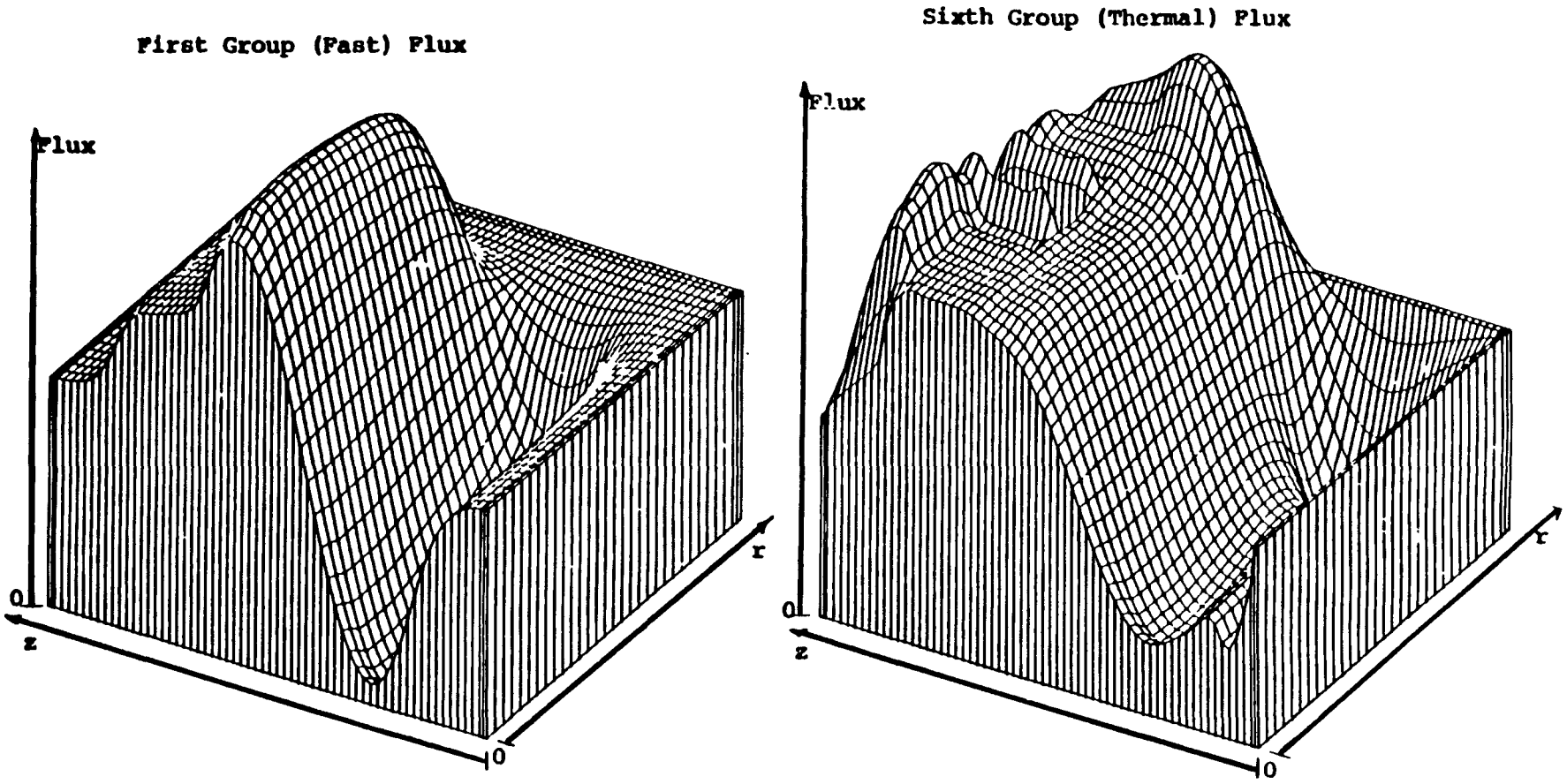

Figure 4.4 First harmonic forward mode for the KAHTER, rodded configuration, three dimensional calculation.

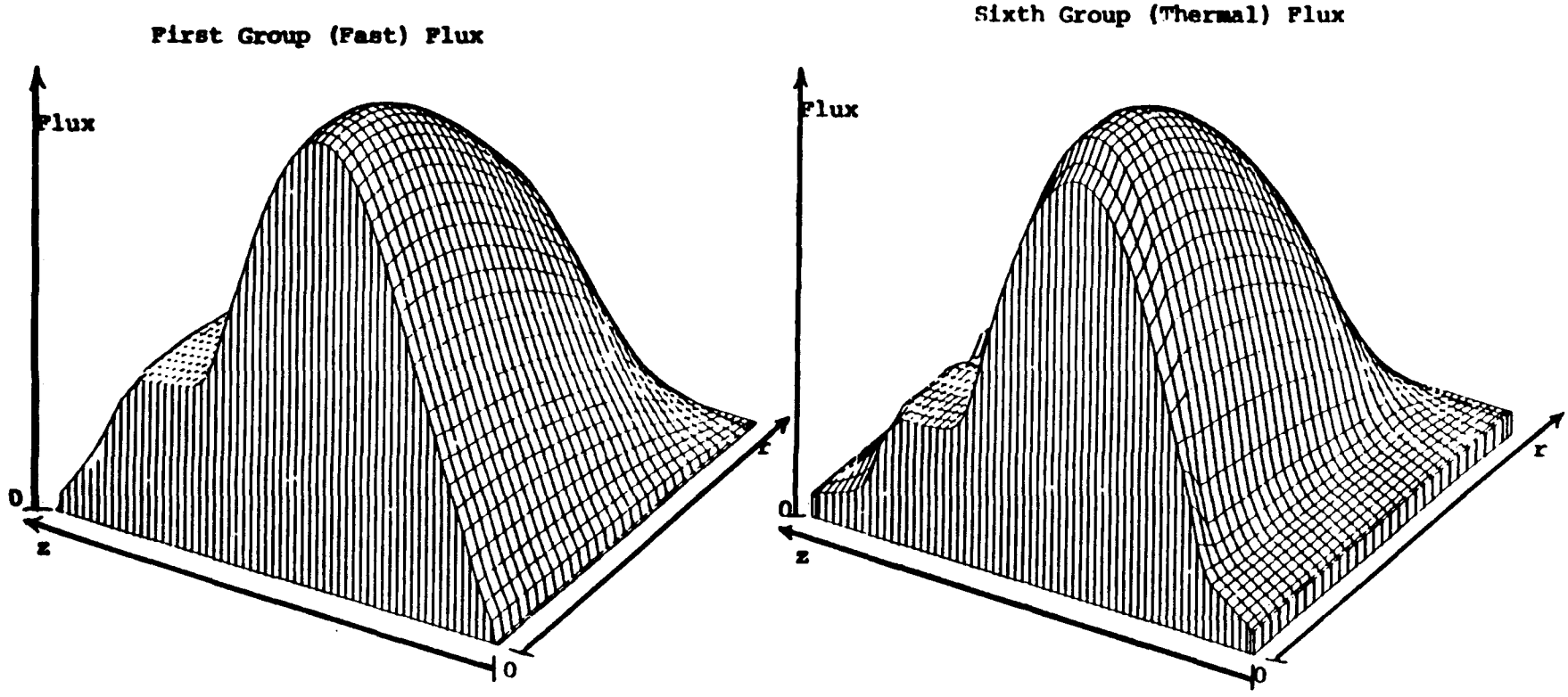

Figure 4.5 Fundamental adjoint mode for the KAHTER, rodded configuration, three-dimensional calculation.

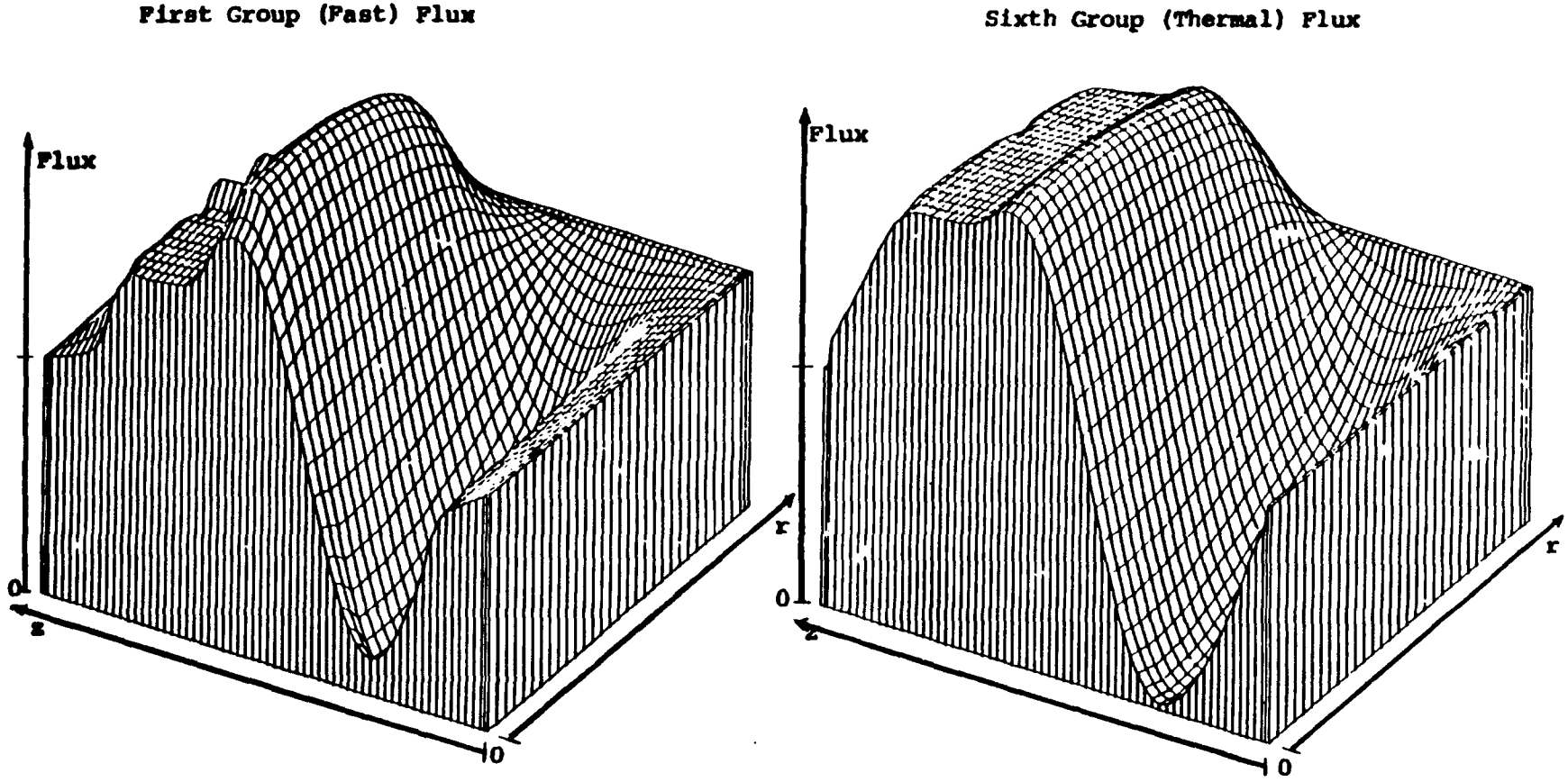

Figure 4.6 First harmonic adjoint mode for the KAHTER, rodded configuration, three-dimensional calculation.

2. Two-Dimensional Lambda Modes for The KAHTER Facility

For calculating the lambda modes for the KAHTER facility in a two-dimensional geometry we first homogenized the core in the azimuthal direction θ, in order to have an average r-z plane representative of the core. The six energy-group cross sections used in the three-dimensional CITATION calculation were condensed into two energy groups. The primary reason for going to a two-dimensional description of the KAHTER was to compare the modal-local formulation with another method known to be accurate. The FX2-TH code, which solves the time-dependent diffusion equation in the framework of the quasi-static method, was used with a two-dimensional KAHTER model for reasons of economy, although it does have a three-dimensional capability. The decrease in the number of groups also helped reduce costs in the space-time analysis with the FX2-TH code without losing important physical information.

The condensation of the group constants, including the diffusion coefficient, into two energy groups and the spatial homogenization were based on a neutron flux weighting, in order to preserve reaction rates in the core. It was found that weighting the diffusion coefficient $D(\underline{r},E,t)$ directly with the flux, rather than the transport cross section $\Sigma_{tr}(\underline{r},E,t)$, provided better agreement, both in flux distribution and in effective multiplication factor, with the three-dimensional six-group CITATION results.

The void region between the top reflector and the core can not be treated, in principle, with the diffusion theory because of the preferential streaming of neutrons in the axial direction escaping from the core. This problem, however, is avoided in the version of the CITATION code in use at the KFA, by allowing directional diffusion coefficients in the void region[32]. Based on the concept of effective diffusion coefficients accounting for voids and anisotropy of the neutron flux,[56] the diffusion coefficient in the void region is multiplied by: 0.09975, 0.09975 and 0.5045 in the radial, azimuthal and axial directions, respectively[32]. Since the 2DBUM code does not have the capability for directional diffusion coefficients, we consider only the decrease in the diffusion coefficient by multiplying it by an average factor of 0.2, without any differentiation with regard to the directions.

The two-dimensional calculations involved 27 meshes in the radial direction, and 41 meshes in the axial direction in a (r-z) geometry. The layout of the mesh and material zones corresponds to the frontal plane of Fig. 4.2. Fig. 4.7 shows the fast and thermal profiles of the three-dimensional CITATION flux distribution, condensed into two groups and averaged over the angular direction. The flux distributions obtained in the two-group, two-dimensional 2DBUM calculation are also shown in Fig. 4.7 and compare well with the CITATION results. It is important to note that the good description of the neutron flux in the void

and top-reflector regions is essential to account accurately for the reactivity effects of the top-reflector rods. For this reason we have attempted to reproduce, as well as possible, the three-dimensional CITATION results.

A modified version of the 2DBUM code was used to obtain the first two harmonic modes of the KAHTER OTTO 5/5 configuration in the two-dimensional model described above. The axial and radial profiles for the first three forward and adjoint modes are shown in Figs. 4.8 through 4.10. In Figs. 4.9 the axial profiles show the characteristic of an axial first harmonic shape. The radial distribution of the first harmonics shown in Figs. 4.9 are negative because they correspond to an axial plane near the bottom of the core. Their profiles are, however, similar to the fundamental mode. This establishes that the first higher harmonic modes for the KAHTER facility possess primarily the characteristics of an axial first harmonic shape. In the second harmonic modes shown in Figs. 4.10 the axial profiles resemble the fundamental axial profiles, and the radial profiles, which are positive in the center and negative in the outer parts of the core, clearly possess the shape of a first radial harmonic. Figs 4.7 through 4.9 represent axial and radial cuts in the two-dimensional pictures shown in Figs. 4.3 through 4.6. The axial profiles correspond to a line along the z-axis in the radial position indicated, and the radial profiles correspond to a line along the radius in the axial position indicated. The normalization in

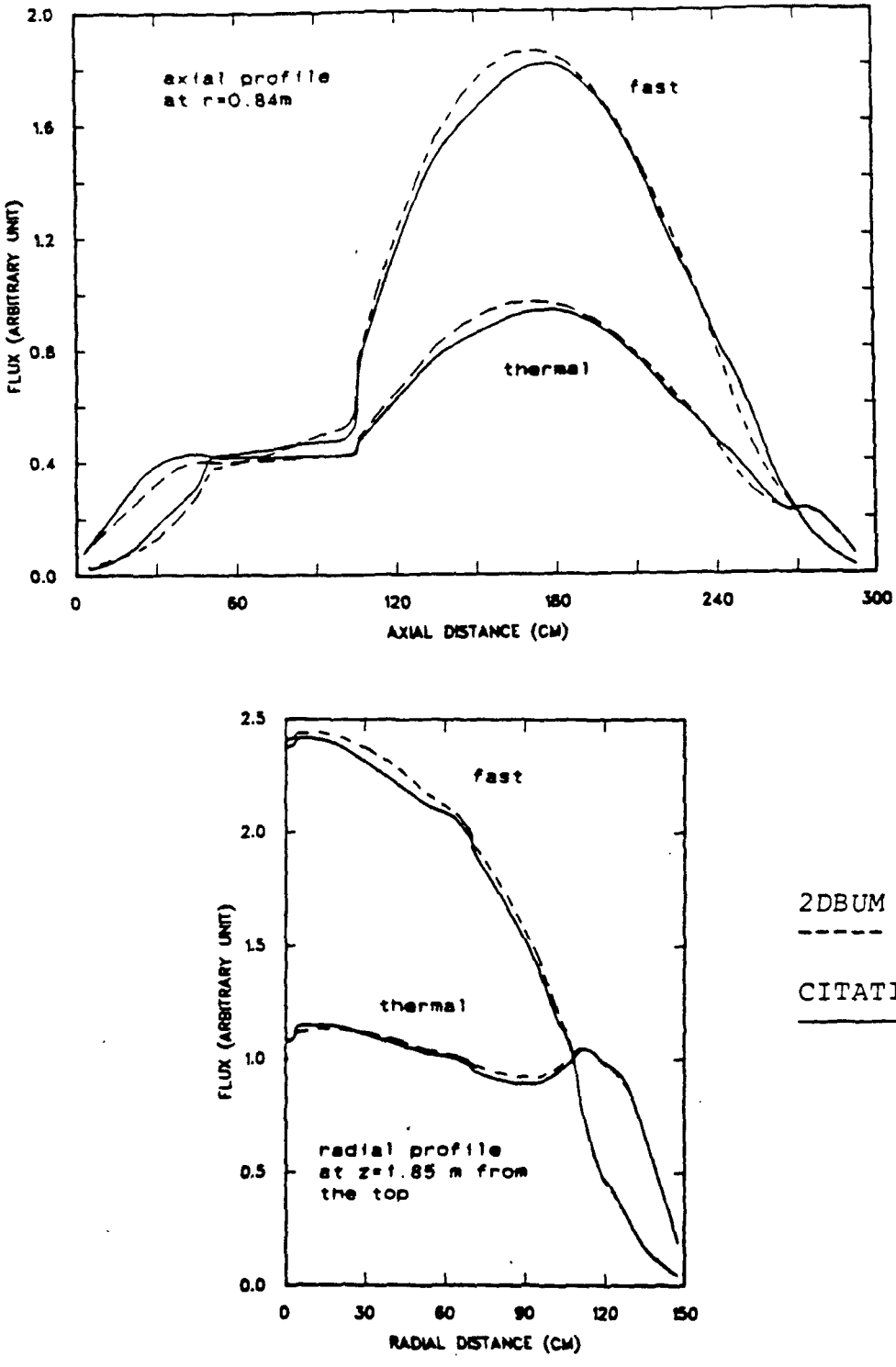

Figure 4.7 Comparison between the condensed CITATION flux distribution and the 2DBUM two-group calculation.

Figs. 4.8 through 4.10 follows the modal orthonormality property.

The eigenvalues corresponding to the lambda modes in three-, two-, and one-dimensional models of the KAHTER facility are shown in Table 4.1. For all three cases the first harmonics are characteristic of a first axial harmonic shape, and consequently have similar eigenvalues. The second higher harmonics in one-dimensional geometry corresponds obviously to a second axial harmonic, but, in two-dimensional geometry, it corresponds to a first radial harmonic, thus producing different eigenvalues. This illustrates the multi-dimensional effects on the harmonic modes and on the eigenvalues.

3. Usefulness of the Lambda Modes for Predicting Perturbed Fluxes

The first higher mode, being asymmetric in the axial direction, can properly represent perturbations in the neutron flux which are also axially asymmetric, such as xenon oscillations and control rod insertion or withdrawal from the core. In the case of a control rod insertion into the core, a primary effect is a shift in the neutron flux to the bottom of the core. This shift can be easily represented by the first axial harmonic since it would decrease the flux at the top and increase it at the bottom.

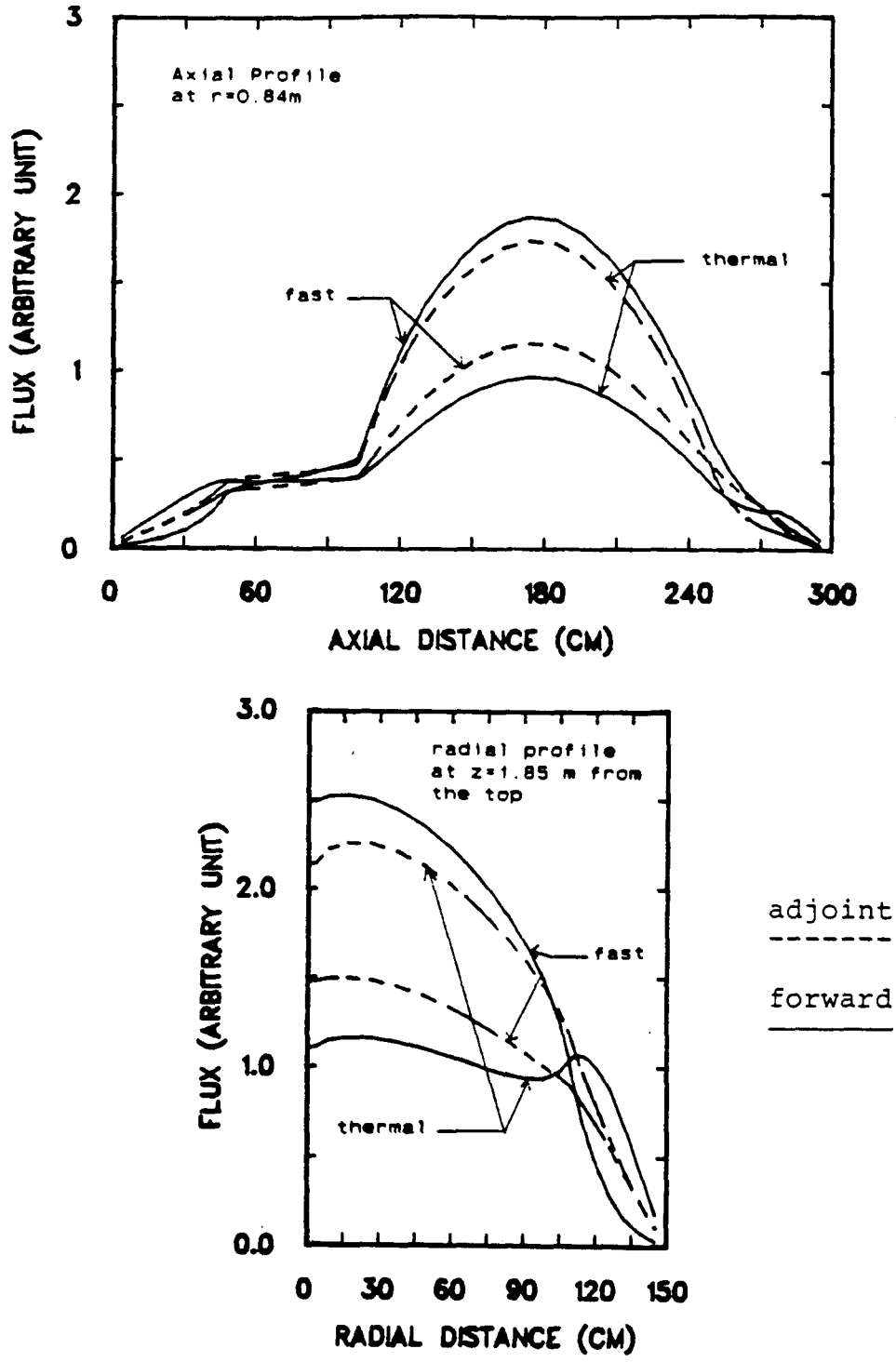

Figure 4.8 Fundamental forward and adjoint modes for the KAHTER facility.

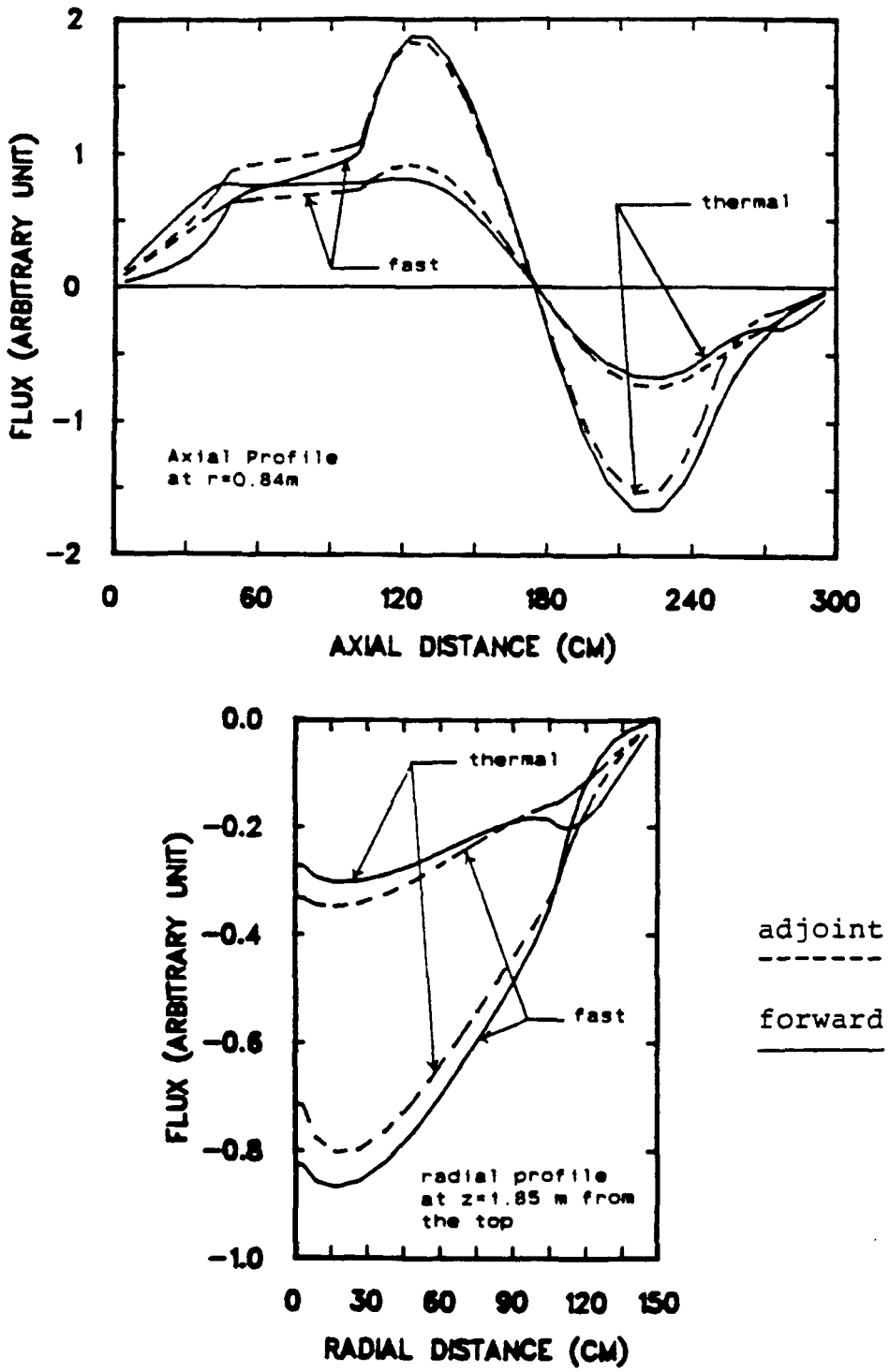

Figure 4.9 First harmonic forward and adjoint modes for the KAHTER facility.

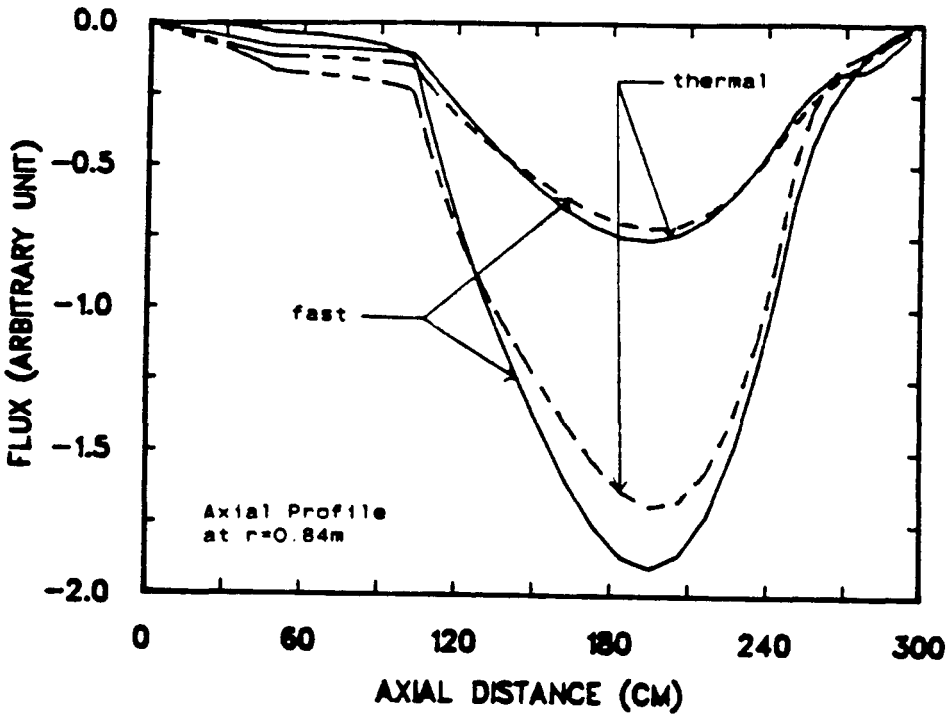

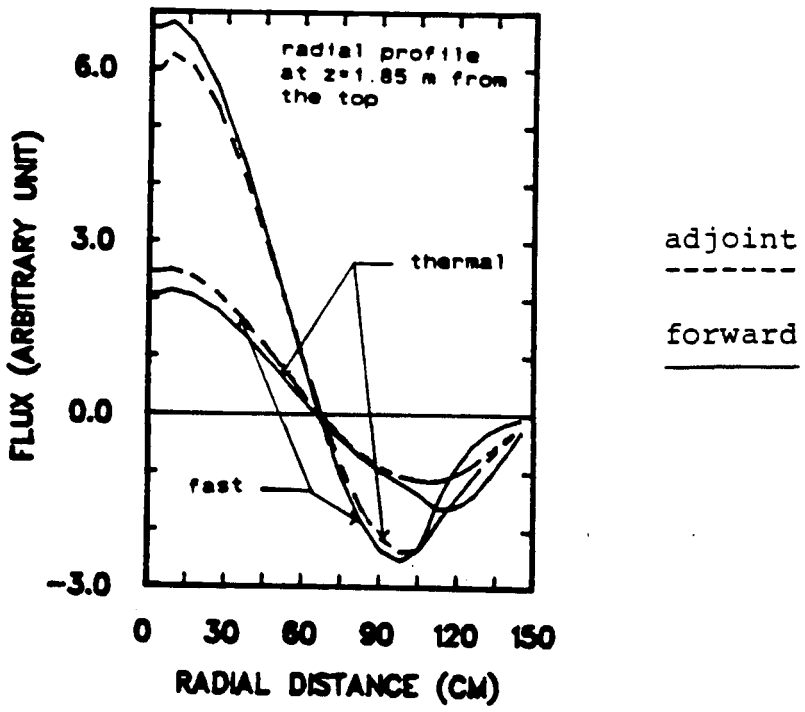

Figure 4.10 Second harmonic forward and adjoint modes for the KAHTER facility.

Table 4.1

Eigenvalues for the KAHTER lambda modes, rodded configuration.

	forward			adjoint		
mode	3-dim r-z-θ	2-dim r-z	1-dim z	3-dim r-z-θ	2-dim r-z	1-dim z
0	0.96957	0.97473	0.97074	0.96912	0.97476	0.97075
1	0.49145	0.55317	0.53952	0.50409	0.55716	0.53943
2	-	0.41536	0.26523	-	0.41358	0.26520

The second harmonic in a (r-z) geometry would efficiently represent perturbations which are radially asymmetric. In the KAHTER facility the motion of the central absorber rod, as well as the motion of the radial-reflector rods cause such asymmetric perturbations. The top-reflector control rods, however, does not excite the second higher harmonic mode very much because its motion will occur near the nodal line of this mode. Thus, we expect that the second harmonic mode will not contribute much for determining perturbed flux distributions caused by the motion of the top-reflector rods.

The next few higher harmonic modes should be excited to a smaller extent by the motion of the top reflector rods because the eigenvalues for these higher modes are very small. The separation between the eigenvalue of a mode from the fundamental mode eigenvalue is a measure of the susceptibility of this mode to excitation. The greater the separation, the more difficult is the excitation. For the case of the KAHTER facility the higher harmonic modes will have eigenvalues below 0.35, which requires stronger perturbations for their excitation. Of course, the fine details in the perturbed flux caused by a rod motion can only be described by the contribution of these several higher harmonic modes, however small their contribution might be.

In the modal-local formulation the fine details of the perturbed flux distribution are obtained through the local function $f(\underline{r},E,t)$, without the need for higher harmonics. In the following section are presented static calculations in one- and three-dimensional geometries that substantiate the validity of the modal-local method for predicting flux perturbations.

C. Accuracy of the Modal-Local Method in Static Calculations

The main purpose of assessing the accuracy of the modal-local method in static calculations is to study the effect of the first-order approximation in the calculation of the local function $f(\underline{r},E)$ and of the number of modes in the estimation of the global function $h(\underline{r},E)$. For this purpose we considered the problem of obtaining the unrodded flux distribution for the KAHTER facility, based on a rodded reference configuration. We used the three-dimensional lambda modes for a rodded KAHTER configuration. The local function $f(\underline{r},E)$, satisfying Eq. (20a) of chapter III, was calculated based on the fixed-source algorithm of the **CITATION code.**

In order to obtain the local function the external source representing the applied perturbation must be known. In our calculations we assumed that the control rod insertion can be represented solely by a perturbation in the

absorption cross sections, thus neglecting totally the perturbations in the scattering cross sections and the diffusion coefficients. The scattering cross section for control rods are very small and their effect can be readily neglected. The diffusion coefficient involves leakage of neutrons, an important effect near the boundaries of any reactor. The control rods are, however, mostly thermal absorbers, and the fast flux does not change much. Thus we assume that the change in the leakage pattern in the region is of small importance.

The local function $f(\underline{r},E)$ representing the withdrawal of the top-reflector rods are shown in Fig. 4.11 for the first (fast) and sixth (thermal) groups. The local function profiles indicate that the influence of the rod withdrawal is limited essentially to the top half of the system. The local function also indicates a much more localized nature of the perturbations in the fast flux than in the thermal flux.

It is clear from Fig. 4.11 that the local function represents the fine details of a perturbed flux that we would otherwise need many higher modes to describe. The incorporation of the local function allows one to use a minimum number of lambda modes for achieving good accuracy in predicting flux perturbations.

For this static calculation, without thermal-hydraulic feedback, Eqs. (8) from Chapter III simplify to:

First Group (Fast) Flux

Sixth Group (Thermal) Flux

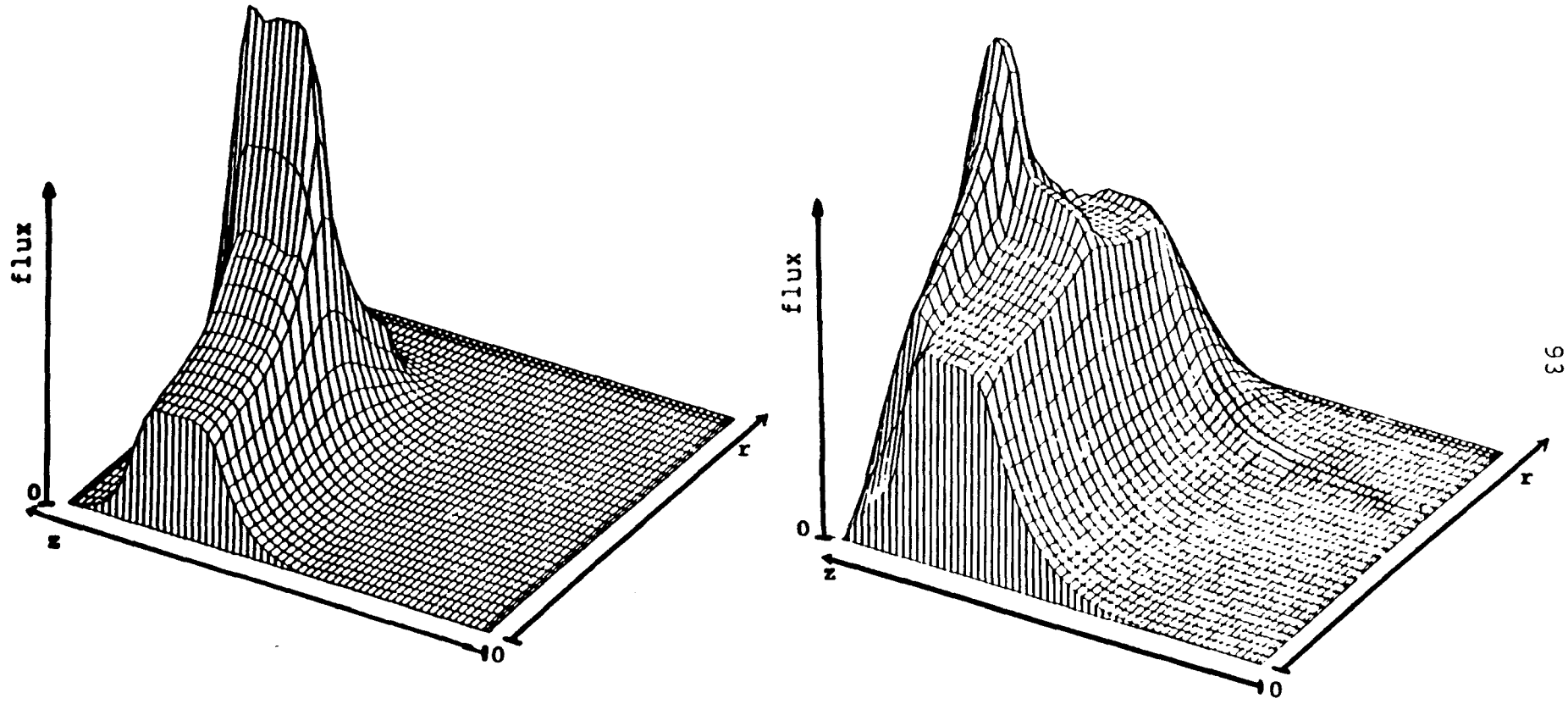

Figure 4.11 Local function for the withdrawal of the top-reflector rods of the KATHER, three-dimensional geometry.

$$a_m = - \frac{\Lambda_m}{\rho_m} [f_{pm} + \sum_{i=1}^{6} f_{dim}], \quad m=1,\ldots,N.$$

The fast and thermal flux distributions obtained with just two modes, the fundamental and the first harmonic modes, and the local function are compared in Figs. 4.12 and 4.13 with the CITATION results. The perturbations in the fast and thermal flux distributions due to the rod withdrawal are plotted in Fig. 4.14 while the fractional error in the thermal flux distribution calculated with the modal-local method, relative to the CITATION results, is shown in Fig. 4.15. Even with the local function included the error is very large in the top reflector especially in the vicinity of the control rods, although throughout the core the error is much smaller, i.e., on the order of 4 to 5% for the fast flux and of 2 to 3% for the thermal flux.

To provide some perspective on the importance of the local function in the modal-local method, we show in Fig. 4.16 the fractional error in the thermal flux distribution calculated through the standard first-order perturbation theory, Eqs. (17) and (18) of Chapter III, again relative to the CITATION result. The perturbation theory cannot predict, with only one mode, the unrodded configuration with an error smaller than 10% away from the rods; the errors are equally much larger in the top-

Modal-Local Calculation

First (Fast) Group

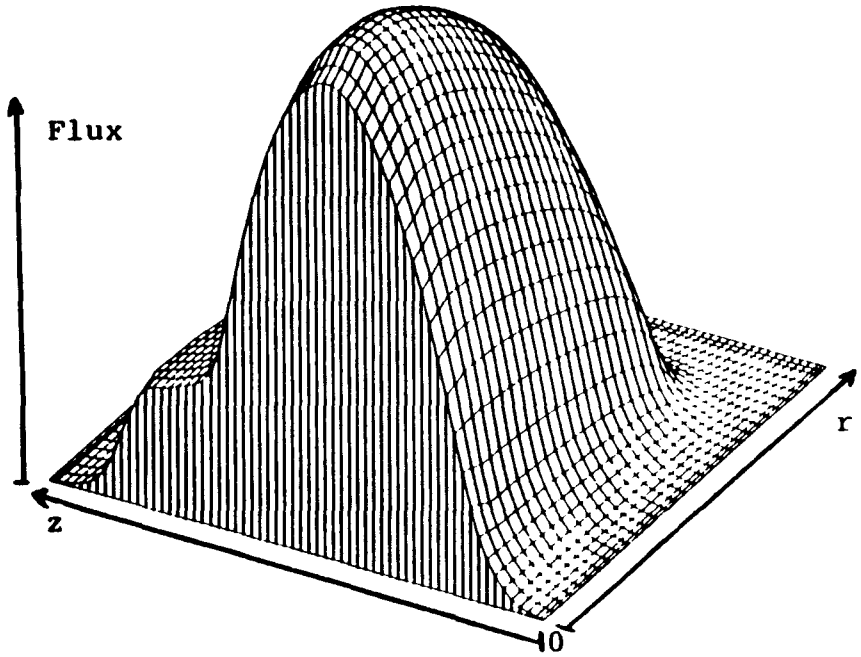

Exact CITATION Calculation

First (Fast) Group

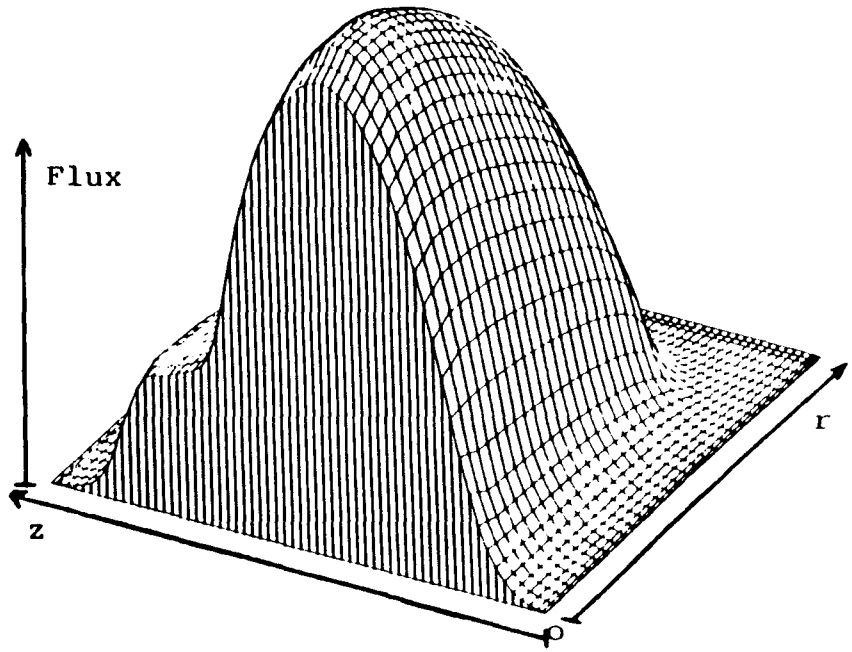

Figure 4.12 Unrodded fast flux distribution, modal-local method vs. exact calculation, three-dimensional geometry.

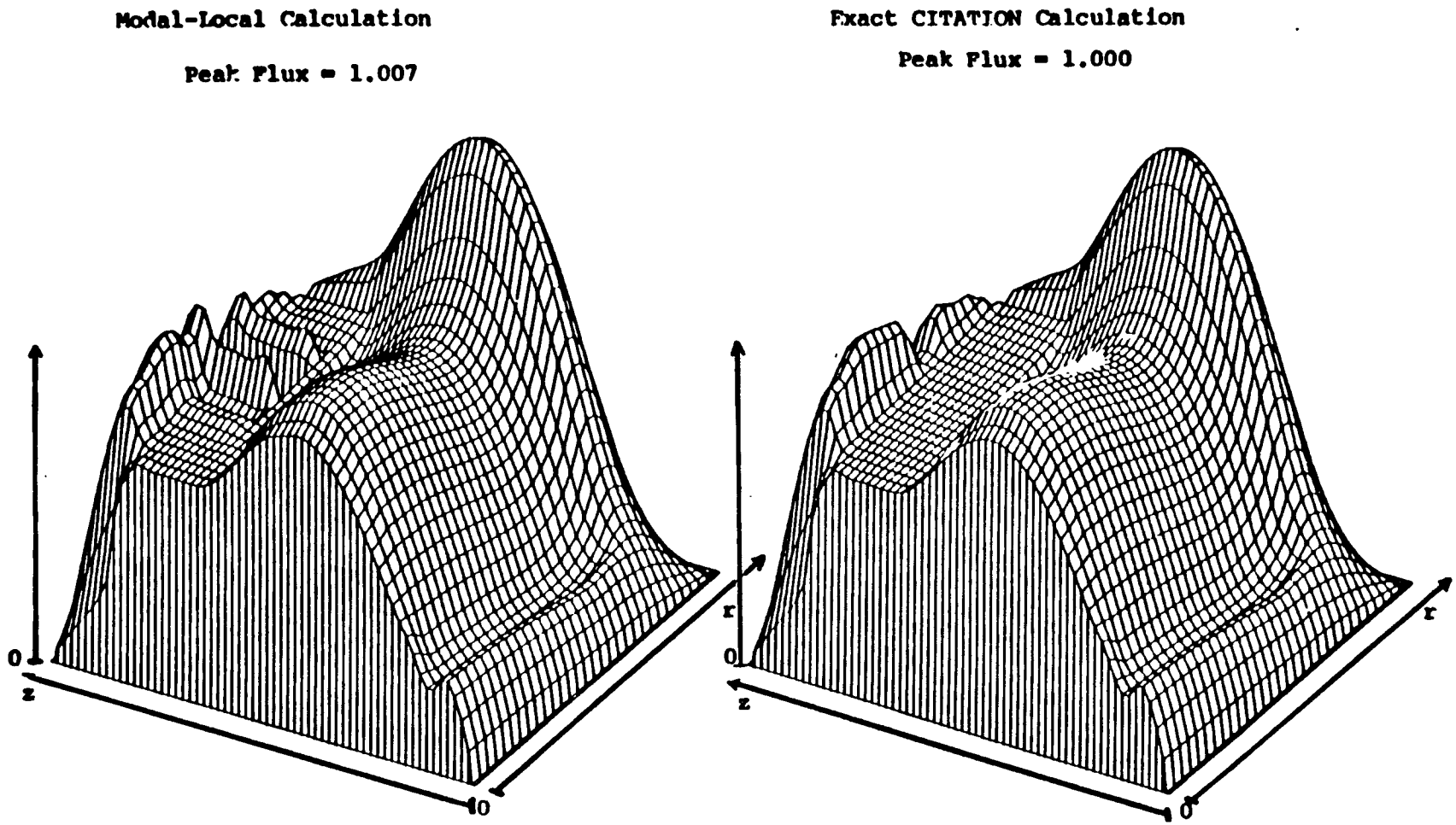

Figure 4.13 Unrodded thermal flux distribution, modal-local method vs. exact calculation, three-dimensional geometry.

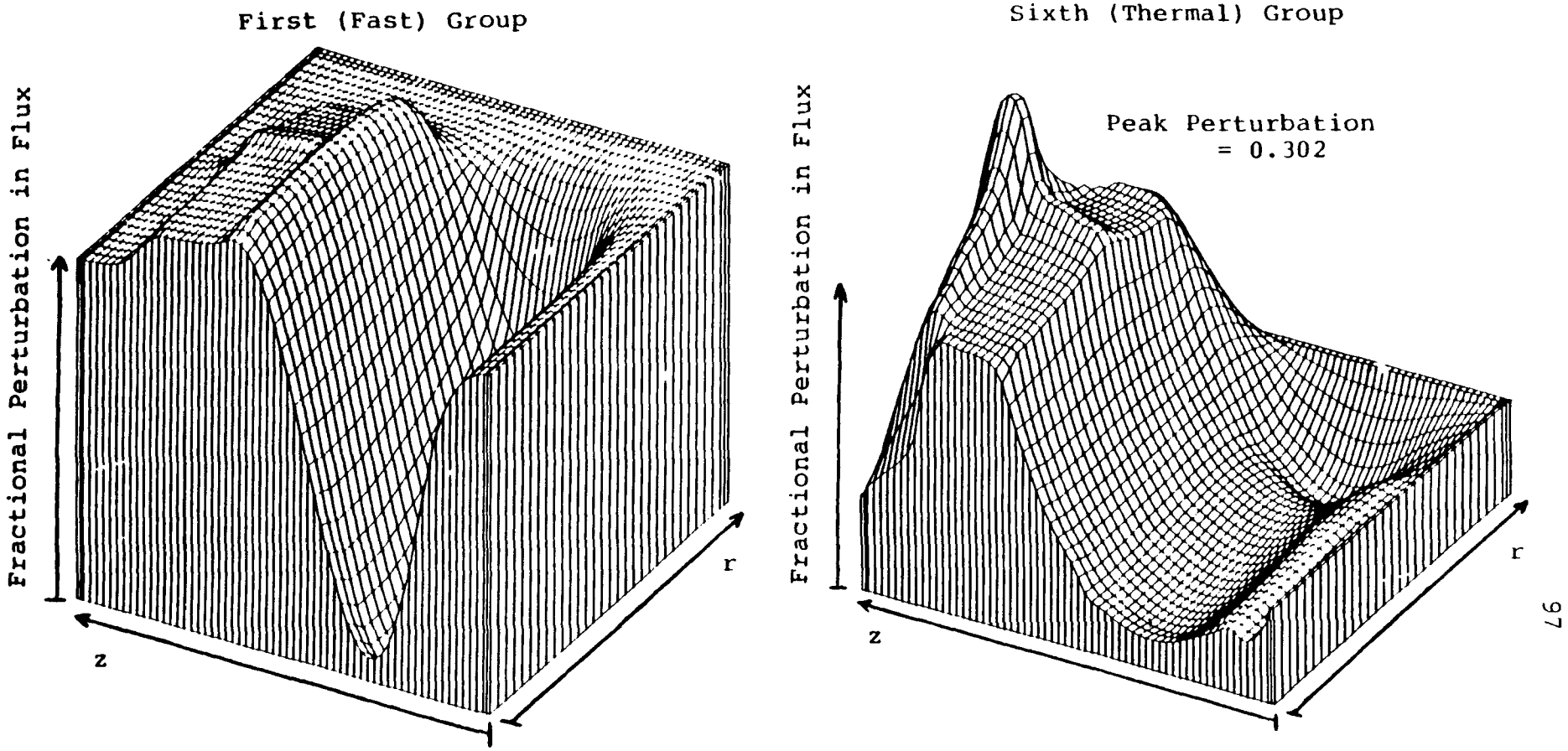

Figure 4.14 Perturbation in flux due to rod withdrawal, three-dimensional geometry.

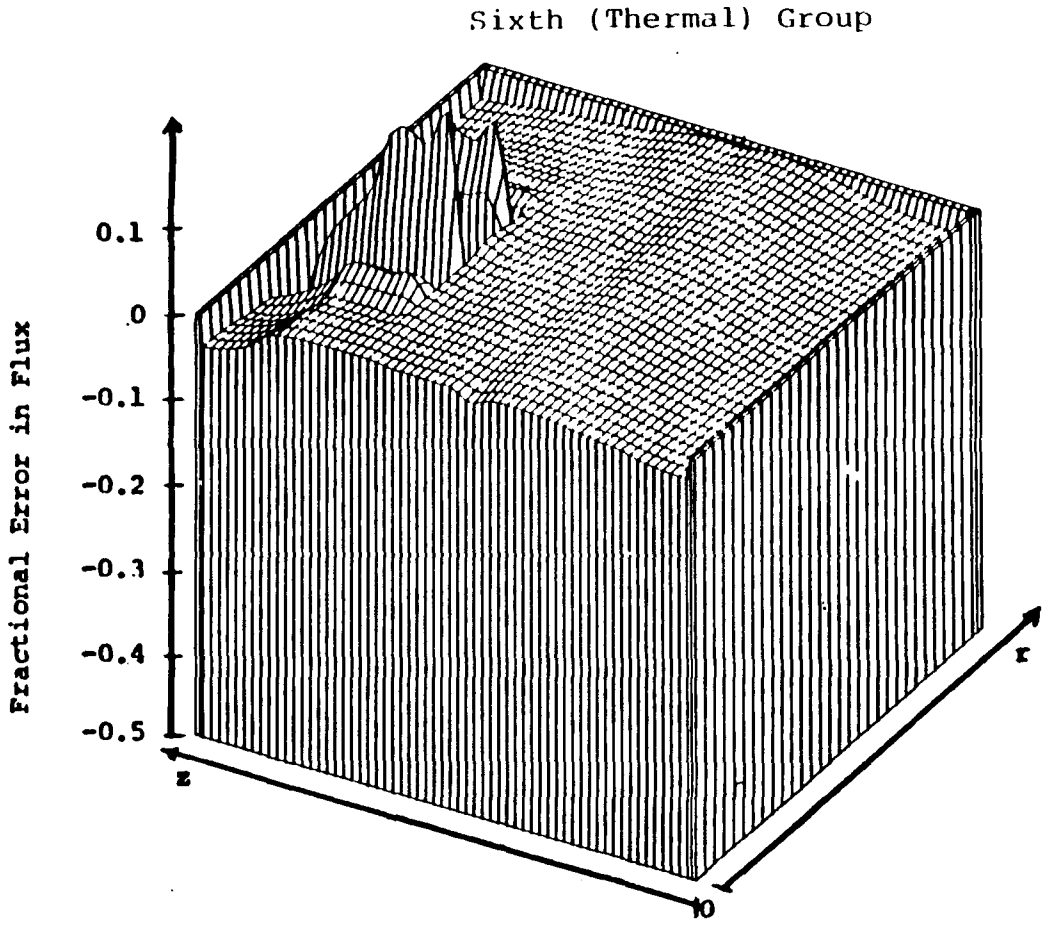

Figure 4.15 Fractional error in flux, modal-local method vs. exact calculation.

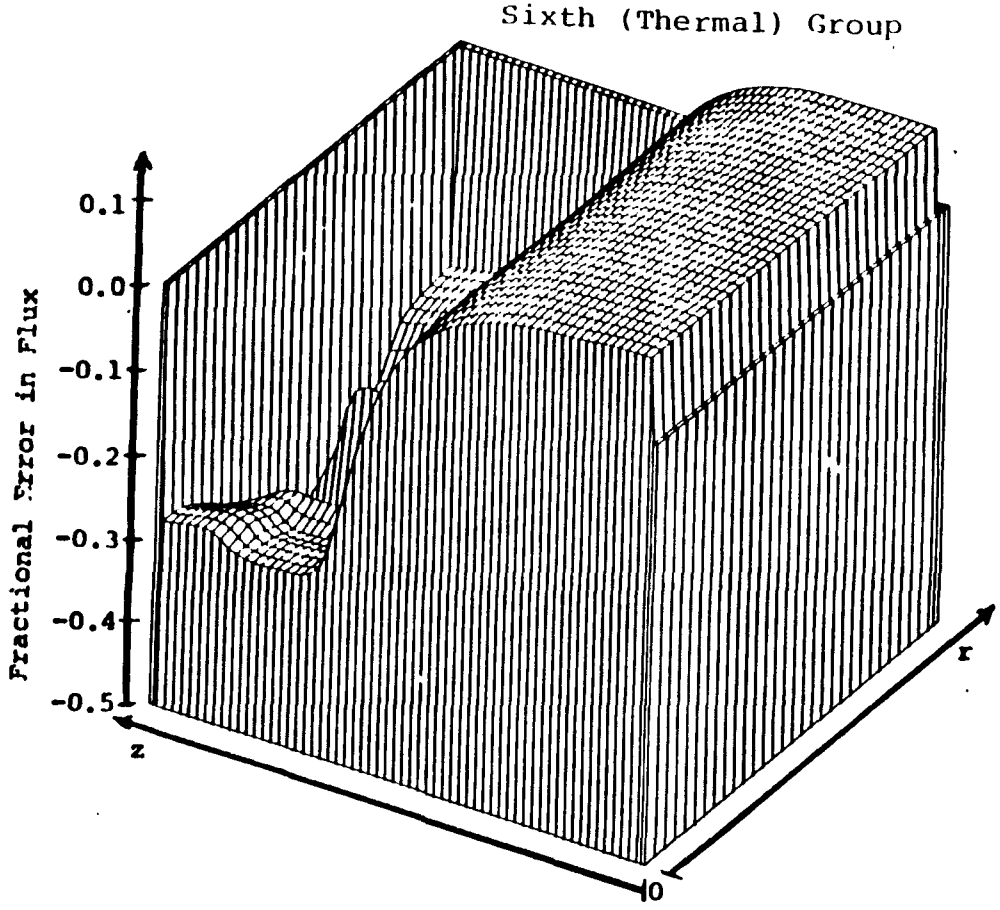

Figure 4.16 Fractional error in flux, standard perturbation theory vs. exact calculation.

reflector region than those shown in Fig. 4.15. The local function $f(\underline{r},E)$ helps to represent the detailed changes in the perturbed flux in the vicinity of the rod movement and yields more accurate expansion coefficients a_m for the lambda modes of the unrodded, perturbed configuration.

The larger errors seen closer to the top-reflector rods are due mostly to the first order approximation in the calculation of the local function. The exact local function should be calculated with the perturbed flux, which is larger in the top-reflector for the perturbed unrodded configuration. The use of the reference flux to calculate the local function (first order approximation) causes the modal-local method to underpredict the perturbed flux around the perturbed area. However, the inclusion of the local function reduces the error substantially when compared with the standard perturbation theory. As shown in Chapter III, the local function in the modal-local method is equivalent to the use of many higher modes.

Improvement in the modal-local method will result if more modes are taken into consideration for estimating $h(\underline{r},E)$. In Fig. 4.17 are shown thermal flux profiles of an one-dimensional axial representation of the KAHTER facility for the reference rodded state, perturbed unrodded state, and the modal-local method predictions with one, two, and five higher modes. One can see that with five higher modes the modal-local result almost coincides with the exact

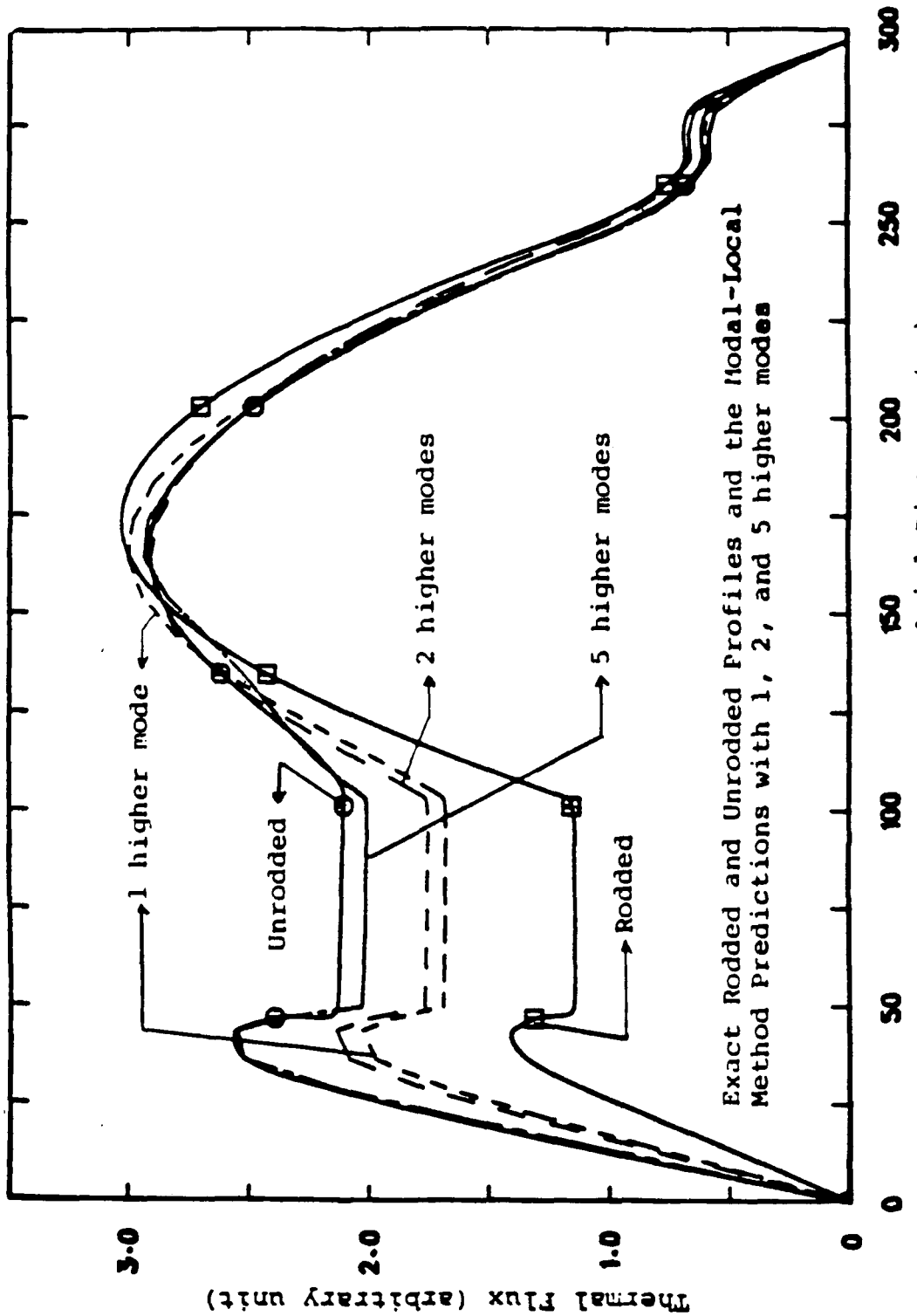

Figure 4.17 One-Dimensional Flux Profiles for the KAHTER Facility.

profile, and that, even with only two higher modes, errors are confined primarily to the vicinity of the control rod. Thus, increasing the number of modes improves the modal-local method prediction of perturbed flux.

In the framework of the expansion techniques, these results demonstrate the improvement provided by the modal-local treatment as compared with the standard modal expansion methods. They also suggest that for the analysis of the KAHTER rod worth data, with detectors located away from the rods, two axial higher modes coupled with the local function may be enough to accurately predict the shape function as a function of time.

D. Verification of the Inverse Kinetics Routine

The algorithm described in Sect. E of Chapter III for solution of the inverse kinetics equation has been tested against direct point kinetics results. The procedure taken was first to generate, with a reliable point kinetics routine[57], the amplitude function n(t) due to some arbitrary reactivity input. Then, this amplitude function n(t) was fed into the inverse kinetics routine, and the reactivity trace obtained was compared with the input reactivity. Tests were made for different types of transients including supercritical and subcritical final states, all giving good agreement between the direct and inverse results.

We present in Table 4.2 the results from a ramp reactivity imput of -1 $/s during 4 seconds, with the reactivity subsequently remaining at -4 $. This transient resembles the rod-drop experiments to be analyzed in the next section and in Chapter V.

The error in reactivity is seen to be very small for calculations with time steps between 1 and 10 ms. The average error in reactivity between the inverse calculations and the input values is less than 0.02 %. Smaller time steps were also tested but no noticeable difference could be be seen. Table 4.2 demonstrates the adequacy of the inverse kinetics algorithm described in Sect. E.2 of Chapter III. Other interesting points observed with respect to this algorithm are its stability and its accuracy almost independent of the time step size. This is an important characteristic since, when one is dealing with experimental data, it is often necessary to accumulate counts over large time intervals in order to improve the statistics. This procedure could affect the accuracy of the results if the algorithm were unstable or inaccurate for large time steps. For the current algorithm it has been found that the interpolation scheme for the amplitude function n(t) works well even for time steps on the order of a tenth of a second.

After having established the degree of confidence in the inverse kinetics algorithm and the performance of the

Table 4.2

Comparison between inverse and direct kinetics with two different time steps. Reactivity in dollars.

time (s)	input* reactivity	inverse† kinetics $\Delta t=0.01$	time (s)	input* reactivity	inverse† kinetics $\Delta t=0.001$
1.005	1.005	1.00473	1.0005	1.0005	1.00042
2.005	2.005	2.00457	2.0005	2.0005	2.00035
3.005	3.005	3.00444	3.0005	3.0005	3.00031
4.005	4.0	3.99938	4.0005	4.0	4.00004
5.005	4.0	3.99934	5.0005	4.0	3.99981

* A point kinetics routine generated the amplitude function with time steps of 0.001 s. This amplitude function was then inputted in the inverse kinetics routine.

† Δt is the time step used in the inverse kinetics calculation.

modal-local method for static problems, we move in the next section to a full space-time kinetics problem.

E. Accuracy of the Modal-Local Method for Space-Time Analysis

For verifying the accuracy of the modal-local method in determining reactivity as a function of time we simulated the rod-drop experiments performed at the KAHTER facility involving the top-reflector rods.[30-32] For the purpose of comparisons the results from the FX2-TH code are taken as our reference. The detector countrates are simulated by the FX2-TH thermal neutron flux at selected locations in the KAHTER facility. From these countrates the modal-local method is required to reproduce the reactivity insertion caused by the drop of the top-reflector rods into the core.

In order to eliminate the spatial dependence of the inverse kinetics, the time-dependent detector correction factors are the most important parameters to be obtained by the modal-local formulation. Other parameters such as $\bar{\beta}(t)$ and $\Lambda(t)$ are also important in the inverse kinetics formulation and will be considered, too.

1. Rod-Drop Simulation with the FX2-TH Code

The two-group, two-dimensional model for the KAHTER facility described in Section B was considered for this rod-drop simulation. The core was discretized in 27 radial

meshes and 41 axial meshes in a (r-z) geometry. In the initial condition the reactor was set critical with the top-reflector rods completely withdrawn. The cross sections representing the empty rod drivers were replaced by the top-reflector rod cross sections in zone 44 in Fig. 4.2. In the void region, the rod cross sections were replaced by those of material 29, for there are no rod guides in the void region. The transient was initiated by inserting the rods into the core at a ramp rate of 0.25 m/s, which is the actual speed of the top-reflector rods in the KAHTER facility. The transient lasted 6.8 s with the rods moving over the period from t = 0 s to t = 4 s. In order to insure that the spatial effects were accounted for, during the insertion period, the FX2-TH code was forced to make a full shape function calculation every 0.6 s. After the top-reflector rods ceased moving this requirement was relaxed to every 1.0 s; it was expected that the shape function would not change much following the rod motion.

The simulation ended at t=6.8 s because little changes in the shape function could be observed. This means that the neutron flux has approached around this time its asymptotic distribution in which the core neutron population would evolve equally as a whole. However, the inverse period of 0.0916 s^{-1} produced by the FX2-TH code at the end of the transient indicates that the reactor was still far from reaching the asymptotic state. The stable inverse period must be smaller than the decay constant , 0.0124 s^{-1},

of the group of the longest-lived delayed neutron precursors. Therefore, part of the delayed neutron precursors $c_i(\underline{r},t)$ were still decaying but their impact in the shape function was very minor.

To confirm these observations, we compare the time-dependent shape function at the end of the transient with the asymptotic shape function, and with the static flux obtained from an eigenvalue calculation describing the final state. The asymptotic shape function was calculated by assuming in Eqs. (3) of Chapter II that:

$$\frac{\partial \psi(\underline{r},E,t)}{\partial t} = 0,$$

$$\frac{1}{n(t)} \frac{dn(t)}{dt} = s, \text{ and}$$

$$\frac{1}{c_i(\underline{r},t)} \frac{\partial c_i(\underline{r},t)}{\partial t} = s,$$

where s is the stable period given by the inhour equation for the final reactivity. The resulting time-independent equation was then solved with the FX2-TH code. In Table 4.3 we compare the asymptotic and the static eigenvalue calculations with the time-dependent shape function. The differences among these three calculations are very small, confirming that the bulk of the spatial redistribution of the neutron flux had already taken place.

Table 4.3

Comparison between time-dependent and static calculations

Stable inverse period obtained from the inhour equation: $s = -0.01231\ s^{-1}$
Inverse period obtained from the FX2-TH code at t=6.8 s: $s = -0.0916\ s^{-1}$
Relative difference between the shape function at 6.8 s and the asymptotic shape function with $s = -0.01231\ s^{-1}$: maximum relative difference = 0.70 %; average relative difference = 0.51 %
Relative difference between the shape function at 6.8 s and the static k-eigenvalue calculation representing the same state: maximum relative difference = 1.0 %; average relative difference = 0.64 %
Static reactivity change between the initial and final states:

k unrodded	k_o rodded	$\frac{k-k_o}{k_o}$	$\frac{k-k_o}{k_o\bar{\beta}}$ ($)
1.0048	0.9743	0.0314	4.577

Dynamic reactivity from FX2-TH: $\rho(t) = 0.0316 = 4.615$ $

A comparison between the dynamic reactivity and the static reactivity is also shown in Table 4.3. The dynamic reactivity is defined as Eq. (5c) of Chapter II. The static reactivity is defined as the relative difference in the effective multiplication factors (eigenvalue of the fundamental lambda mode) of two static calculations: one for the initial state and the other for the final state. It is seen in Table 4.3 that the static and dynamic reactivities from the FX2-TH code are equal for all practical purposes. This was expected since the time-dependent shape function was almost identical to the static neutron flux calculated for the final rodded state.

The FX2-TH code calculates the several kinetics parameters $\rho(t)$, $\bar{\beta}_i(t)$ and $\Lambda(t)$ as defined in Chapter II by Eqs. (5c), (5d) and (5f), respectively, as a function of time. They are then used to solve the point kinetics equations (5a) and (5b) presented in Chapter II to produce the amplitude function, all in the framework of the quasi-static method.

In Figs. 4.18 and 4.19 are shown time-dependent information obtained from the FX2-TH simulation of the rod drop experiment described above. Fig. 4.18 shows the amplitude function $n(t)$ and simulated countrates $R(\underline{r}_o,t)$, the thermal flux as a function of time, at r=1.15 m and z=1.2 m (detector position 1), at r=0.235 m and z=1.8 m (detector position 2), at r=0.54 m and z=2.4 m (detector

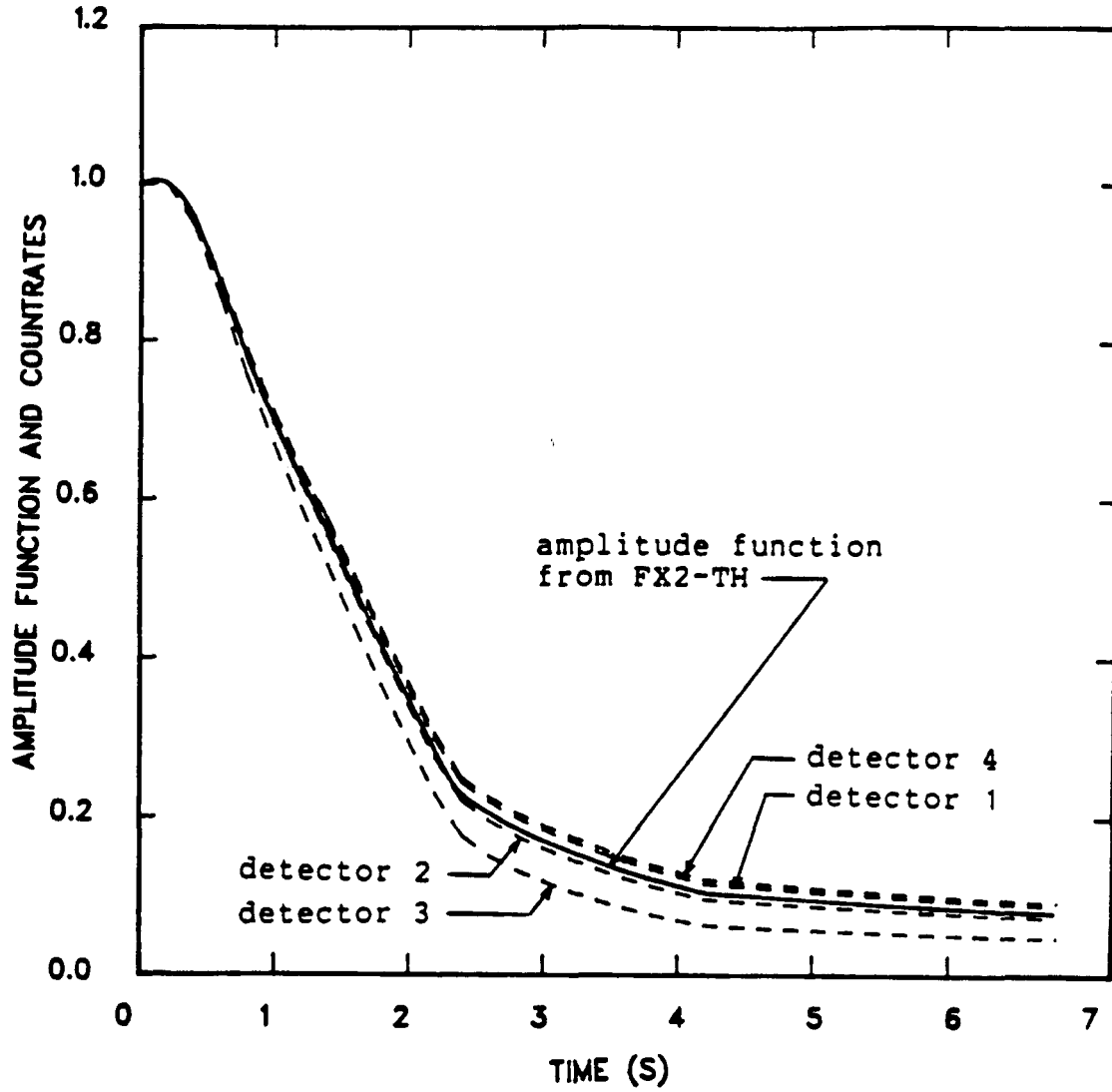

Figure 4.18 Amplitude function and countrates produced by the FX2-TH code simulation.

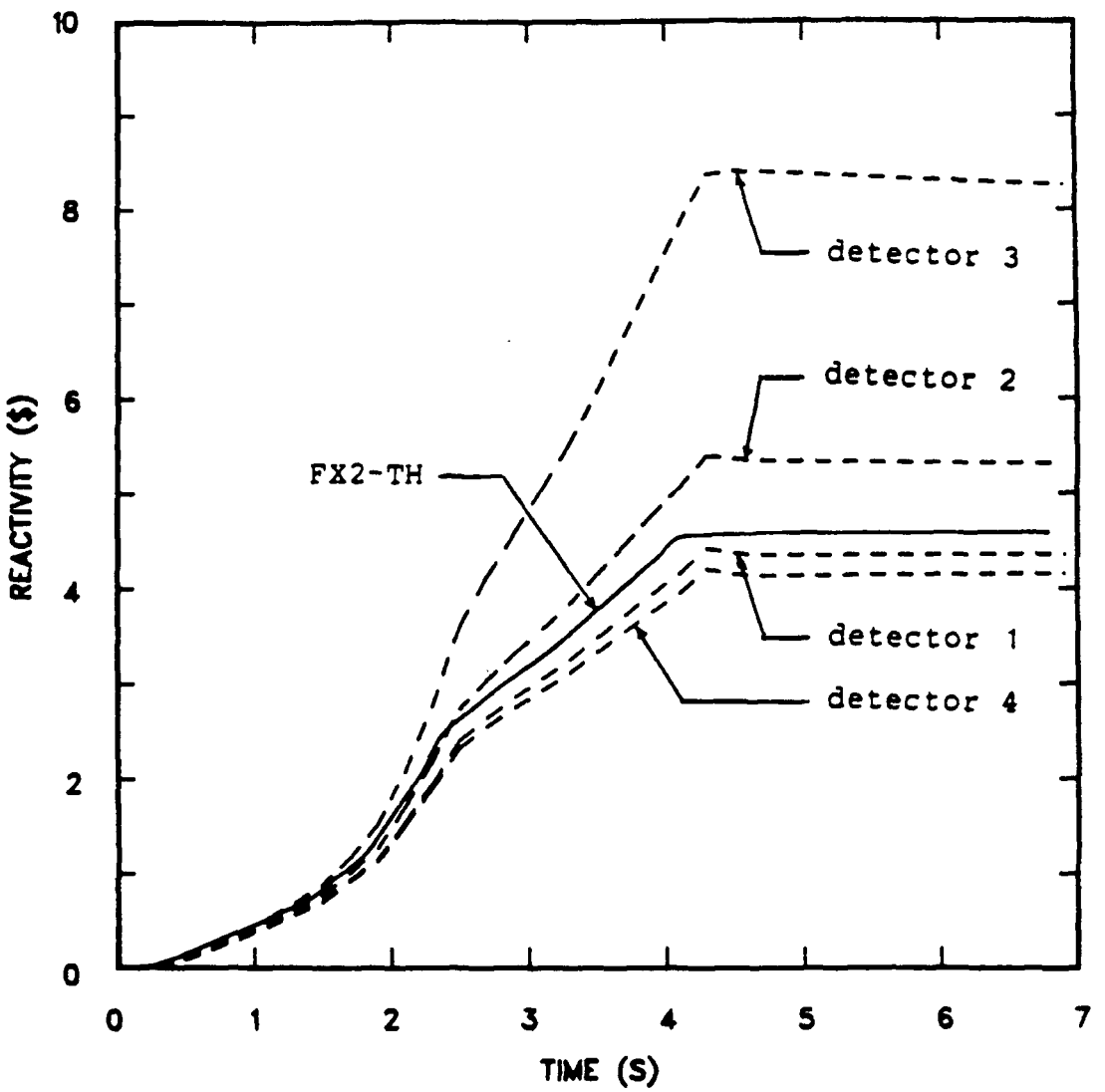

Figure 4.19 Reactivity from the amplitude function and countrates without space-time correction.

position 3), and at r=1.07 m and z=0.4 m (detector position 4). These positions attempt to simulate the actual detector locations at the KAHTER facility.[30-32] The reactivity traces obtained by feeding these detector signals directly to the inverse kinetics routine are shown in Fig. 4.19. The kinetics parameters $\Lambda(t)$ and $\bar{\beta}_i(t)$ were held constant equal to their value from the beginning of the transient. It is seen here that the apparently small differences between the amplitude function and the detector signals produce large errors in the final reactivity values. Table 4.4 shows the kinetics parameters obtained with the FX2-TH code at several points during the transient. Table 4.5 shows the countrates (thermal flux) at the locations 1 through 4 defined above, and the respective reactivities obtained with the direct use of the inverse kinetics routine.

Clearly Fig. 4.19 and Table 4.5 indicate that the assumption of countrates taken as the amplitude function is a poor approximation when spatial effects are present during the transient. Depending on the detector location the error can be very great. In the next section we present the results from the modal-local simulation of this same transient.

2. Rod-drop Simulation with the Modal-Local Method

The modal-local simulation requires, prior to the analysis itself, a set of lambda modes for some reference

Table 4.4

Kinetics parameters and amplitude function produced by the FX2-TH code during the rod-drop simulation.

time (s)	$\Lambda(t)$ (ms)	$\tilde{\beta}(t)$	$\rho(t)$ ($)	n(t)
0.0	1.089	6.853×10^{-3}	0.0	1.0
1.0	1.079	6.853×10^{-3}	-0.567	0.6341
1.8	1.064	6.853×10^{-3}	-1.483	0.3739
2.8	1.044	6.853×10^{-3}	-3.146	0.1746
4.0	1.030	6.853×10^{-3}	-4.616	0.1063
4.8	1.029	6.853×10^{-3}	-4.615	0.0957
5.8	1.029	6.853×10^{-3}	-4.614	0.0859
6.8	1.029	6.853×10^{-3}	-4.614	0.0780

Table 4.5

Reactivity from simulated countrates from four core locations.

	detector 1		detector 2		detector 3		detector 4	
time (s)	R(t)	ρ(t) ($)	R(t)	ρ(t) ($)	R(t)	ρ(t) ($)	R(t)	ρ(t) ($)
0.	1.0	-0.002	1.0	-0.003	1.0	-0.007	1.0	-0.002
1.0	0.636	-0.577	0.621	-0.613	0.591	-0.694	0.639	-0.568
1.8	0.365	-1.539	0.342	-1.694	0.297	-2.067	0.371	-1.503
2.8	0.185	-3.049	0.162	-3.573	0.120	-5.044	0.191	-2.920
4.0	0.117	-4.413	0.097	-5.388	0.064	-8.359	0.122	-4.197
4.8	0.106	-4.350	0.088	-5.331	0.057	-8.360	0.111	-4.135
5.8	0.095	-4.358	0.079	-5.319	0.052	-8.299	0.100	-4.149
6.8	0.088	-4.360	0.073	-5.311	0.048	-8.260	0.092	-4.153

configuration of the core, and a set of local functions at several intermediate states during the transient. The two-dimensional lambda modes presented in Sect. B were utilized here for the calculation of the modal function $h(\underline{r},E,t)$. The local functions obeying Eq. (3) of Chapter III were obtained for several intermediate states through fixed source calculations performed with the 2DBUM code. The fixed source representing the perturbation introduced in the core is found at a given time by simply determining the top-reflector rod position. This is easily done since the rods are inserted with constant speed into the core. As before, we neglected the perturbations in scattering and leakage, and represented the rod insertion solely by changes in the absorption cross sections.

The local functions corresponding to 0 s, 1.076 s, 2.062 s, and 3.031 s are shown in Figs. 4.20 and 4.21. Again, the local function clearly represents the fine details of the flux perturbation and is restricted mostly to the top part of the core. For intermediate times, the local function is obtained by linear interpolation in accordance with the quasi-static approach. The axial profiles are given along the top-reflector rods, while the radial profiles are selected at the top reflector.

In Fig. 4.22 are illustrated the reactivity traces obtained from the modal-local method for the countrates presented in Fig. 4.18. The agreement is very good for all

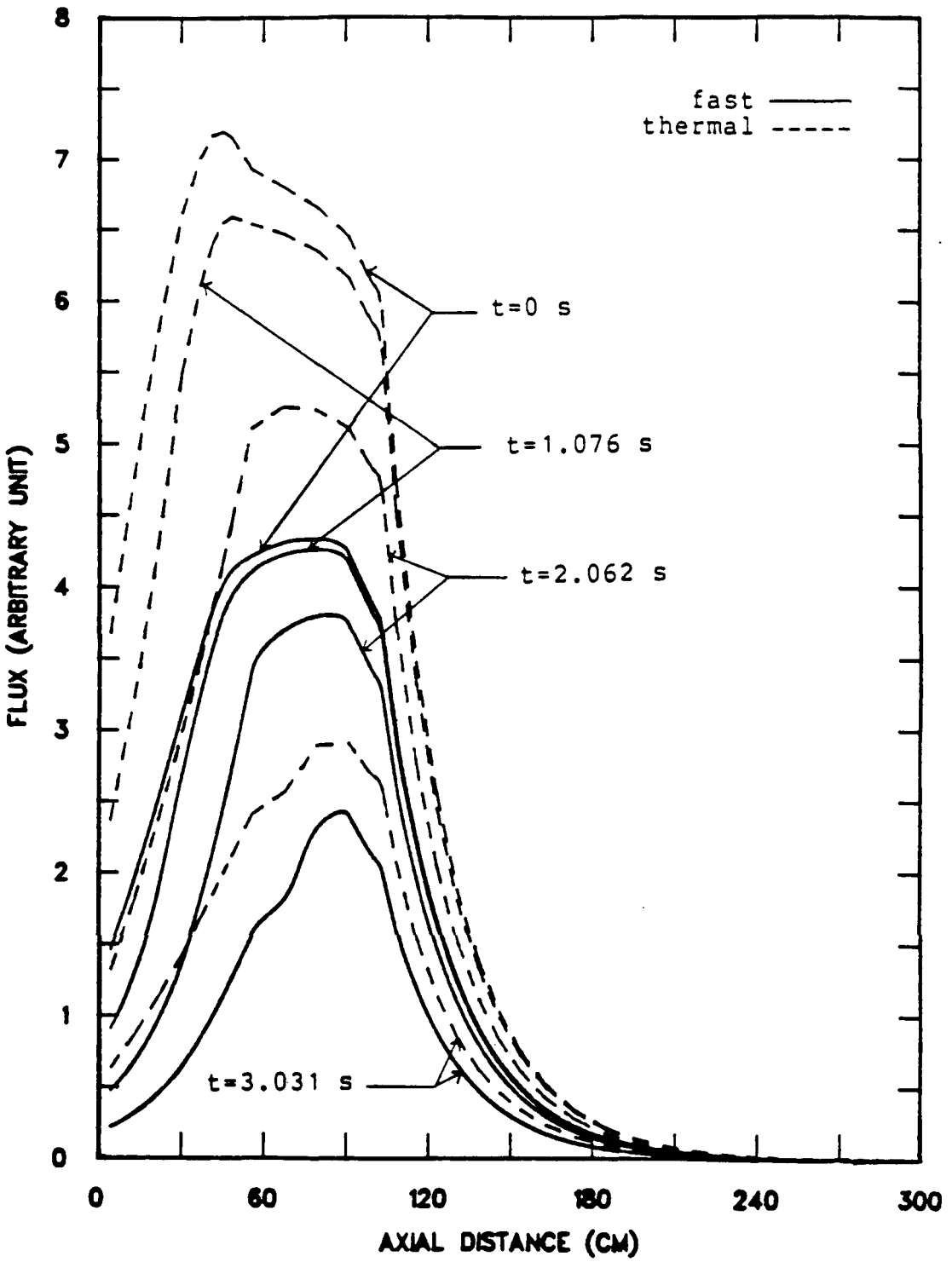

Figure 4.20 Local function at several points during the transient.

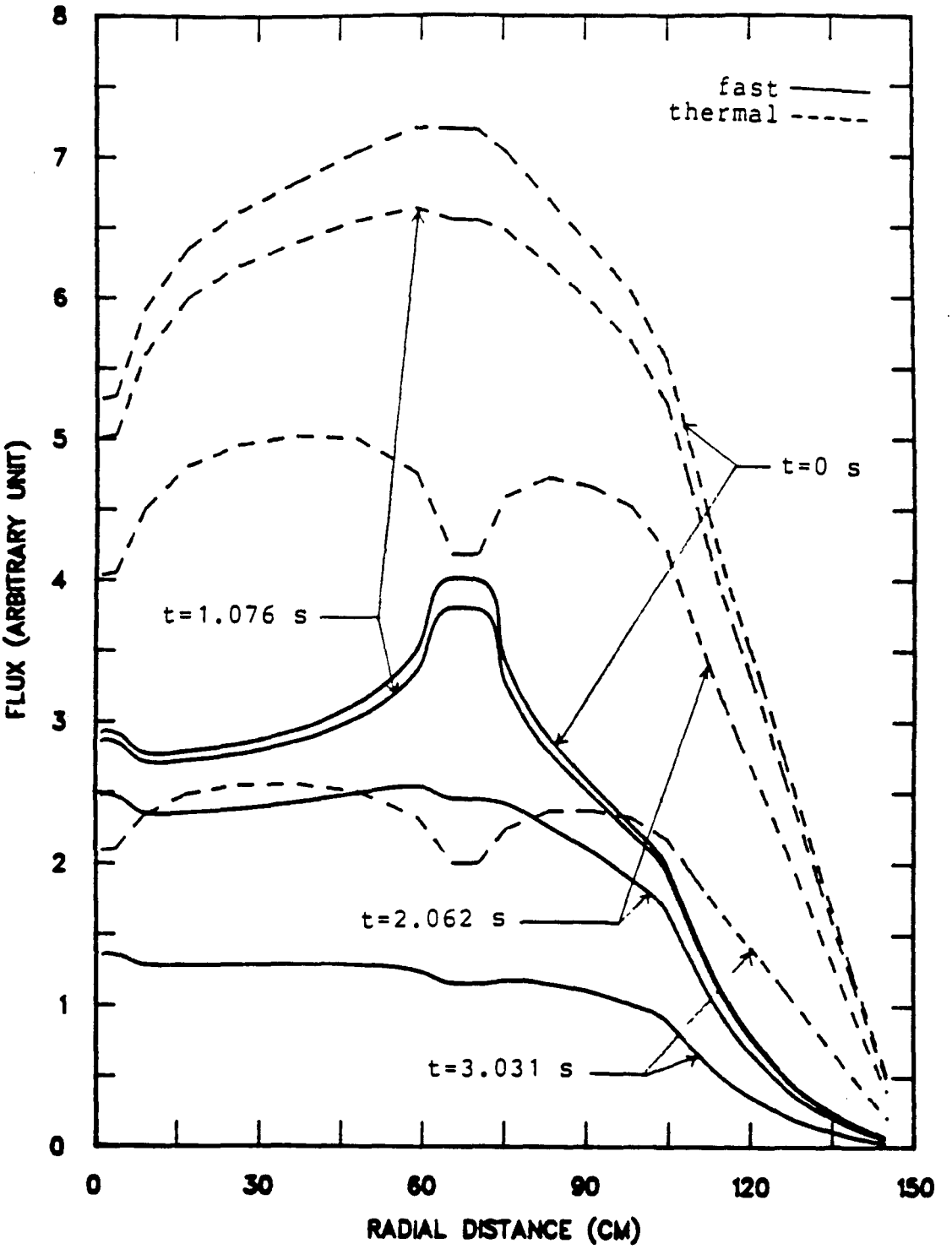

Figure 4.21 Local function at several points during the transient.

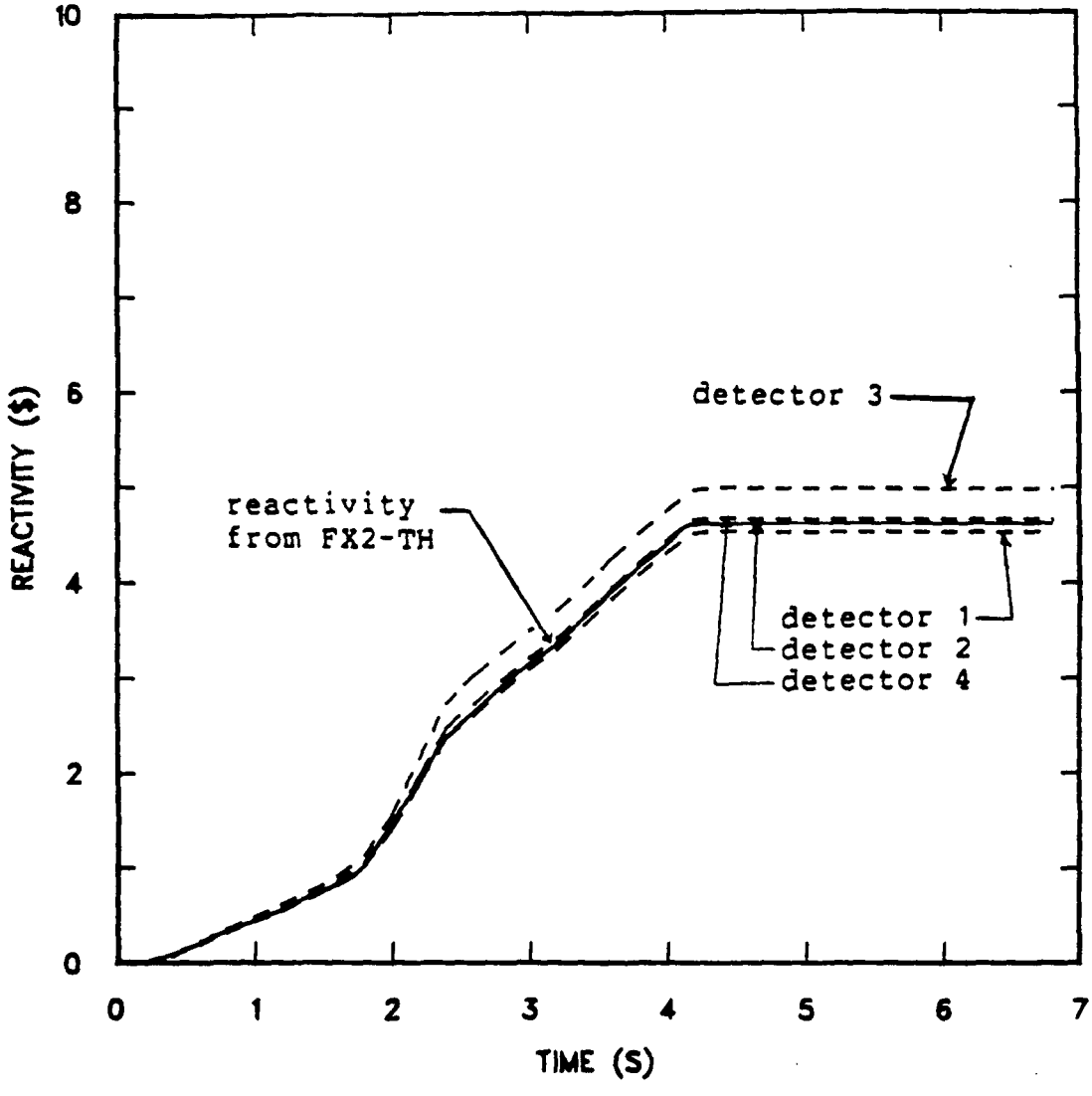

Figure 4.22 Reactivity with space-time correction from the modal-local method.

detectors except perhaps for detector 3, closest to the top-reflector rods. The correction factors produced by the modal-local method are compared in Fig. 4.23 with those from the FX2-TH code. Here, since the thermal flux at detector location is taken as the detector signals, the correction factors are simply the shape function at the detector locations. Table 4.6 shows the kinetics parameters $\Lambda(t)$ and $\bar{\beta}(t)$, the modal coefficients $a_m(t)$ for the modal function $h(\underline{r},E,t)$, and the ratio of local function and shape function weighted by $\phi_o^\dagger(\underline{r},E)\,\frac{1}{v}$. This ratio illustrates the relative contribution of the local function to the shape function. Table 4.7 shows the amplitude function obtained by the modal-local method for detectors 1 through 4 and the corresponding reactivities, for several intermediate times during the transient.

3. Analysis of the Results

In this section we will analyze the results obtained for the rod-drop simulation performed with the FX2-TH code and the modal-local method. We will first assess the importance of the amplitude function and the time-dependent kinetics parameters in the inverse kinetics equation. The time-dependent generation time can play an important role in determining the correct reactivity, especially when the perturbation introduced in the core causes large tilts in the neutron flux distribution.

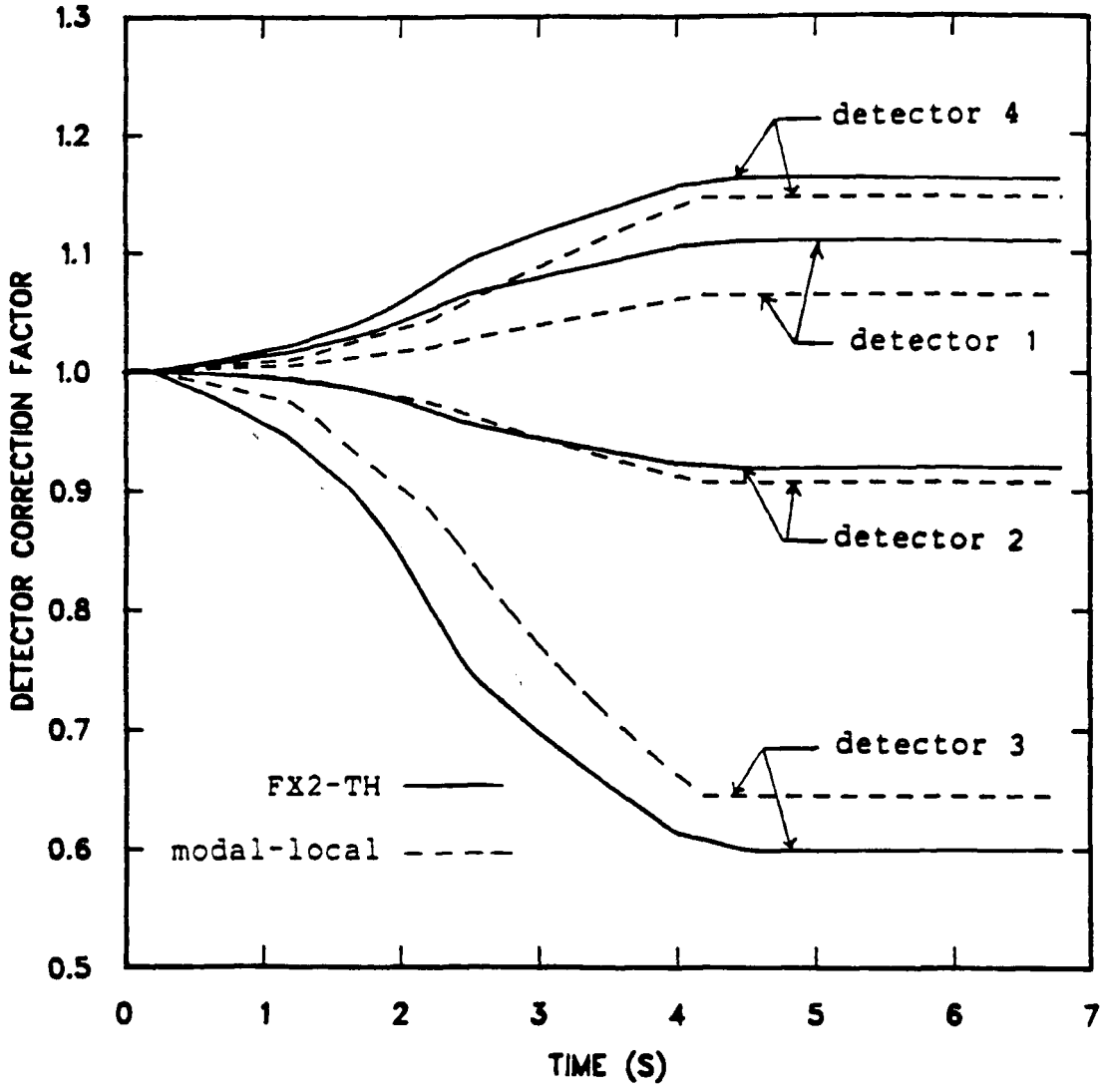

Figure 4.23 Correction factors from the FX2-TH code and modal-local method for detectors 1 through 4.

Table 4.6

Kinetics parameters, modal expansion coefficients for $h(\underline{r},E,t)$, and a local function ratio.

time (s)	$\bar{\beta}(t)$	$\Lambda(t)$ (ms)	$a_o(t)$	$a_1(t)$	$a_2(t)$	$\frac{\langle \phi_o^\dagger, \frac{1}{v} f(t) \rangle^*}{\langle \phi_o^\dagger, \frac{1}{v} \psi(t) \rangle}$
0.0	6.852-3 †	1.066	0.9407	0.0407	-0.0023	0.0318
1.0	6.852-3	1.063	0.9449	0.0385	-0.0021	0.0273
1.8	6.852-3	1.056	0.9560	0.0318	-0.0017	0.0236
2.8	6.853-3	1.043	0.9768	0.0185	-0.0009	0.0132
4.0	6.853-3	1.030	0.9993	0.0032	-0.0001	0.0
4.8	6.853-3	1.030	0.9994	0.0031	-0.0001	0.0
5.8	6.853-3	1.030	0.9994	0.0031	-0.0001	0.0
6.8	6.853-3	1.030	0.9994	0.0031	-0.0001	0.0

* This ratio can be interpreted as the contribution of the local function to the shape function.

† 6.852-3 reads 6.852×10^{-3}.

Table 4.7

Amplitude function and reactivity with correction factors from the modal-local method.

	detector 1		detector 2		detector 3		detector 4	
time (s)	n(t)	ρ(t) ($)	n(t)	ρ(t) ($)	n(t)	ρ(t) ($)	n(t)	ρ(t) ($)
0.0	1.0	0.0	1.0	0.0	1.0	0.0	1.0	0.0
1.0	0.641	-0.558	0.633	-0.579	0.616	-0.622	0.642	-0.556
1.8	0.382	-1.410	0.379	-1.458	0.357	-1.563	0.380	-1.418
2.8	0.181	-3.093	0.175	-3.209	0.162	-3.496	0.178	-3.145
4.0	0.111	-4.521	0.108	-4.649	0.101	-4.971	0.108	-4.662
4.8	0.100	-4.523	0.097	-4.653	0.091	-4.979	0.097	-4.660
5.8	0.090	-4.523	0.087	-4.653	0.081	-4.975	0.087	-4.659
6.8	0.081	-4.524	0.079	-4.652	0.075	-4.972	0.079	-4.659

For estimation of the shape function as a function of time the modal-local method presents basically four approximations: (a) the limited number of modes for the global function $h(\underline{r},E,t)$, (b) the first-order perturbation in the local function calculation, (c) the neglect of cross terms in the modal coefficient equations, and (d) the neglect of time derivative in the local function calculation. The first two of these approximations have been studied in the Sect. C where we noted that the modal-local method predicts accurately the perturbed flux or shape function away from the perturbation. In this section we will study how these four approximations, including the first two, affect the determination of the detector correction factors and kinetics parameters.

Importance of the detector correction factors

From Fig. 4.19 one sees that space-time effects do not allow the use of countrates directly to obtain reactivity through the inverse kinetics equation. The error can be very large and is dependent on the detector location. The reactivity insertion is overpredicted by detector 3 located only 0.09 m from the top-reflector rods in the radial direction. This is due to the thermal flux depression around the control rods with their large in the thermal neutron absorption cross section. Fig. 4.18 clearly shows that the signal from detector 3 decays more rapidly during the transient. The direct consequence of this is the

greater final reactivity produced by detector 3 when no space-time corrections are considered, as shown in Fig. 4.19 and Table 4.5. The other detectors located in positions away from the top-reflector rods produce smaller errors in the final reactivity, but still require in general space-time corrections.

Fig. 4.23 shows that the correction factors are very much position-dependent and that they evolve in time in distinct manner. This can be explained by analyzing the shape function development as a function of time. The perturbation in the shape function due to the top-reflector rod insertion is primarily one of shifting the shape function to the bottom of the core. Thus, one sees that detectors 1 and 4, located in the bottom part of the core, require a correction greater than 1 because the shape function tilts towards them. Conversely, detectors 2 and 3, located in the top part of the core, require a correction smaller than 1 because the shape function is tilting away from them. Detector 3, which is closest to the top-reflector rods, requires the greatest correction since the shape function is very depressed around the control rods because of their strong absorption of thermal neutrons.

Importance of the time-dependent kinetics parameters

The effective delayed neutron fraction $\bar{\beta}(t)$ accounts for the difference in fission spectrum between prompt and

delayed neutrons, and has a direct influence on the reactivity. The parameter changes during a transient only if the spectrum or the energy dependency of the shape function $\psi(\underline{r},E,t)$ in the fast energy range is perturbed. Since we are using a two-group model to describe the spectral effects, it is impossible to see any difference between prompt and delayed neutrons; their spectra are lumped together in the same fast group. Therefore, as is shown in Tables 4.4 and 4.6, the effective delayed neutron fraction did not change during this simulation.

The generation time $\Lambda(t)$ changes about 5.8 % during the transient according to the FX2-TH results shown in Table 4.4, while the modal-local method produced a change of 3.4 % based on the results shown in Table 4.6. The importance of $\Lambda(t)$ can be better understood by noticing that, in Eq. (6) of Chapter II, it appears both inside and outside the convolution integral in the inverse kinetics equation. If the generation time is held constant during the transient, it could be taken out of the integral to cancel with the one outside the integral. If its time dependency is considered, the convolution integral can be said to be multiplied by the ratio between generation times at the current time and some average value of previous times. Its maximum effect will be given by the ratio of the final to initial generation time. For this rod-drop simulation, the neglect of the time dependency of the generation time has been found to increase the final

reactivity by about 4 %, indicating that this effect is large and should not be overlooked.

Errors in the estimation of the reactivity

The reactivity at a given time t obtained through the inverse kinetics equation depends on the amplitude function and the kinetics parameters during the transient. In general, errors in n(t), $\Lambda(t)$ and $\bar{\beta}(t)$ during the transient affect the reactivity. With a constant $\bar{\beta}(t)$, however, the errors are due only to the estimates of n(t) and $\Lambda(t)$, which appear in the inverse kinetics equation in the ratio $\frac{n}{\Lambda}$. In Table 4.8 are shown the error in the ratio $\frac{n}{\Lambda}$ and the corresponding error in reactivity produced by the modal-local method for the four detector locations at t=6.8 s.

In order to understand how the amplitude function and the kinetics parameters affect the reactivity, consider the effect of the ratio $\frac{n}{\Lambda}$ in the inverse kinetics Eq. (6) of Chapter II. The convolution integral in the inverse kinetics equation is the term which contributes the largest error to the reactivity. The other term $\Lambda \frac{\dot{n}}{n}$ is very small, of the order of 10^{-4}, so that errors in it can be neglected. The error in the convolution integral $\rho_d(t)$ can be given by the following expression:

Table 4.8

Relative errors in $\frac{n}{\Lambda}$ and reactivity between the FX2-TH code and modal-local method.

detector	error in n/Λ at 6.8 s (%)	error in $\rho(t)$ at t=6.8 s (%)
1	1.90	1.4
2	-0.91	-0.1
3	-9.22	-6.7
4	-0.89	-2.2

Tabela errada...

$$\delta\rho_d(t) = \rho_d(t) - \rho_{do}(t) = \frac{\delta y(t)}{y(t)}\,\rho_{do}(t)$$

$$- \frac{1}{y(t)} \sum_{i=1}^{6} \lambda_i \int_{-\infty}^{t} \delta y(t')\bar{\beta}_i\, e^{\lambda_i(t'-t)}dt'$$

with $y(t) = \frac{n(t)}{\Lambda(t)}$ and $\delta y(t) = y(t) - y_o(t)$, where the ρ_{do} and y_o refer to the results obtained from the FX2-TH code and ρ_d and y refer to the modal-local estimates. The error in the convolution integral $\delta\rho_d(t)$ has two components: one due to the error in $y(t)$ at time t, and another due to errors in $y(t)$ during the transient. The relative error in the reactivity will then be given by:

$$\frac{\rho(t) - \rho_o(t)}{\rho_o(t)} \simeq \frac{\delta\rho_d(t)}{\rho_o(t)}$$

where $\rho_o(t)$ is the FX2-TH reactivity.

In Fig. 4.24 we show the absolute deviation $\delta y(t)$ during the transient for the four detectors. For detectors 1, 2, and 3 there is a cancellation of errors between the two terms of $\delta\rho_d$ because $\delta y(t)$ during the transient and at the end of the transient is in the same direction. For detector 4, $\delta y(t)$ starts positive and then becomes negative, which causes a summation of errors. This explains why detector 2, with almost the same final relative error in

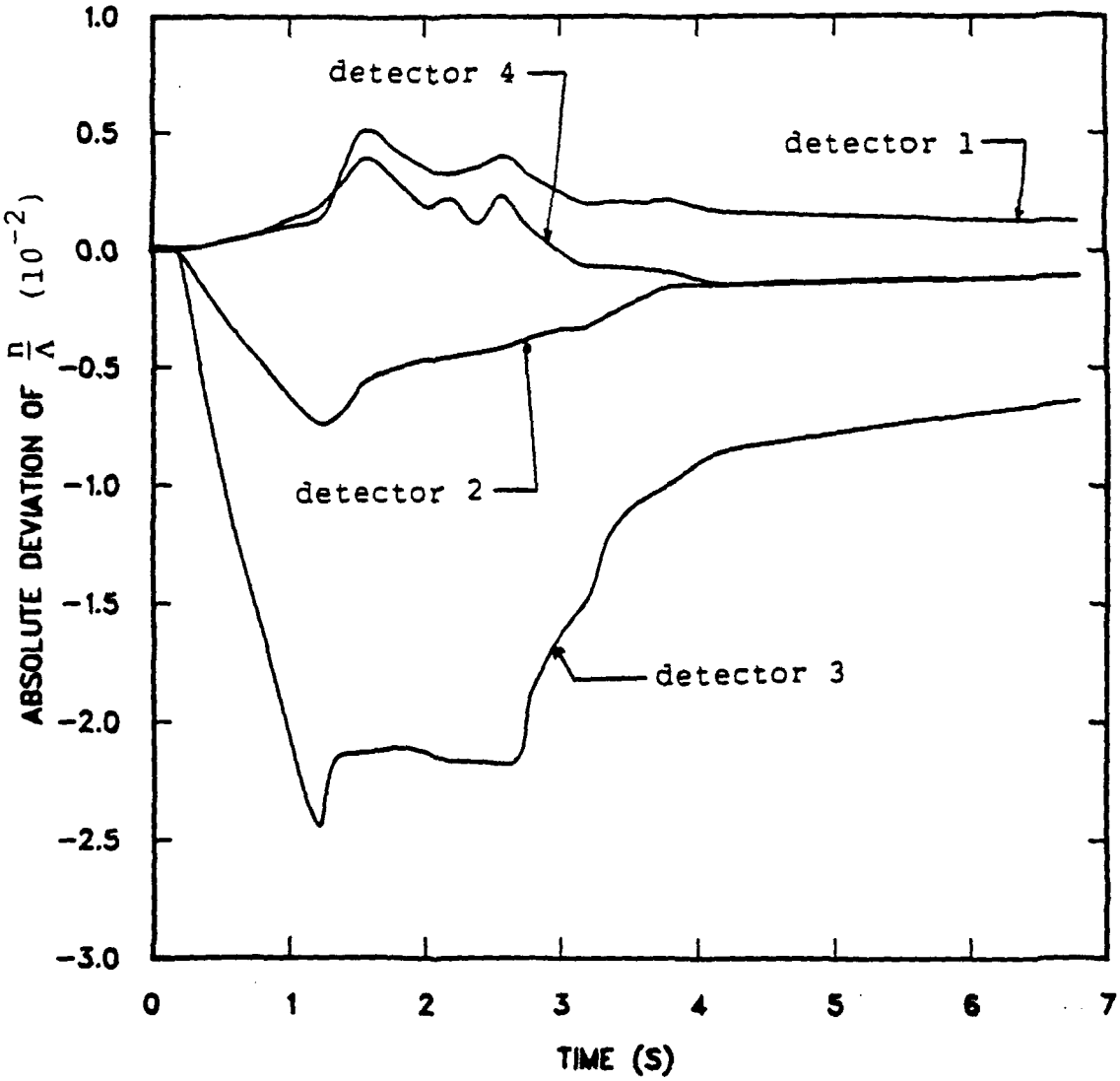

Figure 4.24 Absolute deviation of $\frac{n}{\Lambda}$ between the modal-local method and the FX2-TH code.

y(t) as detector 4, produces more accurate results as shown in Table 4.8.

This cancellation of errors is better understood by noticing that the reactivity is basically the ratio of some weighted average value of y(t) throughout the transient to the final value of y(t). If one encounters small errors in the same direction in y(t) during the whole transient the ratio does not change much. However, if the errors are in different directions, as in the case of detector 4, in which the numerator is larger ($\delta y>0$ in the beginning of the transient), and the denominator is smaller ($\delta y<0$ at the end of the transient), the error in the ratio will be compounded.

Approximations in the local function

The discrepancies between the parameters produced by the FX2-TH code and the estimates from the modal-local method are due to the errors in the modal-local prediction of the shape function during the transient. In Sect. C we have shown for, static calculations, that the first-order perturbation approximation in the local function calculation was responsible for greater errors in the shape function near the perturbation location. The reference flux for the rodded configuration used to calculate the source of the local function was smaller than those of the perturbed states. The magnitude of the local function is then smaller

than what it would be if the exact shape function was considered. In Figs. 4.25 through 4.28 are shown the fast and thermal shape functions predicted by the FX2-TH code and the modal-local method for three times during the transient, t=0 s, t=1.8 s and t=6.8 s. The axial profiles, taken at a radial position r=0.84 m show a good agreement between the modal-local and the FX2-TH shape functions. The radial profiles, taken in the top-reflector, clearly show that near the perturbation the modal-local method can not predict the shape function as well even with the inclusion of the local function. The relative errors average around 10 % there.

The other approximation in the calculation of the local function was the neglect of the time derivative term. For assessing its impact on the local function we have performed a static calculation in which we assumed:

$$\frac{1}{f(\underline{r},E,t)} \frac{\partial f(\underline{r},E,t)}{\partial t} = s$$

where $s = -0.25\ s^{-1}$ was obtained as an average value for the whole core around t= 2.062 s. Although the time-derivative term is only approximately represented by the above model, it can provide us with useful information. The new local function was calculated with the the 2DBUM code by incorporating the term $\frac{s}{v}$ in the absorption cross section. Little difference was noted in the local function, with agreement better than 0.1 % with that obtained with Eq. (3)

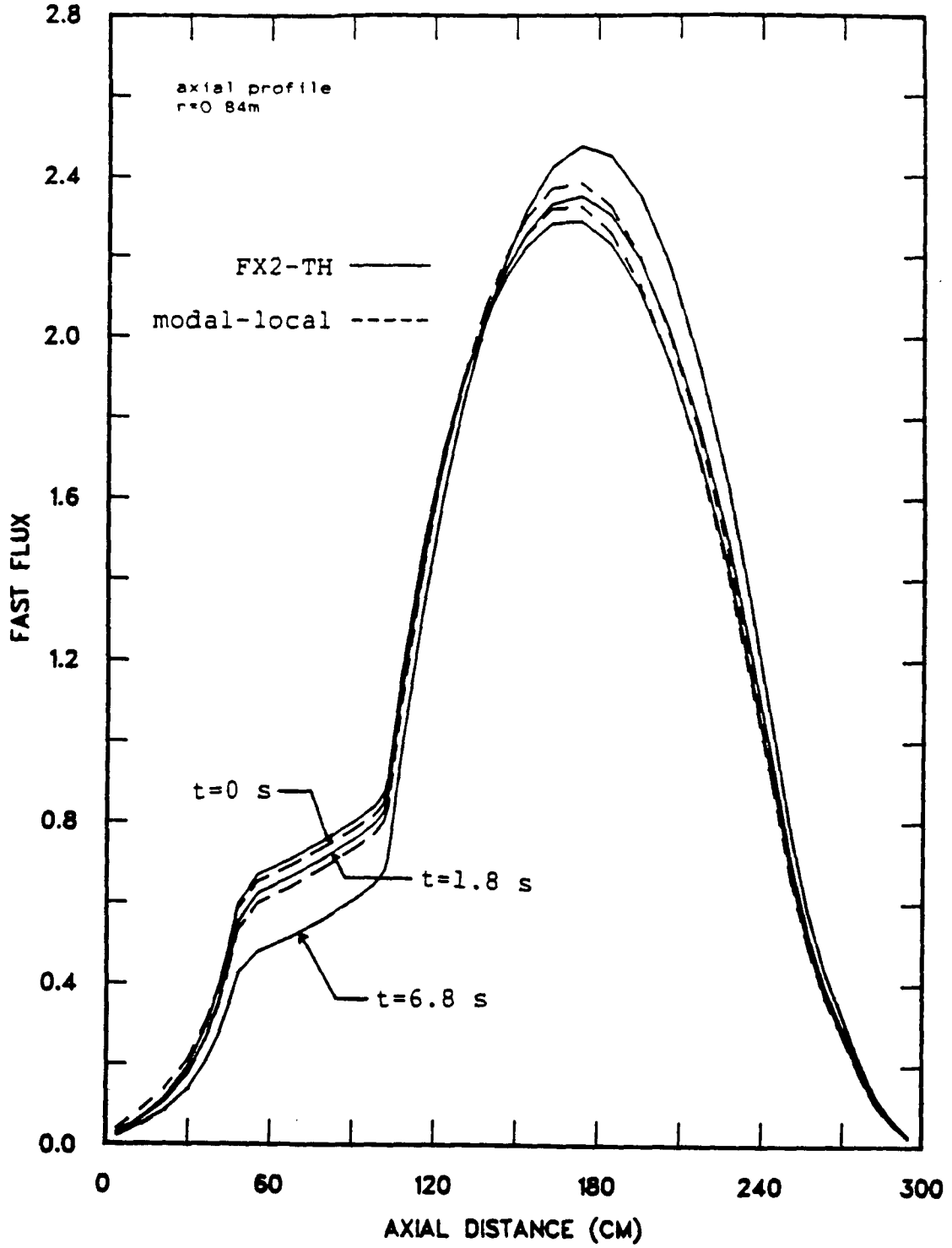

Figure 4.25 Shape function as a function of time produced by the FX2-TH code and the modal-local method.

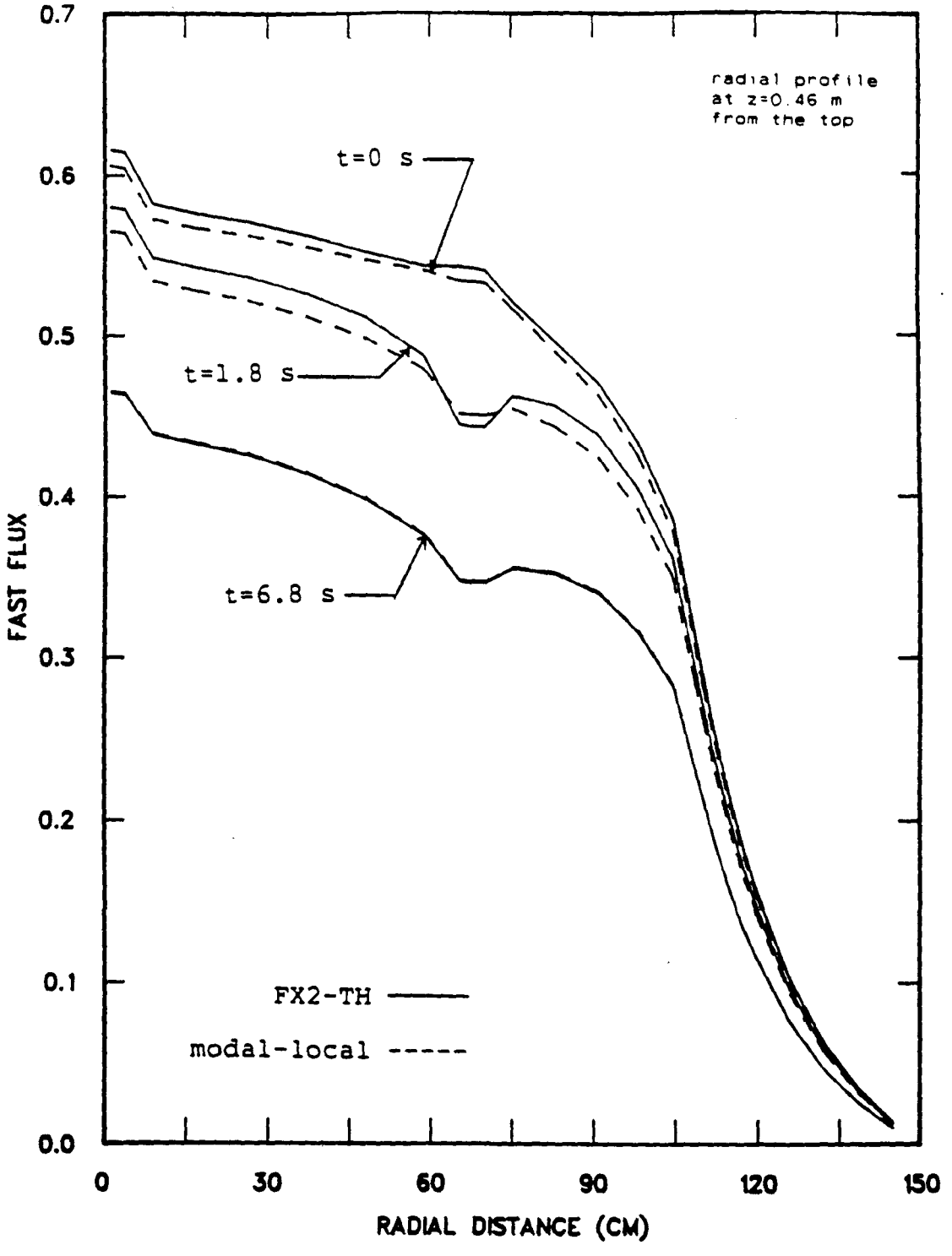

Figure 4.26 Shape function as a function of time produced by the FX2-TH code and the modal-local method.

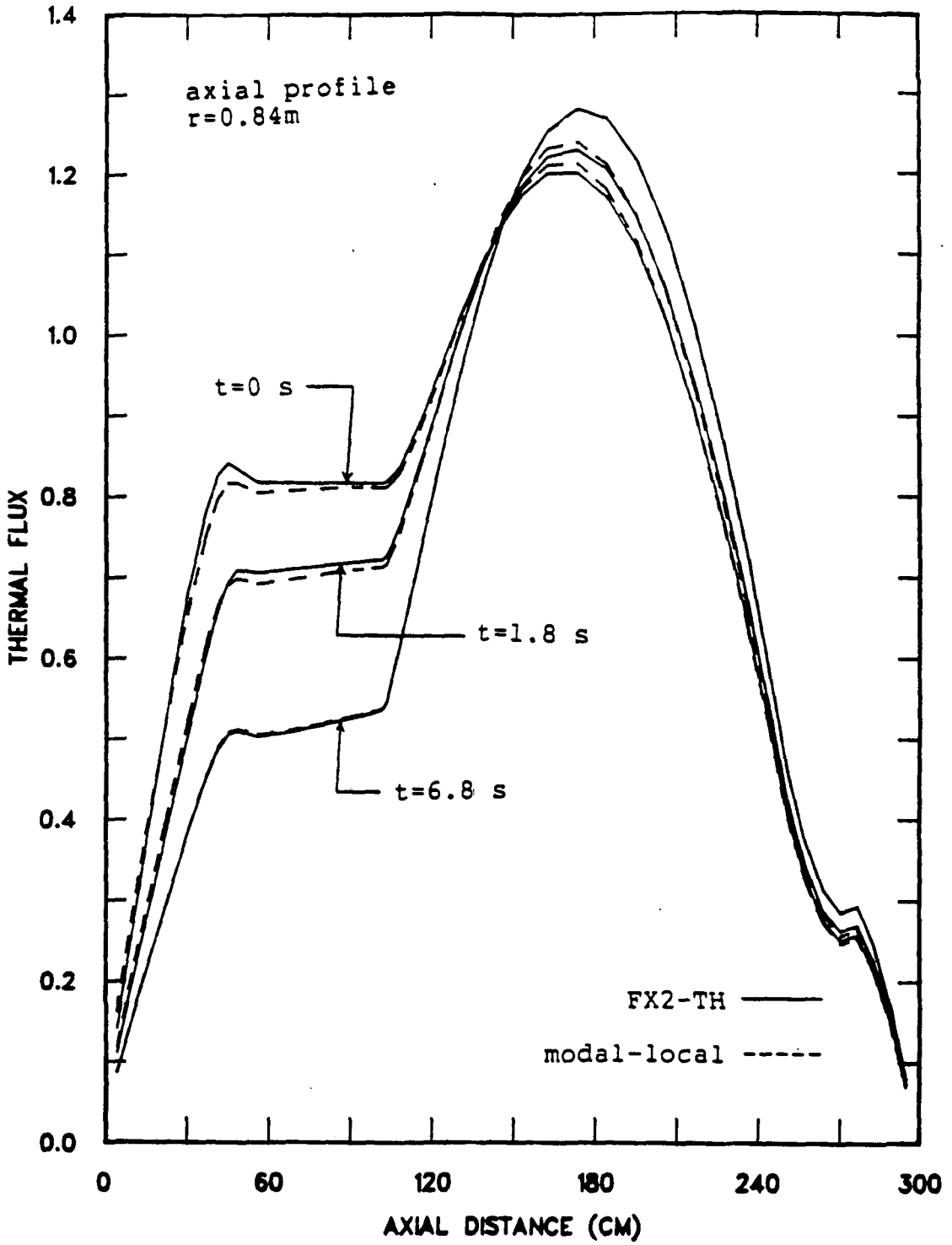

Figure 4.27 Shape function as a function of time produced by the FX2-TH code and the modal-local method.

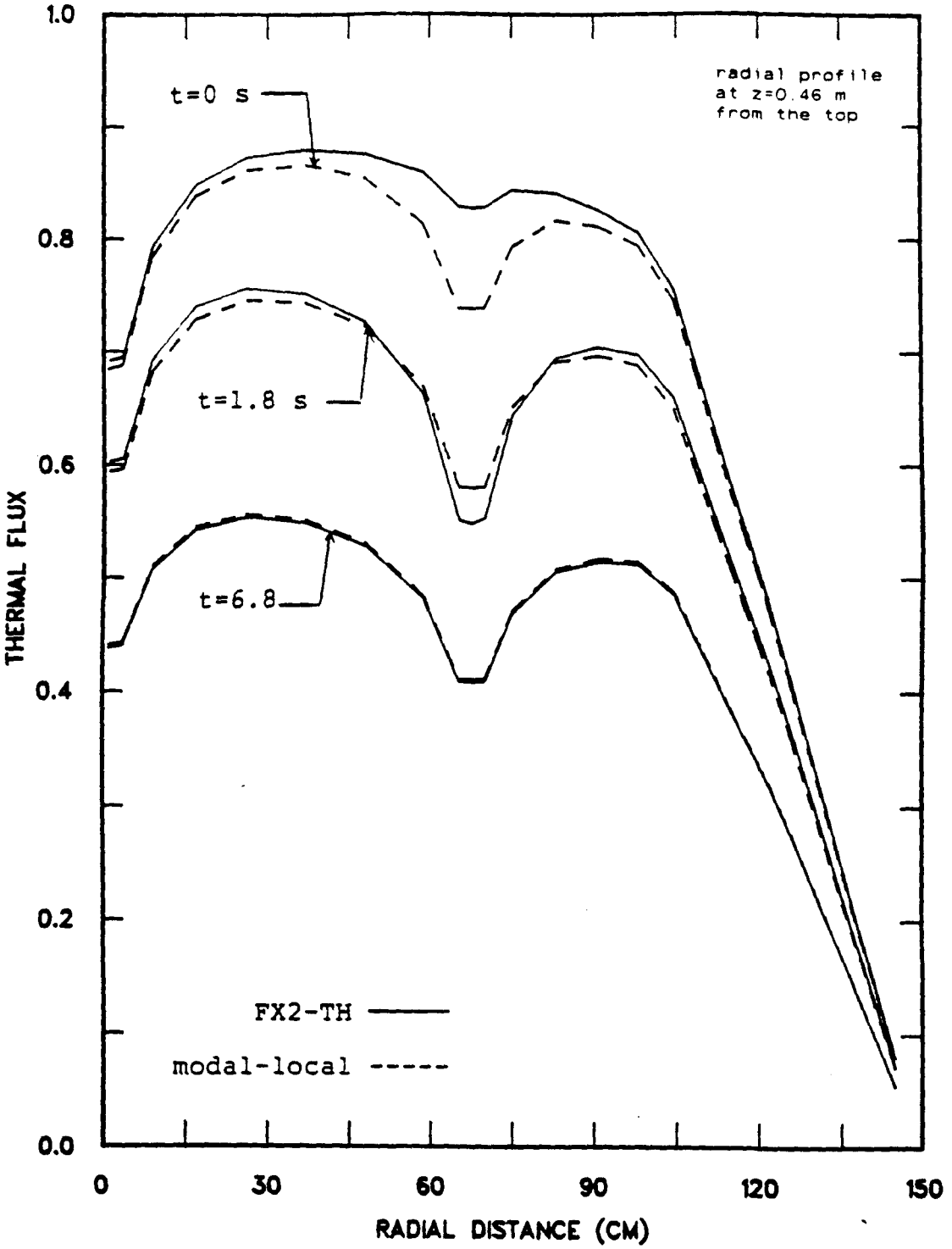

Figure 4.28 Shape function as a function of time produced by the FX2-TH code and the modal-local method.

of Chapter III. This was expected since the thermal and fast neutron speeds are very large, causing the term $\frac{s}{v}$ to be very small. Therefore, the neglect of the time derivative term in the local function equation is a good approximation.

In the quasi-static implementation of the modal-local method, the local function is linearly interpolated between the times it is not pre-calculated. In order to insure the overall accuracy, one should pre-calculate the local function with sufficient frequency during the transient so that the interpolations adequately approximate the correct $f(\underline{r},E,t)$.

Approximations in the modal function

The approximations made in the calculation of the modal function $h(\underline{r},E,t)$ are the neglect of the cross integrals, e.g., $\langle\phi_m^\dagger,\frac{1}{v}\phi_n\rangle$ and $\langle\phi_m^\dagger,(M_{po}-L_o)\phi_n\rangle$, $m\neq n$, and the limited number of modes considered in the expansion. The neglect of the cross integrals is not a necessary approximation in the modal-local method, but it proves to be convenient since it decouples the equations for the modal coefficients. The integrals $\langle\phi_m^\dagger,(M_{po}-L_o)\phi_n\rangle$, $m\neq n$, would not be zero only because of the slight difference between the prompt neutron and total fission spectra. In a two-energy group model, however, there is no difference between the two spectra, and hence no approximation has actually been made in our two-group analysis with respect to these integrals.

The integrals $<\phi_m^\dagger, \frac{1}{v}\phi_n>$, $m \neq n$, are not zero because $\frac{1}{v}$ and M_{po} have distinct energy and spatial distribution in the reactor core, especially in the KAHTER facility which has large void and reflector regions. We have noticed that the cross integrals, with $m \neq n$, for the KAHTER facility are at least an order of magnitude smaller than the integrals with $m=n$. The coupling terms in the modal coefficient equations due to the cross integrals are considered were found to be two orders of magnitude smaller than the others, and altered the modal coefficients by less than 1 %. Thus, the neglect of these cross terms is also a good approximation, even for the KAHTER facility. For light water reactors the neglect of these integrals will be even a better approximation because they are usually two orders of magnitude smaller than the integrals with $m=n$.

The other approximation in the calculation of the modal function $h(\underline{r},E,t)$ is the limited number of modes. It has been shown in Sect. C that an increased number of modes improves the modal-local estimation of the shape function. As in any modal expansion technique, the number of modes required for achieving a desired accuracy is problem dependent. Usually for problems involving distributed perturbations in the core, only a few modes may be sufficient. Very localized perturbations require a larger number of modes because higher harmonics are likely to be excited.

A final point to make is the possibility of estimating the detector correction factors and the kinetics parameters through static calculations representing the initial and final state of the reactor core. As shown in Table 4.3 the time-dependent shape function can be accurately represented by the flux from a static calculation. This can provide limiting values for the kinetics parameters and for the detector correction factors. If the static corrections are made sometime before the end of the transient, due to cancellation of errors, the final reactivity may be estimated fairly accurately. If the reactivity as a function of time is desired, a number of static calculations will be required to estimate properly the shape function throughout the transient.

Now that we have considered a space-time problem at zero power to test the accuracy of the modal-local method, we will consider in the next section a problem in which thermal hydraulic effects have to be accounted for.

F. Reactivity Measurements in the Power Reactor Environment

In power reactors one should consider the thermal hydraulic effects which can substantially affect the outcome of the transient, and, hence, the safety of a nuclear power plant. The power-reactor problem becomes more involved because of the thermal-hydraulic feedback, but, on the other hand, the external perturbations are less stringent. The

reactivity changes allowed in a reactor at the operating power range are usually on the order of few cents.

To assess the accuracy of the modal-local method in the presence of thermal hydraulic feedback we simulate a differential rod-worth measurement similar to the one described in Sect. D of Chapter II. A simple axial model for a typical pressurized water reactor representing an average coolant channel was chosen in this study. The FX2-TH code provide the reference calculation for this simulation, against which the modal-local method is tested.

The simulation of the differential rod worth at power conditions with the FX2-TH code and the modal-local method are presented in Sects. 1 and 2, respectively. In Sect. 3 we discuss the results and make some concluding remarks.

1. Simulation with the FX2-TH Code

This simulation considers an one-dimensional axial, two-group representation of a loosely coupled pressurized water reactor (PWR). The reactor core is 3.6 m long with a 0.3 m reflector each on the top and bottom. The model to estimate the fuel and coolant temperatures is based on Eqs. (10) of Chapter III for an average coolant channel composed of a fuel rod and surrounding coolant. The rod motion is represented by a linear change in the thermal absorption cross section over 2 seconds in a 0.1 m mesh located 2.7 m from the bottom of the reactor.

In Fig. 4.29 is shown a simplified sketch of the PWR core and in Table 4.9 are shown the neutronic and thermal hydraulic parameters. The functional dependency of the cross sections with temperature are assumed to be given by the simple relationships in Table 4.9. The fast absorption cross section is assumed to change as the square root of the fuel temperature, representing the Doppler effect. The density effects due to the coolant or moderator temperature variation are represented by changes in the thermal absorption cross sections as a linear function of moderator temperature.

The reactivity coefficients presented in Table 4.9 were obtained by performing static neutronic calculations with the thermal hydraulic feedback effects included. Each of the reactivity coefficients was obtained by dividing the reactivity change due to the temperature variation by the average temperature variation. The reactivity change was given by the relative difference between eigenvalues representing the states with and without temperature effects.

The transient starts with the control rods being withdrawn from the core by 0.1 m during 2 s. This causes an introduction of positive reactivity into the core which makes the power to rise about 10 % in the next 4 s. As the power rises, the thermal hydraulic feedback effects start to contribute negative reactivity, decreasing the growth rate

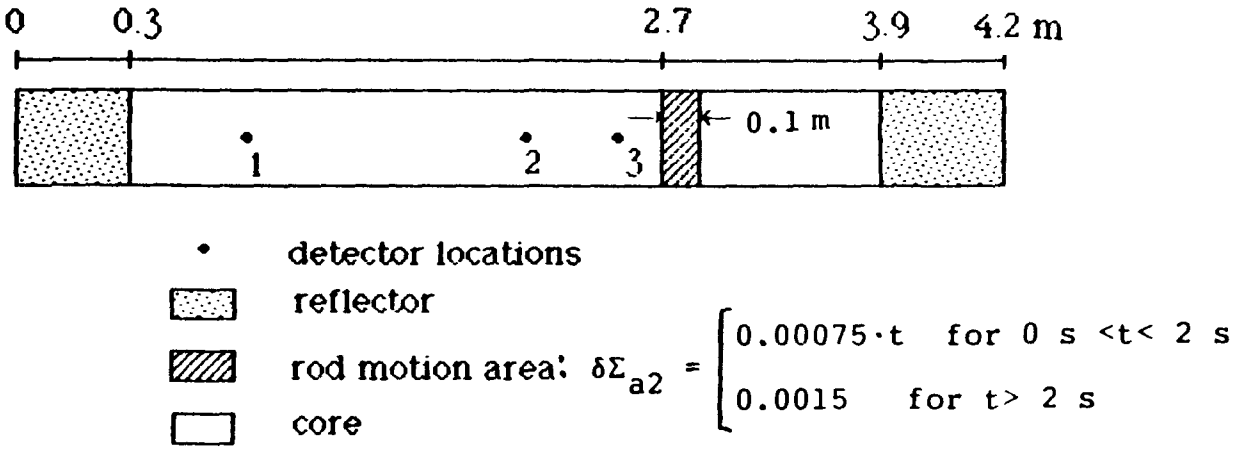

Figure 4.29 Layout of the one-dimensional PWR.

Table 4.9

Neutronic and thermal hydraulic data for the PWR model.

Neutronic Data

region	group	D	Σ_a	Σ_r	$\nu\Sigma_f$
core	1	1.454	0.009604	0.01631	0.006606
	2	0.3949	0.10100	0.0	0.1206
reflector	1	1.417	0.0004838	0.03143	0.0
	2	0.278	0.009818	0.0	0.0

total delayed neutron fraction: $\beta = 0.006853$

speeds: $v_1 = 2.189\text{x}10^{+5}$ m/s, $v_2 = 2.665\text{x}10^{+3}$ m/s

Feedback Coefficients

Doppler effect: $\frac{\partial \Sigma_{a1}}{\partial \sqrt{T_f}} = 1.0036\text{x}10^{-5}\ \text{cm}^{-1}/\sqrt{\text{K}}$

moderator temperature: $\frac{\partial \Sigma_{a2}}{\partial T_c} = 8.5\text{x}10^{-6}\ \text{cm}^{-1}/\text{K}$

reference fuel temperature: 750 K

reference coolant temperature: 557 K

Doppler coefficient of reactivity: $\frac{\partial \rho}{\partial \langle T_f \rangle} = -1.011\text{x}10^{-5}\ \text{K}^{-1}$

moderator temperature coefficient of reactivity:

$$\frac{\partial \rho}{\partial \langle T_c \rangle} = -6.495\text{x}10^{-5}\ \text{K}^{-1}$$

Thermal Hydraulic Data

average channel power = 61.209 kW

average coolant temperature rise = 27 K

coolant volume fraction = 0.5931

$T_{in} = 557.02$ K

$\rho_c C_c = 3.991\ \frac{\text{MJ}}{\text{m}^3\ \text{K}}$

$\rho_f C_f = 3.630\ \frac{\text{MJ}}{\text{m}^3\ \text{K}}$

$C_c = 5.52\ \frac{\text{kJ}}{\text{kg K}}$

$G = 3500\ \frac{\text{kg}}{\text{m}^2\ \text{s}}$

$U = 5.34\ \frac{\text{kJ}}{\text{m}^2\ \text{K s}}$

of the net reactivity. After the rods have ceased moving, the net reactivity starts to decrease because the external perturbation is stabilized and the thermal hydraulic feedback continues to introduce negative reactivity into the core.

In Fig. 4.30 are plotted the total power, the net reactivity, the external reactivity, and the feedback reactivity as a function of time obtained from the FX2-TH code. The feedback effect reduces the net reactivity after t=2 s, and consequently causes a slower rise in power. During the transient the kinetics parameters remained essentially unchanged because of the relatively small perturbation in the shape function: the effective delayed neutron fraction $\bar{\beta} = 6.853 \times 10^{-3}$ and the generation time $\Lambda = 29.5\ \mu s$.

For the modal-local analysis we chose three detectors located at z=2.95 m, at z=1.95 m, and at z=0.55 m from the bottom reflector. As before the thermal flux at these locations were taken as the detector signals. The signals from these three detectors and the respective reactivities obtained by feeding them directly into the inverse kinetics routine are plotted in Fig. 4.31 and 4.32. The relatively small perturbation introduced into the core has induced sufficient spatial redistribution of neutron flux during the transient so that correction factors are required for an accurate inverse kinetics analysis. As expected, detector 3

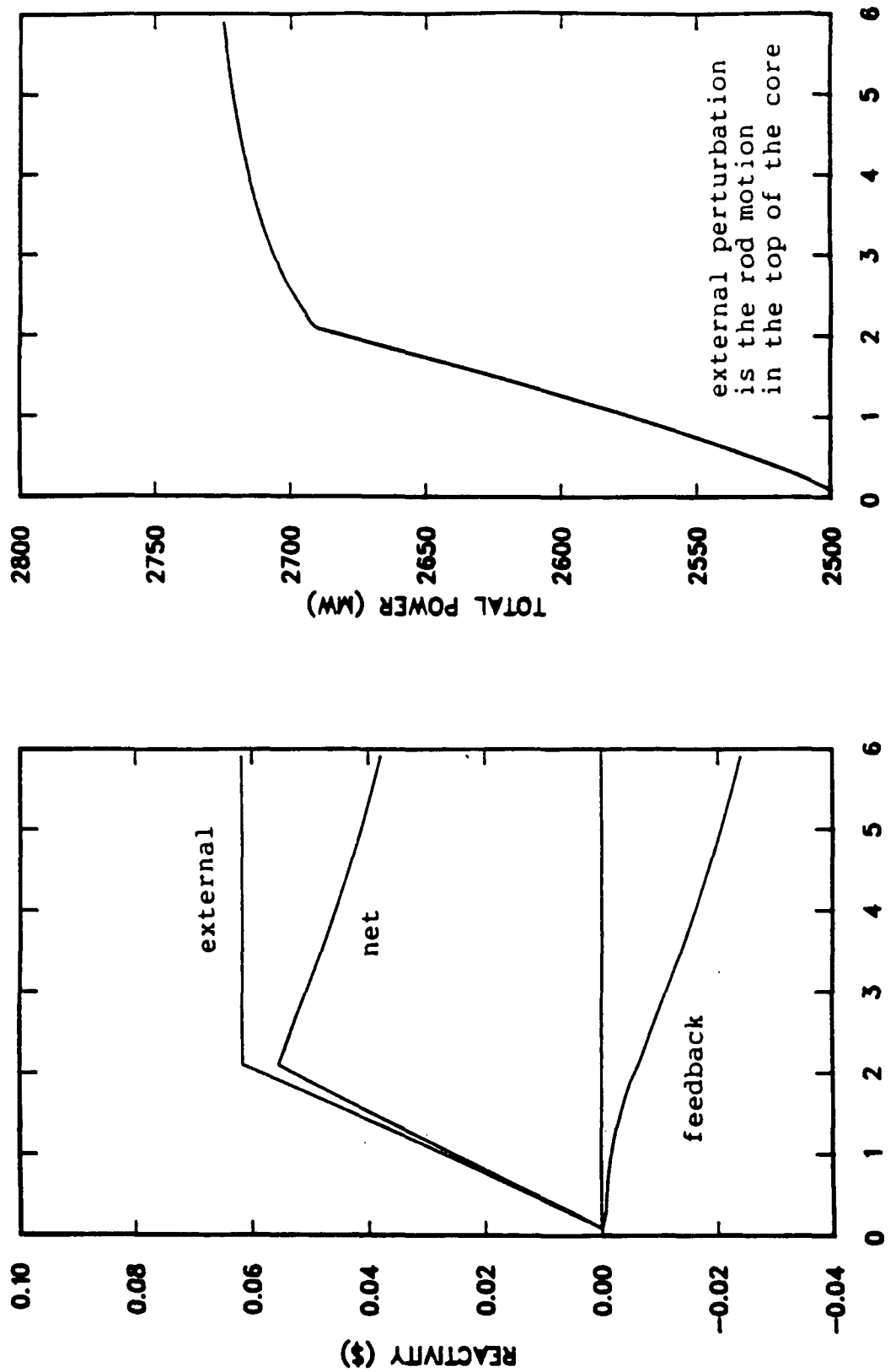

Figure 4.30 Reactivities and power as a function of time obtained from the FX2-TH code.

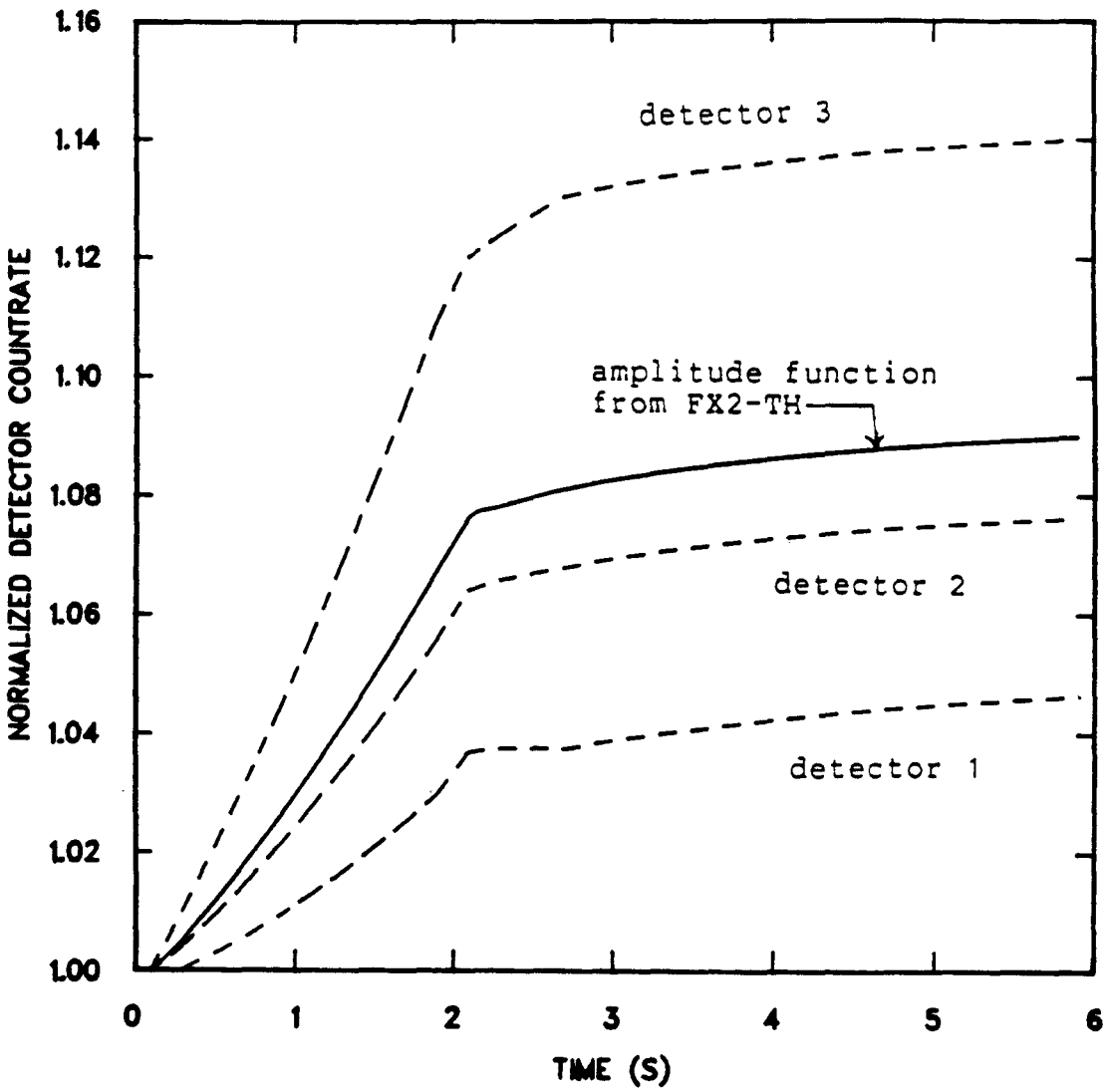

Figure 4.31 Detector signals from detectors 1 through 3 as a function of time.

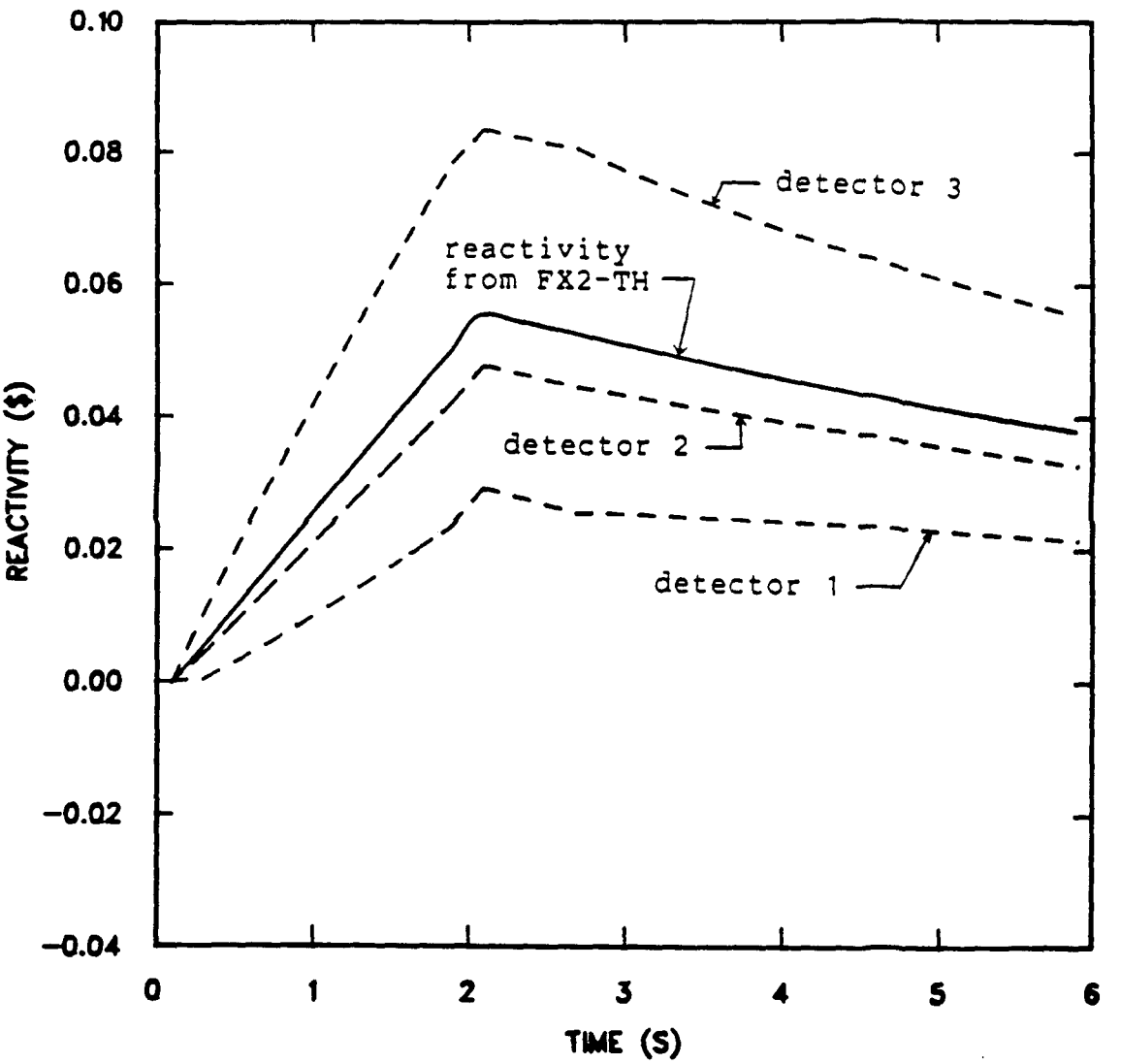

Figure 4.32 Net reactivity with no space-time correction obtained with the inverse kinetics equation.

placed near the rod motion yields a severe overprediction in reactivity. Detector 1 near the bottom of the core produces a severe underprediction, while detector 2, in the center of the core, seems to be located in a region where the shape function changes the least. It is worthwhile to recall that the inverse kinetics equation yields only the net instantaneous reactivity. The individual reactivity components should be obtained in a different manner.

2. Simulation with the Modal-Local Method

For obtaining the necessary parameters for the modal-local analysis of this transient, a set of five forward and adjoint lambda modes were calculated with the 2DBUM code in one-dimensional geometry and two energy groups. We have considered here a larger number of modes because the external perturbation is rather localized, over a 0.1 m mesh in a 4.2 m reactor. A local function due to the control rod motion was calculated corresponding to t=2 s. For times between 0 and 2 s the local function was linearly interpolated in the framework of the modal-local method. In Figs. 4.33 through 4.36 are shown the forward lambda modes and the local function. The normalization of the modes follows the modal orthonormality property.

The reference state chosen for the calculation of the lambda modes was the initial state at t=0 s, before the control rods were moved. It corresponds to a steady-state

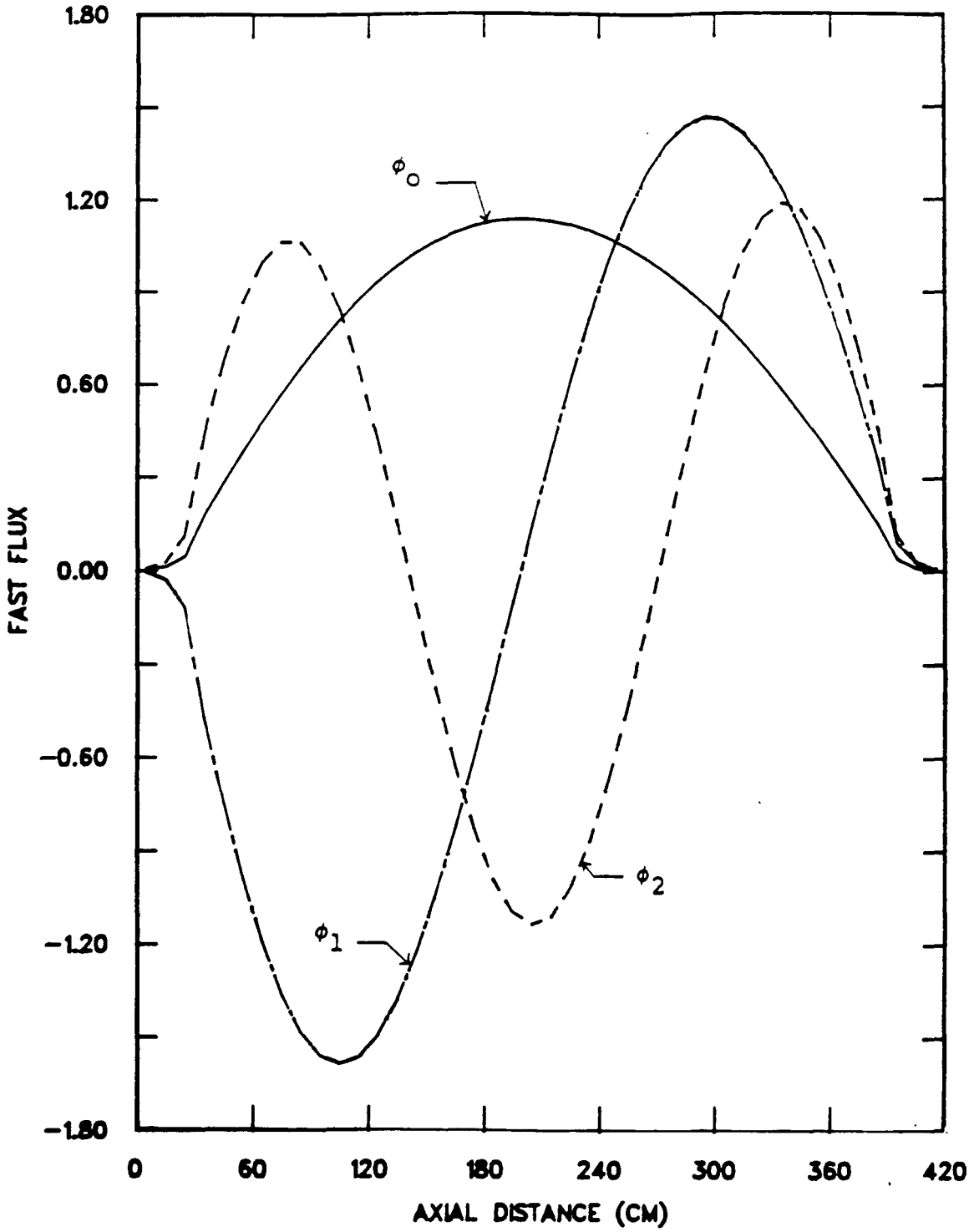

Figure 4.33 Fast lambda modes for the PWR.

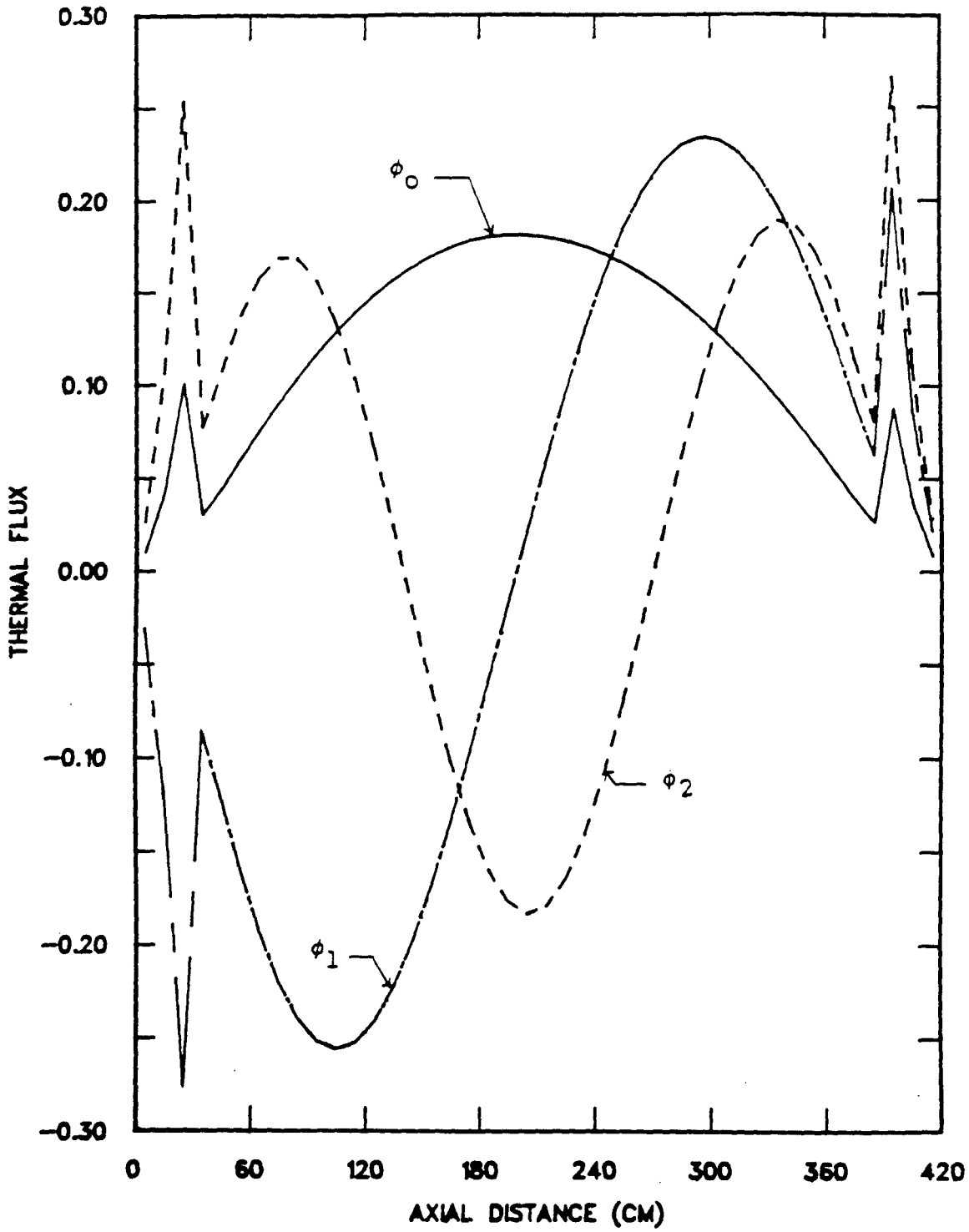

Figure 4.34 Thermal lambda modes for the PWR.

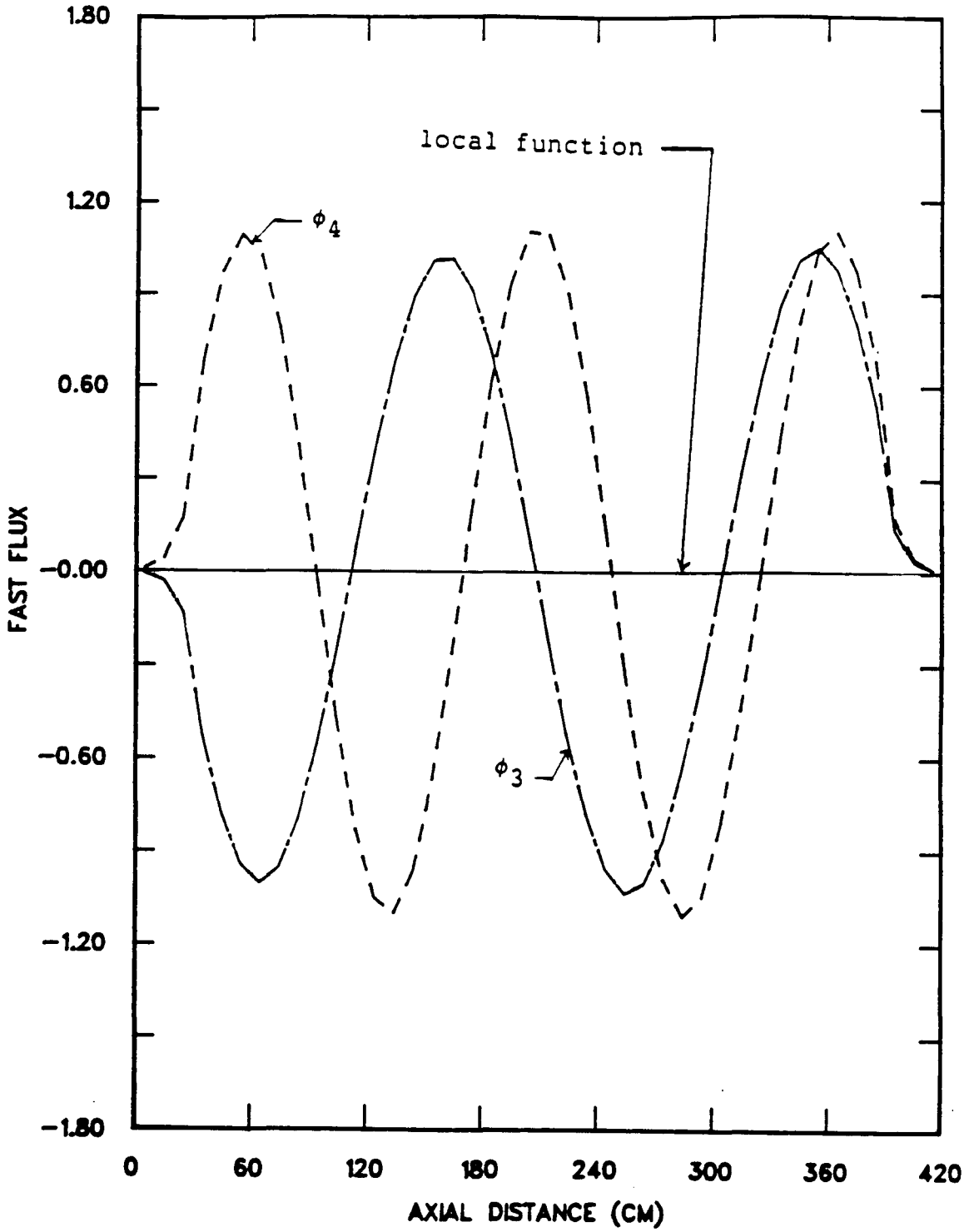

Figure 4.35 Fast lambda modes and local function for the PWR.

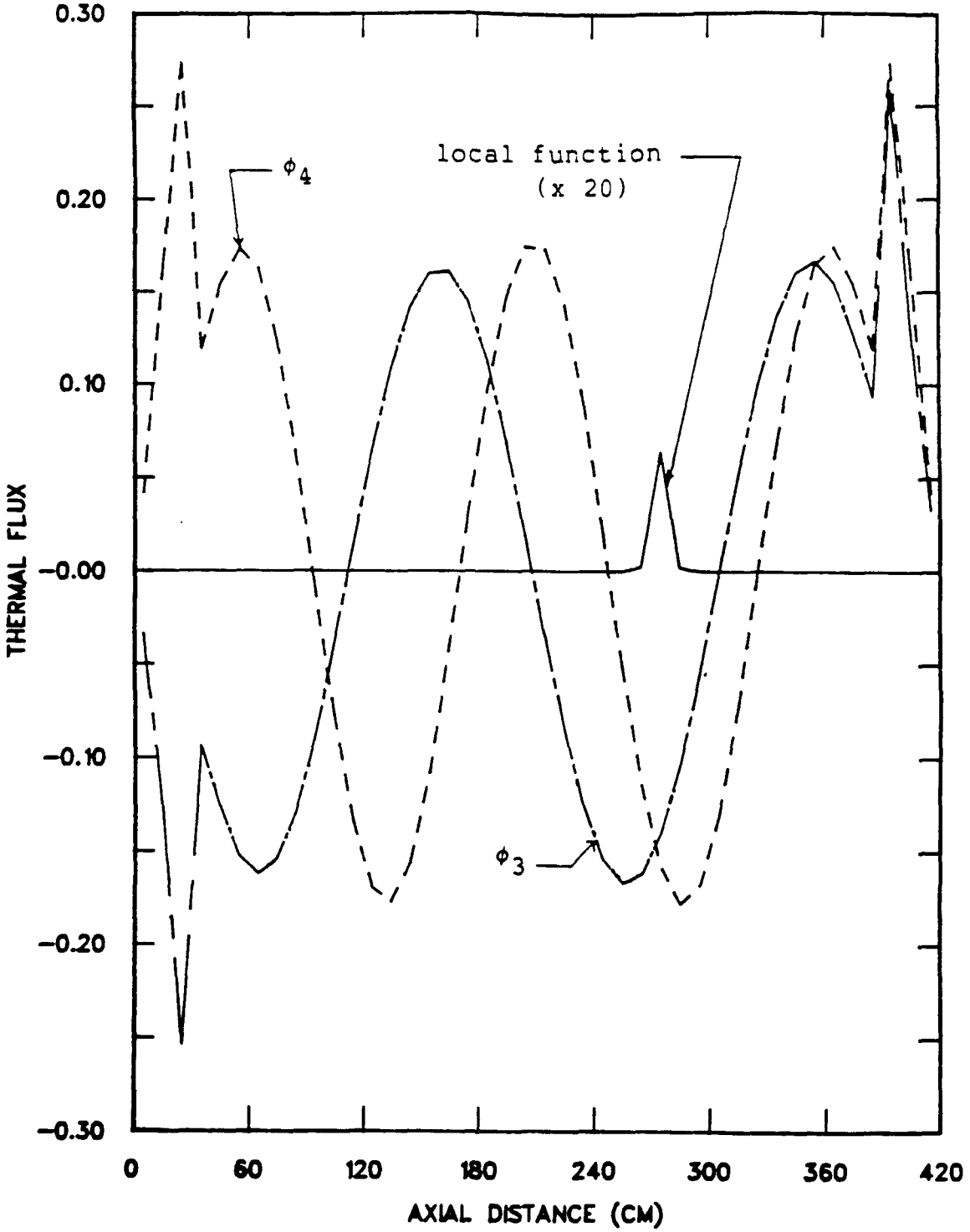

Figure 4.36 Thermal lambda modes and local function for the PWR.

condition with an equilibrium temperature distribution in the core. This condition was obtained through a coupled thermal-hydraulic and neutronic calculation with the FX2-TH code. The lambda modes correspond to the set of cross sections presented in Table 4.9 with the absorption cross sections changed pointwise according to the temperature distribution in the core. The modes are found to be slightly tilted to the bottom part of the core because the fuel and coolant temperatures in the top part of the core are higher. Near the core-reflector interfaces can also be seen the thermal flux peaks due to the increased slowing down of fast neutrons in the reflectors.

The local function is also shown in Figs. 4.35 and 4.36. The rod motion is represented through a change only in the thermal absorption cross section so that the fast local function remains identically zero. Due to the small magnitude of the perturbation and its rather localized nature, the thermal local function has been amplified 20-folds in Fig. 4.36.

The influence of the external perturbation and the thermal hydraulic feedback in the shape function can be estimated by comparing during the transient $f_{pm}(t)$ and $\xi_m(t)$ defined in Sect. III.A. The former represents the contribution of the local function or external perturbation, while the latter the contribution of the feedback effects. In Table 4.10 are shown both f_{pm} and ξ_m as a function of

time for the five modes considered in this simulation. We note f_{pm} increases in magnitude as the rod is moved out of the core and remains unchanged after the rod ceases moving at t=2 s. The term f_{p2} is small throughout the transient because one of the nodal points of ϕ_2 occurs near the perturbation location. The feedback integrals ξ_m grow throughout the transient as the thermal hydraulic feedback effects increase. They remain small for modes 3, 4, and 5, indicating that the perturbation in the shape function due to the feedback is more smooth and gradual. The bulk of the perturbation in the shape function is caused by the rod motion since f_{pm} is greater than ξ_m throughout the transient. The expansion coefficients $a_m(t)$ and a ratio describing the local function contribution to the shape function are shown as a function of time in Table 4.11. The shape function after the rod motion is terminated changes very little indicating the feedback effects on the shape function are minor.

In Fig. 4.37 are shown the correction factors obtained with the modal-local method for the three detectors, with the corrected net reactivity traces shown in Fig. 4.38. The three detectors provide accurate net reactivity traces after the detector correction factors are applied to the countrates. Detector 3 still overpredicts the reactivity somewhat because the correction factor from the modal-local method is slightly smaller than the FX2-TH value. This error is perhaps inevitable because detector 3 is located

Table 4.10

Integrals* as a function of time produced by the modal-local method.

time (s)	f_{po}	f_{p1}	f_{p2}	f_{p3}	f_{p4}	ξ_o	ξ_1	ξ_2	ξ_3	ξ_4
0.0	0.0	0.0	0.0	0.0	0.0	0.0	0.0	0.0	0.0	0.0
1.0	6.6035	5.5165	1.0331	-7.1960	-6.8385	-0.2292	-0.0804	0.0256	0.0386	0.0174
2.0	13.207	11.033	2.0663	-14.392	-13.677	-1.1518	-0.4193	0.1158	0.1853	0.0819
3.0	13.207	11.033	2.0663	-14.392	-13.677	-3.4844	-0.9474	0.2355	0.3959	0.1643
4.0	13.207	11.033	2.0663	-14.392	-13.677	-3.6451	-1.4616	0.3388	0.5882	0.2259
5.0	13.207	11.033	2.0663	-14.392	-13.677	-4.6252	-1.9425	0.4288	0.7654	0.2721
6.0	13.207	11.033	2.0663	-14.392	-13.677	-5.4380	-2.3828	0.5058	0.9255	0.3058

* The rod motion and the thermal hydraulic feedback are represented by f_{pn} and ξ_n, respectively.

Table 4.11

Modal expansion coefficients for $h(\underline{r},E,t)$, and a local function ratios produced by the modal-local method.

time (s)	a_o	a_1	a_2	a_3	a_4	$\frac{\langle \phi_o^\dagger, \frac{1}{v} f(t) \rangle^*}{\langle \phi_o^\dagger, \frac{1}{v} \psi(t) \rangle}$
0.0	1.0	0.0	0.0	0.0	0.0	0.0
1.0	0.9998	0.0095	0.0009	-0.0036	-0.0022	2.4-4
2.0	0.9995	0.0199	0.0019	-0.0074	-0.0041	4.9-4
3.0	0.9995	0.0202	0.0021	-0.0075	-0.0045	4.9-4
4.0	0.9995	0.0199	0.0022	-0.0074	-0.0045	4.9-4
5.0	0.9995	0.0197	0.0023	-0.0074	-0.0045	4.9-4
6.0	0.9995	0.0193	0.0023	-0.0073	-0.0046	4.9-4

* This ratio can be intrepreted as the contribution of the local function to the shape function.

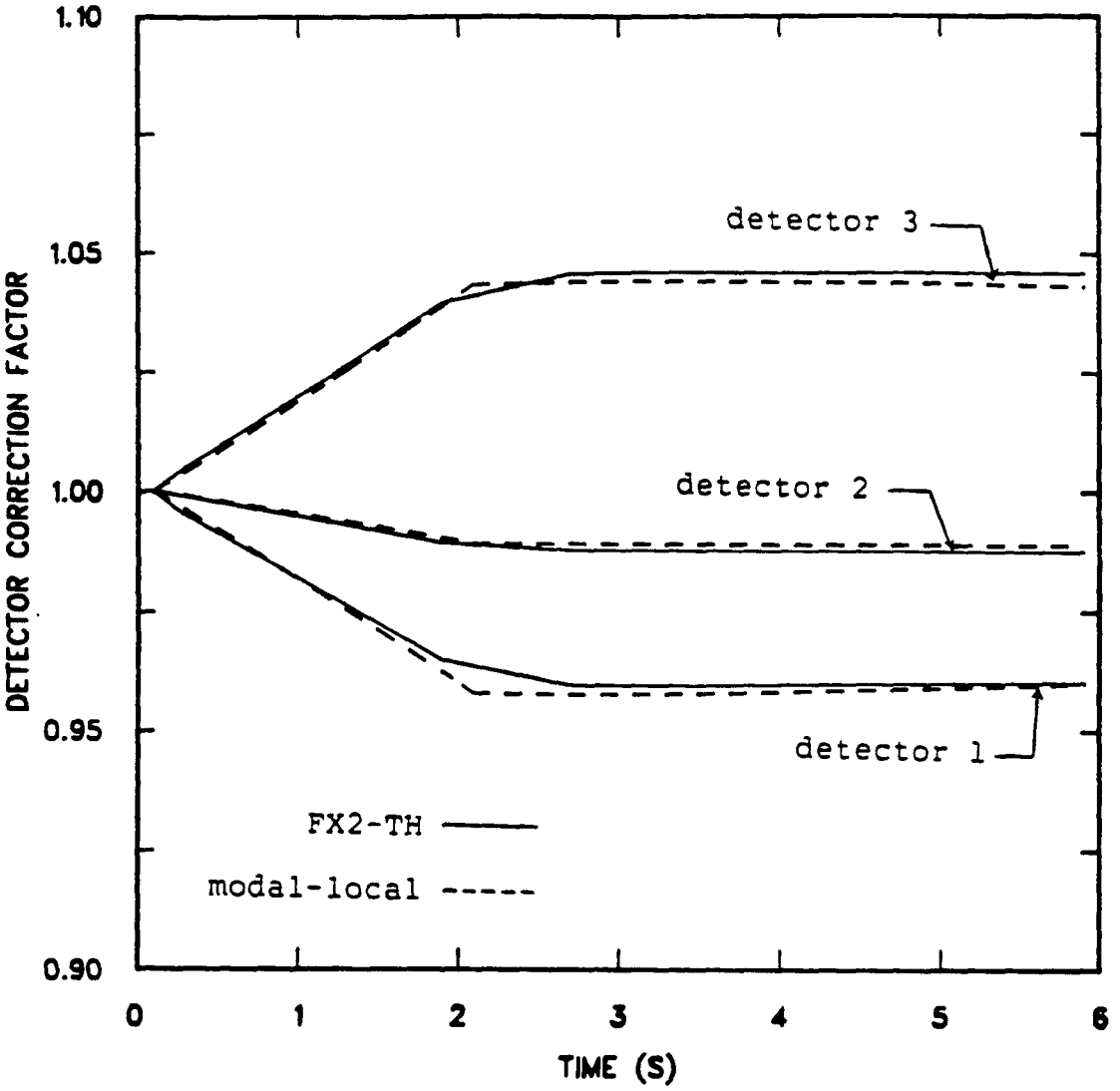

Figure 4.37 Correction factors as a function of time for detectors 1 through 3.

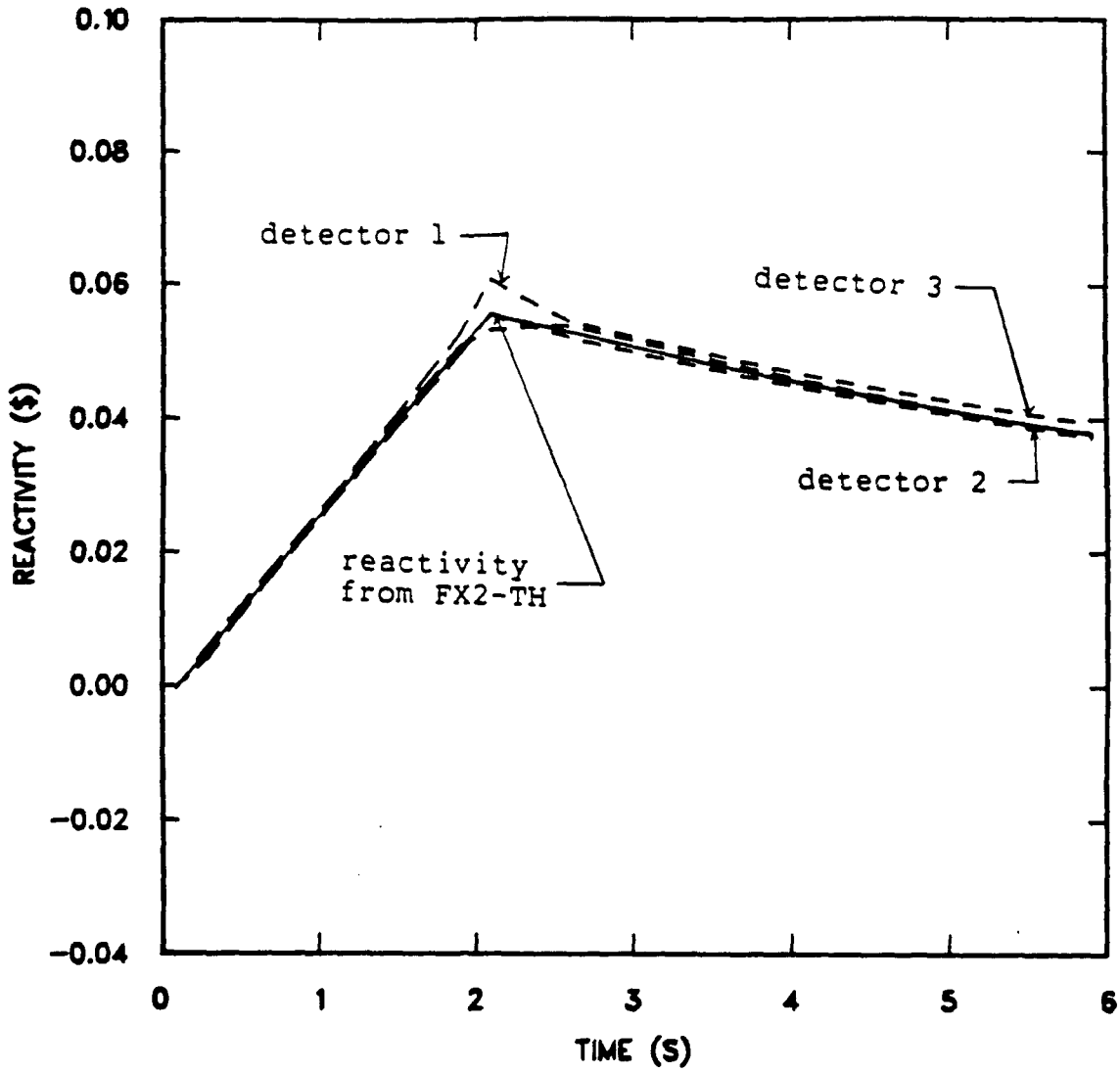

Figure 4.38 Corrected net reactivity as a function of time given by the modal-local method.

very near the control rods motion. The correction factor for detector 1 shows a visible error around t=2 s causing the discrepancy seen in the net reactivity trace of Fig. 4.38.

The feedback reactivity is estimated through Eq. (12b) of Chapter III with the perturbation operators and shape function produced by the modal-local method. For the purpose of finding a unique control rod reactivity during the transient we take the average of the three net reactivity traces presented in Fig. 4.38. Another possible procedure would be taking an average of the amplitude functions from the several detectors an then with it obtain a unique reactivity. The external reactivity is found as the difference between the averaged net reactivity and the feedback reactivity. In Table 4.12 are compared the reactivity components and the net reactivity from the modal-local method and the FX2-TH code at several points during the transient. In Fig. 4.39 the net reactivity, the feedback reactivity, and the external reactivity obtained with the modal-local method are also compared with those from the FX2-TH code. In Table 4.12

In Figs. 4.40 and 4.41 are compared the shape function at t=0 and t=6 s obtained from the modal-local method with those from the FX2-TH code. It is seen that apparently small redistribution in neutron flux can not be neglected in an inverse kinetics analysis. The rather localized

Table 4.12

Comparison of the net reactivity and its components between the modal-local method and the FX2-TH code.

time (s)	FX2-TH			modal-local		
	ρ_{net}	ρ_{feed}	ρ_{ext}	ρ_{net}	ρ_{feed}	ρ_{ext}
0.0	0.0	0.0	0.0	0.0	0.0	0.0
1.0	0.0280	-0.0018	0.0298	0.0283	-0.0015	0.0298
2.0	0.0555	-0.0061	0.0617	0.0565	-0.0061	0.0626
3.0	0.0502	-0.0150	0.0617	0.0506	-0.0117	0.0624
4.0	0.0452	-0.0165	0.0617	0.0455	-0.0166	0.0621
5.0	0.0408	-0.0209	0.0617	0.0411	-0.0207	0.0617
6.0	0.0371	-0.0241	0.0617	0.0373	-0.0240	0.0612

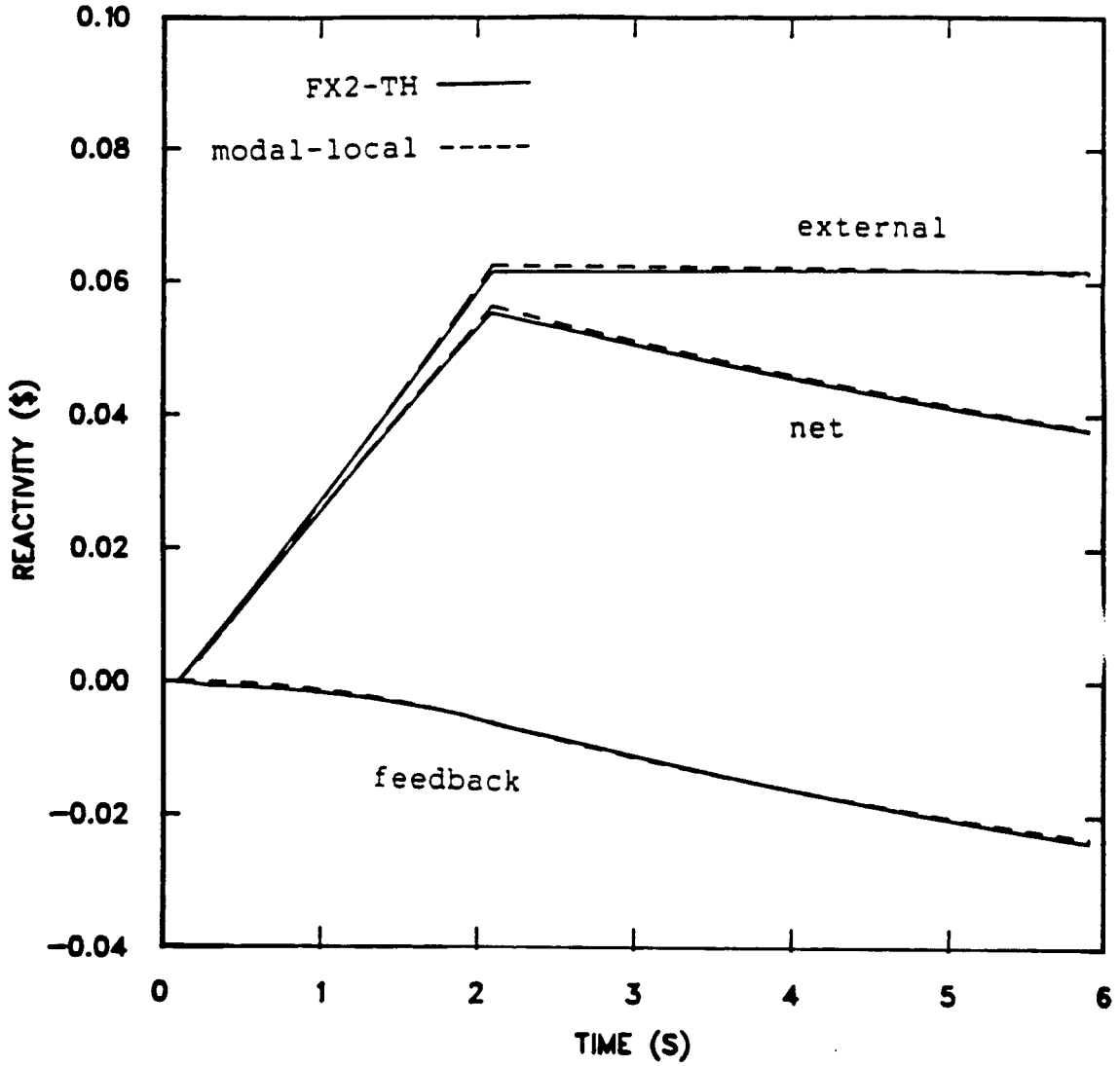

Figure 4.39 Comparison of net and component reactivities between the modal-local method and the FX2-TH code.

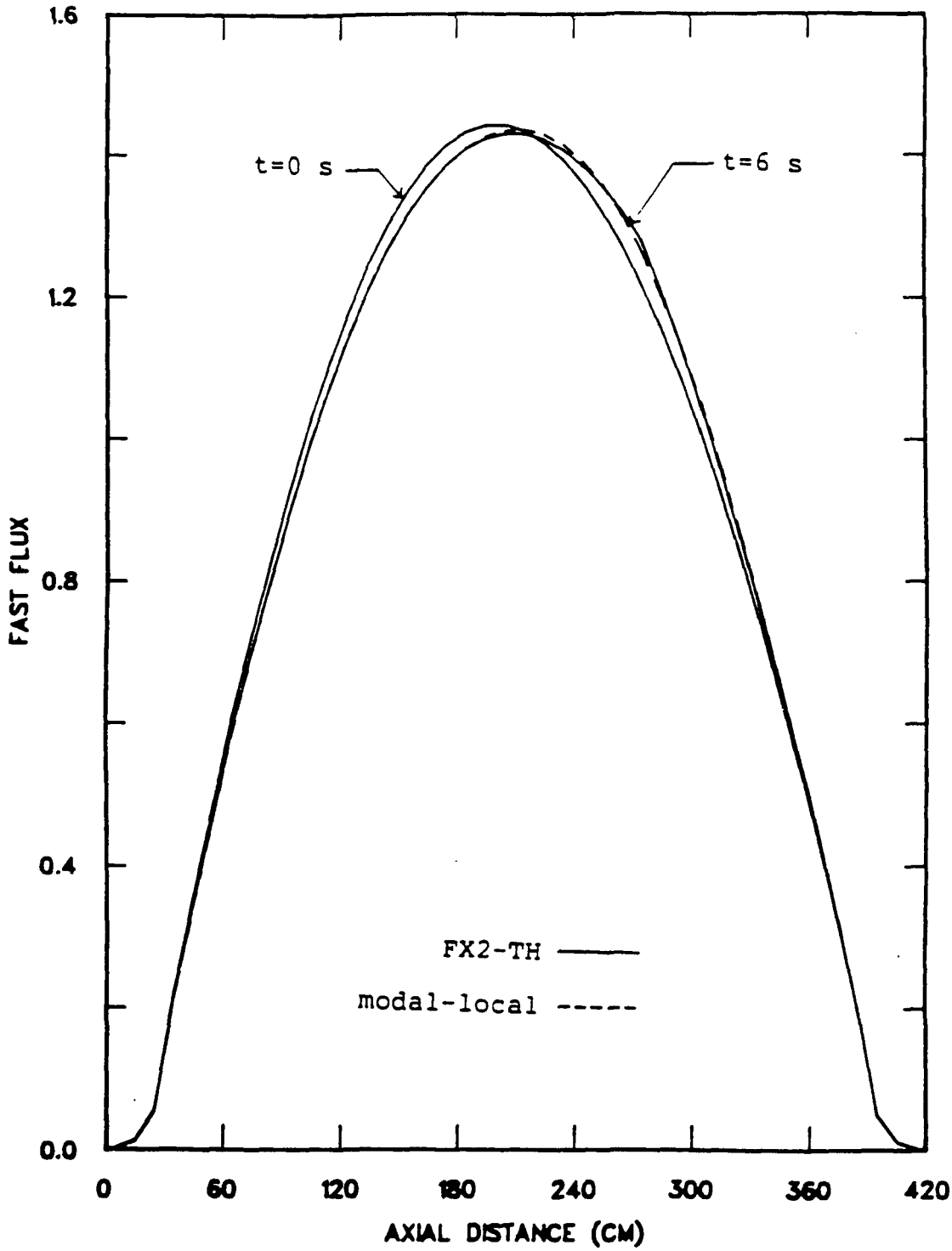

Figure 4.40 Comparison of the fast shape function between the modal-local method and FX2-TH code at the end of the transient.

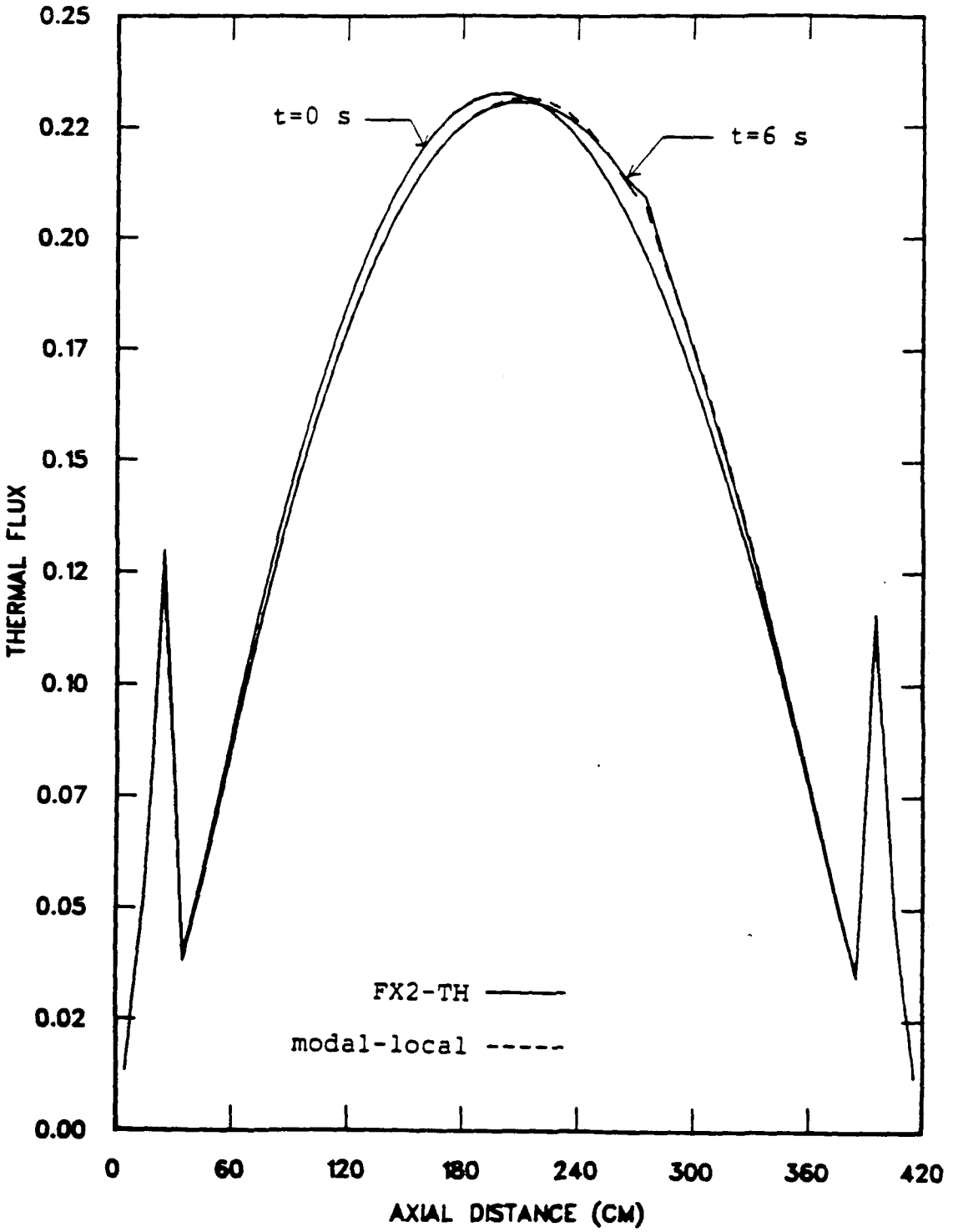

Figure 4.41 Thermal shape function comparison between the modal-local method and FX2-TH code at the end of the transient.

perturbation in the core causes a tilt in the flux toward the top of the core, and locally, a bump is seen in the thermal flux profile which is represented by the local function of Fig. 4.36. The kinetics parameters from the modal-local method essentially remained constant during the transient and coincide with those from the FX2-TH code.

3. Analysis of the Results

In this transient the kinetics parameters did not change, so the only source of error in the reactivity is in the amplitude function. That is the ratio $y=\frac{n}{\Lambda}$, introduced in the previous section, is here subject only to errors in the amplitude function n(t). The errors in the n(t) estimates come from the small discrepancies in the modal-local correction factors shown in Fig. 4.37.

In Table 4.13 are shown the the relative errors, at the end of the transient, in the estimated amplitude functions and net reactivities for the three detectors, compared with the FX2-TH results. The reactivity is very sensitive to small errors in the estimated amplitude function because the total reactivity change is small, of the order of few cents. The average reactivity components obtained from the three detectors are accurate to 0.5 %.

In power reactors determination of not only the detector correction factors but also the reactivity components depends on how well the shape function can be

Table 4.13

Errors in the amplitude function and reactivity between the modal-local method and the FX2-TH code at the end of transient.

detector	error in n(t) (%)	error in $\rho_{net}(t)$ (%)
1	-0.05	-1.1
2	-0.13	-1.5
3	0.25	3.8
Error of the average net reactivity = 0.41 %.		
Error of the feedback reactivity = 0.5 %		

predicted during the transient. The feedback reactivity, in particular, requires that the thermal hydraulic model be accurate. In Fig. 4.42 are shown the change in the fuel and coolant temperature at the end of the transient. The thermal hydraulic model adopted in the modal-local method has reproduced the FX2-TH results with a fair degree of accuracy. The maximum change in fuel temperature takes place around the region of greatest neutron flux increase during the transient. The coolant temperature is increased as the coolant flows upward along the channel.

In Figs. 4.43 and 4.44 are illustrated the perturbations in the shape functions at the end of the transient. The modal-local method has predicted very accurately the perturbation despite the discrepancies in the fuel and coolant temperature distributions. This is because the influence of the thermal hydraulic feedback on the shape function is small as was shown in Table 4.10 in which f_{pm} are much greater than ξ_m.

The utility of the local function can once more be seen in Fig. 4.44 for the perturbation in the thermal shape function. Without the inclusion of the local function the error near the control rods would be much larger. In Fig. 4.43 there is no local function component for the fast shape function because it is identically zero for the fast group. The perturbation in the operators M_p and L was

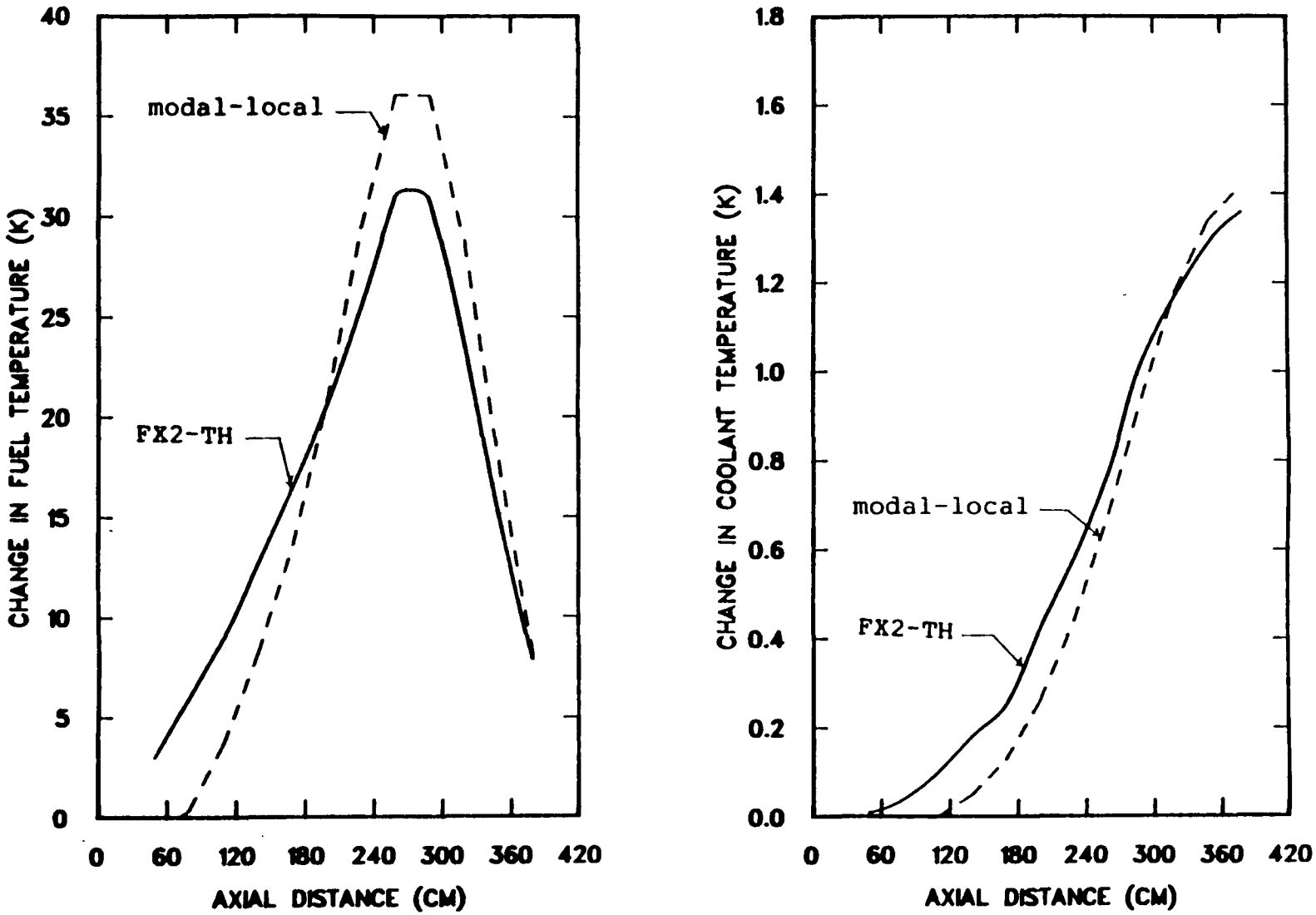

Figure 4.42 Perturbation in fuel and coolant temperature between the beginning and end of the transient.

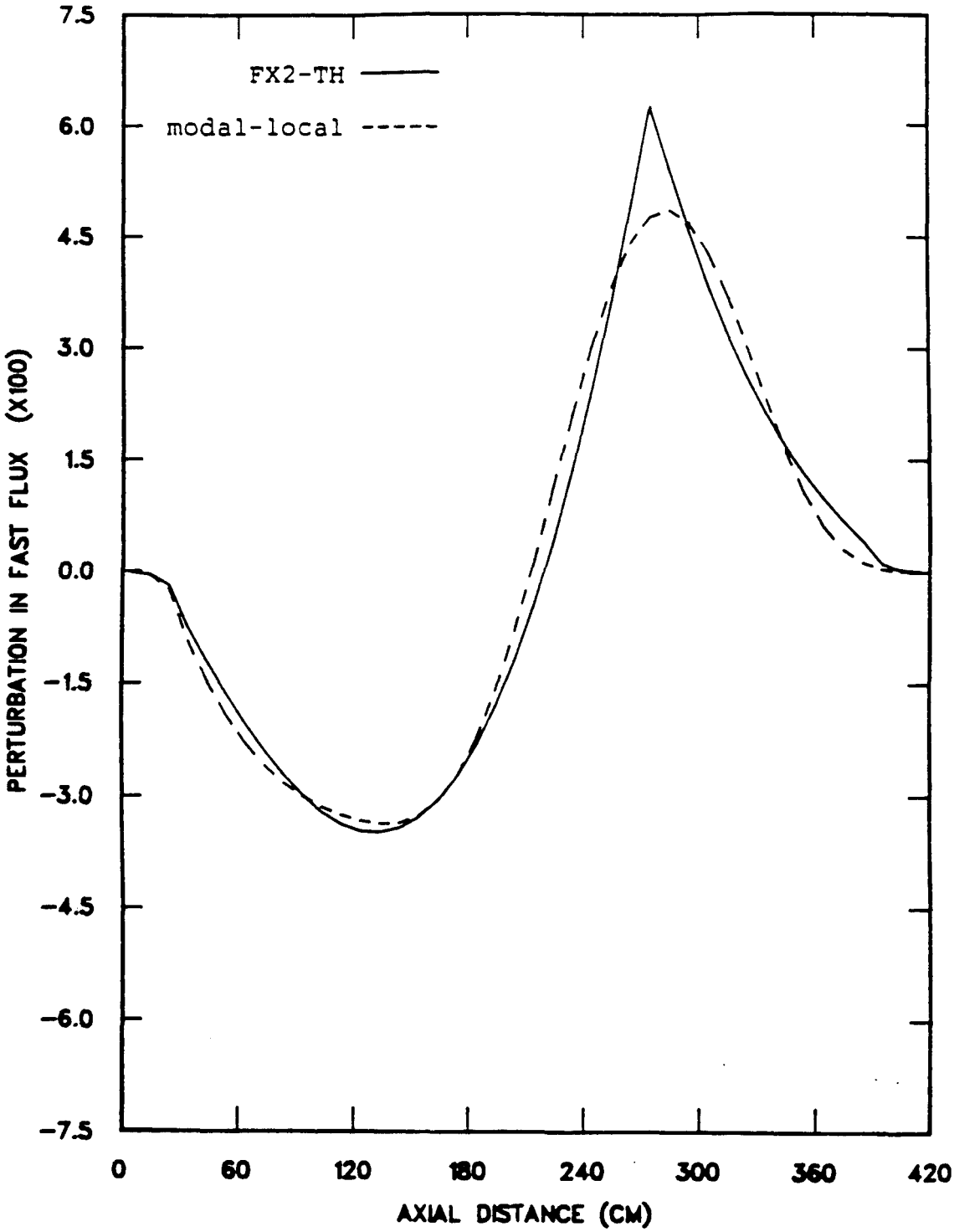

Figure 4.43 Perturbation in the fast shape function between the beginning and end of the transient.

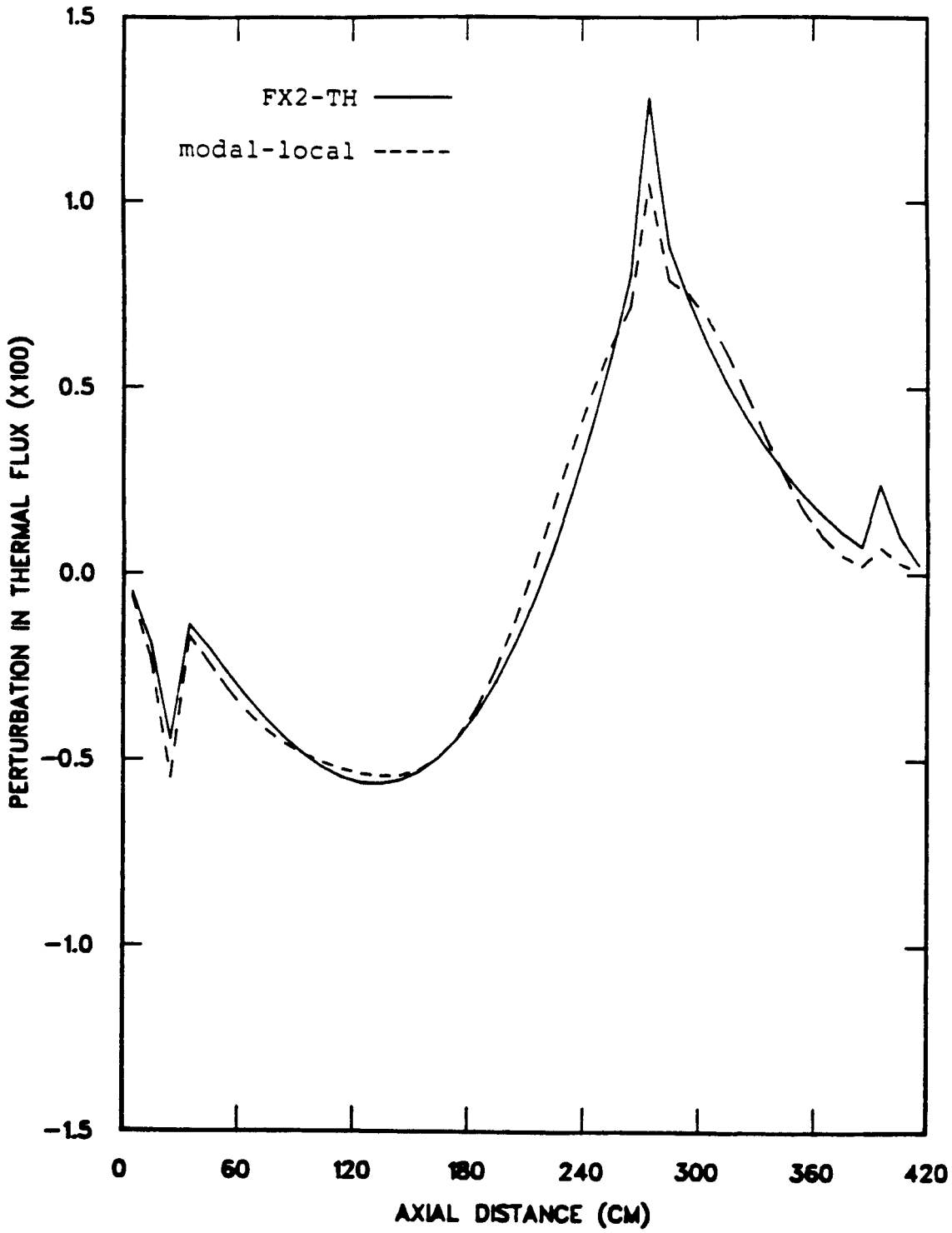

Figure 4.44 Perturbation in the thermal shape function between the beginning and end of the transient.

restricted to the thermal absorption cross section in our model.

It is seen in Fig. 44 that near the rod motion the modal-local method could not predict very well the shape function even with the inclusion of the local function. The estimation of the external reactivity component through Eq. (12) of Chapter II will result in large errors. Therefore, the external reactivity has been obtained in an indirect way through determination of the feedback component of the reactivity.

Having completed evaluation of the accuracy of the modal-local method in various situations we move to Chapter V where an application of the method is carried out for determining both integral and differential rod worths from actual measurements.

CHAPTER V

ANALYSIS OF THE KAHTER ROD-WORTH MEASUREMENTS

In this chapter we present analysis of rod worth measurements with the modal-local method. The rod-drop experiments were performed with the top-reflector control rods at the KAHTER facility in 1979. The data showed a large neutron flux redistribution during the measurements, and, hence, are a good test for the modal-local method. The previous analysis[31] of of the KAHTER reactivity data obtained the correction factors for the detectors through static eigenvalue calculations for the rodded and unrodded KAHTER configurations alone. Although this technique corresponds to an adiabatic approximation[34] in the space-time analysis, it appears to have provided a rather accurate means of accounting for the detector position dependence of the reactivity data. For analysis of partially inserted rod worth data, this adiabatic treatment would require static eigenvalue calculations at several intermediate reactor configurations, making the method rather impractical to apply. This indeed was one of the primary considerations in initiating the present investigation.

The rod-drop experiments performed with the top-reflector rods of the KAHTER facility have been simulated with the FX2-TH code in Chapter IV. The simulation demonstrated that the motion of the top-reflector rods excite primarily the first higher harmonic mode which is the first axial mode. The second harmonic mode, the first radial mode, was not excited because the rod motion happened to be near its nodal line.

Based on these results we can expect that the lambda modes obtained in Sect. IV.B for the KAHTER facility with the CITATION code will be sufficient to estimate the modal function $h(\underline{r},E,t)$. The CITATION calculations were done in a three-dimensional r-z-θ geometry with six energy groups with the rodded configuration as the reference state. The two modes obtained for the KAHTER facility are the fundamental and the first axial harmonic modes.

The local function was obtained for twelve intermediate rod positions representing the rod insertion as a function of time. The time-dependent shape function obtained by the modal-local method provided the correction factors needed for the utilization of detector signals as the amplitude function in the inverse kinetics routine. In Sect. A we describe briefly the rod-drop experiments and the location of the detectors used in the tests, followed by the results and discussion of our analysis in Sects. B and C.

A. A Brief Description of the Rod Worth Measurements

Rod drop experiments were carried out at the KAHTER facility with the flux distribution monitored by neutron detectors placed at several locations in the core and in the reflectors. The KAHTER facility has several axial and radial channels for measurements as shown in Fig. 5.1. In the axial channels the detectors can scan the core almost from top to bottom. The detector countrates taken at channels A4, A6, A7, and A8 at different axial locations were analyzed. For the integral rod worth analysis the detector signals obtained at axial positions, 0.4, 1.2, 1.8, and 2.4 m from the bottom of the core, were investigated. The detector locations are shown in a side view of the KAHTER facility in Fig. 5.2. More details on the measurement system of KAHTER may be found in Ref. 32.

In all the rod drop experiments considered here, the bank of 8 top reflector control rods was inserted into the core, with collection of the data lasting 10 s. The rod insertion in the case of the integral rod worth measurements took place over a period of about 4 s. The counts were accumulated in intervals of 20.016 ms and a detector dead time of 1.5 μs was accounted for in our analysis.

B. Space-Time Analysis of the Rod Worth Data

For this application of the coupled modal-local method we considered the countrate data for the integral rod worth

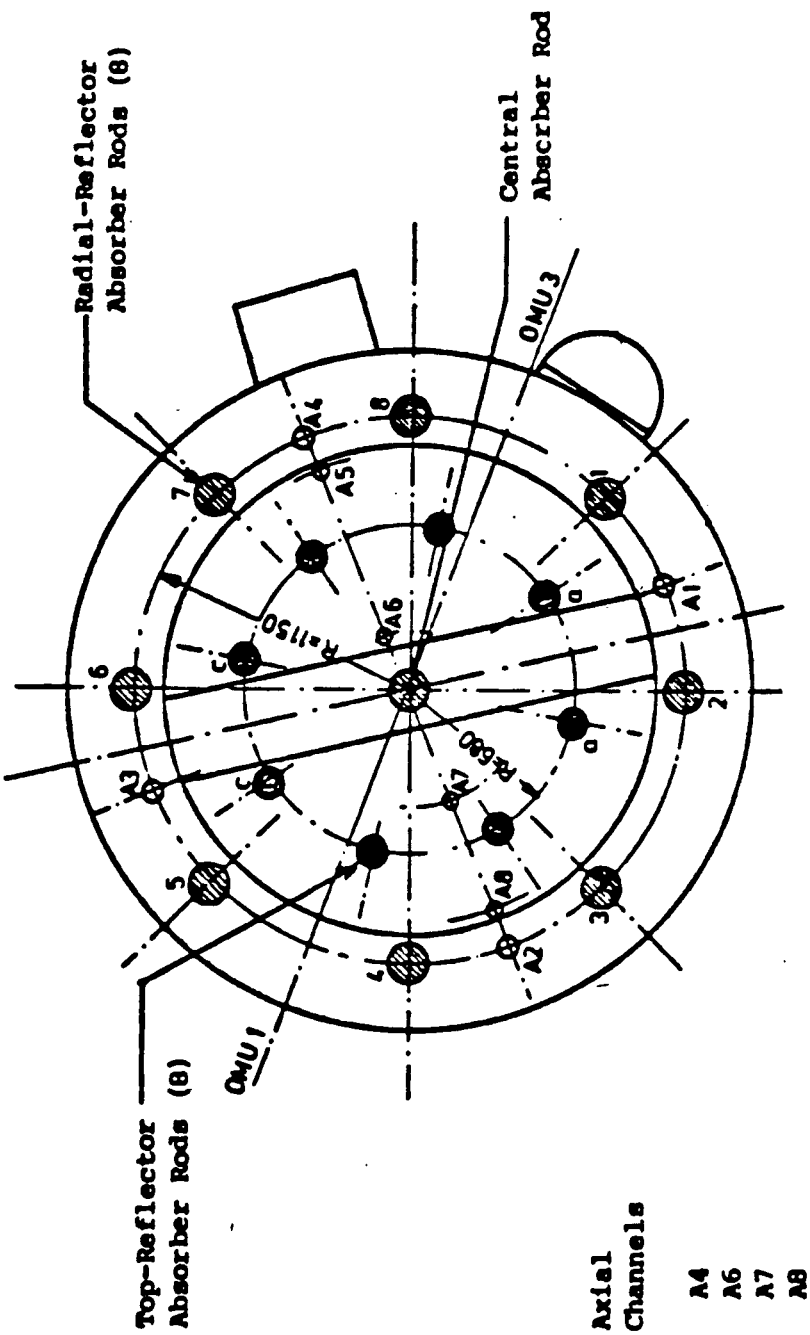

Figure 5.1 Detector channel layout for the KAHTER facility, top view.

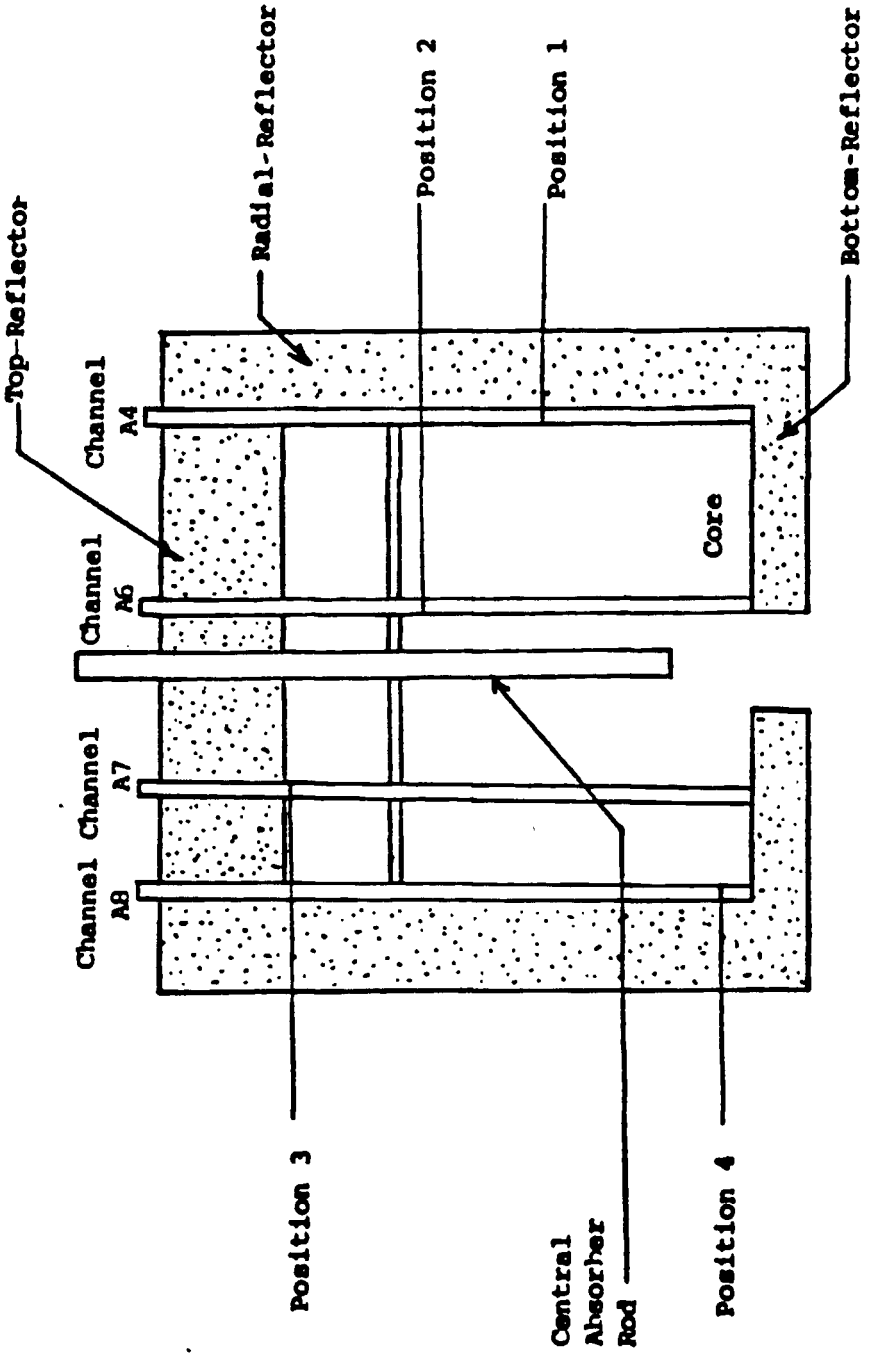

Figure 5.2 Detector locations at the KAHTER facility, side view.

measurements collected at the channels A4, A6, A7, and A8. The detectors were located successively at 0.4, 1.2, 1.8, and 2.4 m from the bottom of the core. The countrates as a function of time for the rod positions 1 to 4 are shown in Fig. 5.3. The integral rod worths obtained by feeding the countrates directly into the inverse kinetics routine are shown in Table 5.1. The tabulated reactivity worths are obtained by averaging the reactivity values, following the complete insertion of the rods, over a period between 7.6 s and 9.6 s from the beginning of the transient. The standard deviations associated with the statistical fluctuations in the time-averaged reactivity worths are also shown in Table 5.1.

The reactivity worths as a function of time are plotted in Fig. 5.4 for all four detector in channel A4 at height of 1.2 m, in A6 at 1.8 m, in A7 at 2.4 m and in channel A8 at 0.4 m corresponding to positions 1 through 4 in Fig. 5.2. Fluctuations in the countrates and reactivity worths, in addition to the dependence on detector position, are readily recognizable in Fig. 5.4 and Table 5.1. It is interesting to notice that the relatively small variations in the countrates for the different detectors produced rather large discrepancy in reactivity, showing how sensitive the inverse kinetics equation is to the amplitude function.

While calculating the local function for the unrodded state, we noticed that it was essentially non-zero only in

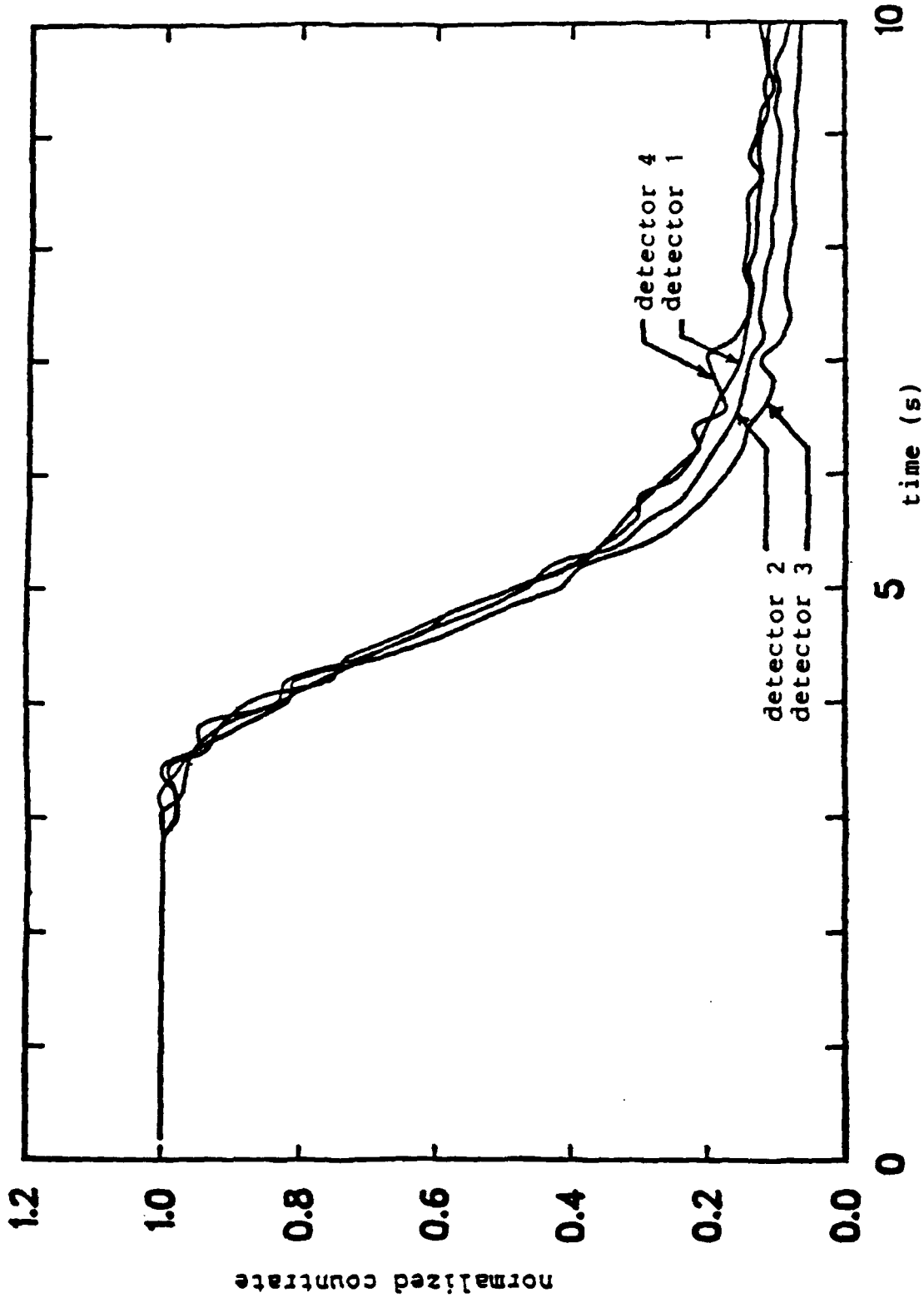

Figure 5.3 Countrates vs. time for integral rod worth measurements.

Table 5.1

Integral rod worths without space-time correction.

Axial Detector Location (m)	Reactivity ($) + Standard Deviation ($)			
	Channel A4	Channel A6	Channel A7	Channel A8
0.4	3.392 ± 0.215	3.264 ± 0.279	3.295 ± 0.227	3.311 ± 0.392
1.2	3.482 ± 0.135	3.533 ± 0.125	3.538 ± 0.110	3.628 ± 0.155
1.8	4.290 ± 0.201	4.319 ± 0.135	4.375 ± 0.111	4.162 ± 0.244
2.4	5.421 ± 0.289	5.445 ± 0.219	5.977 ± 0.284	5.657 ± 0.194

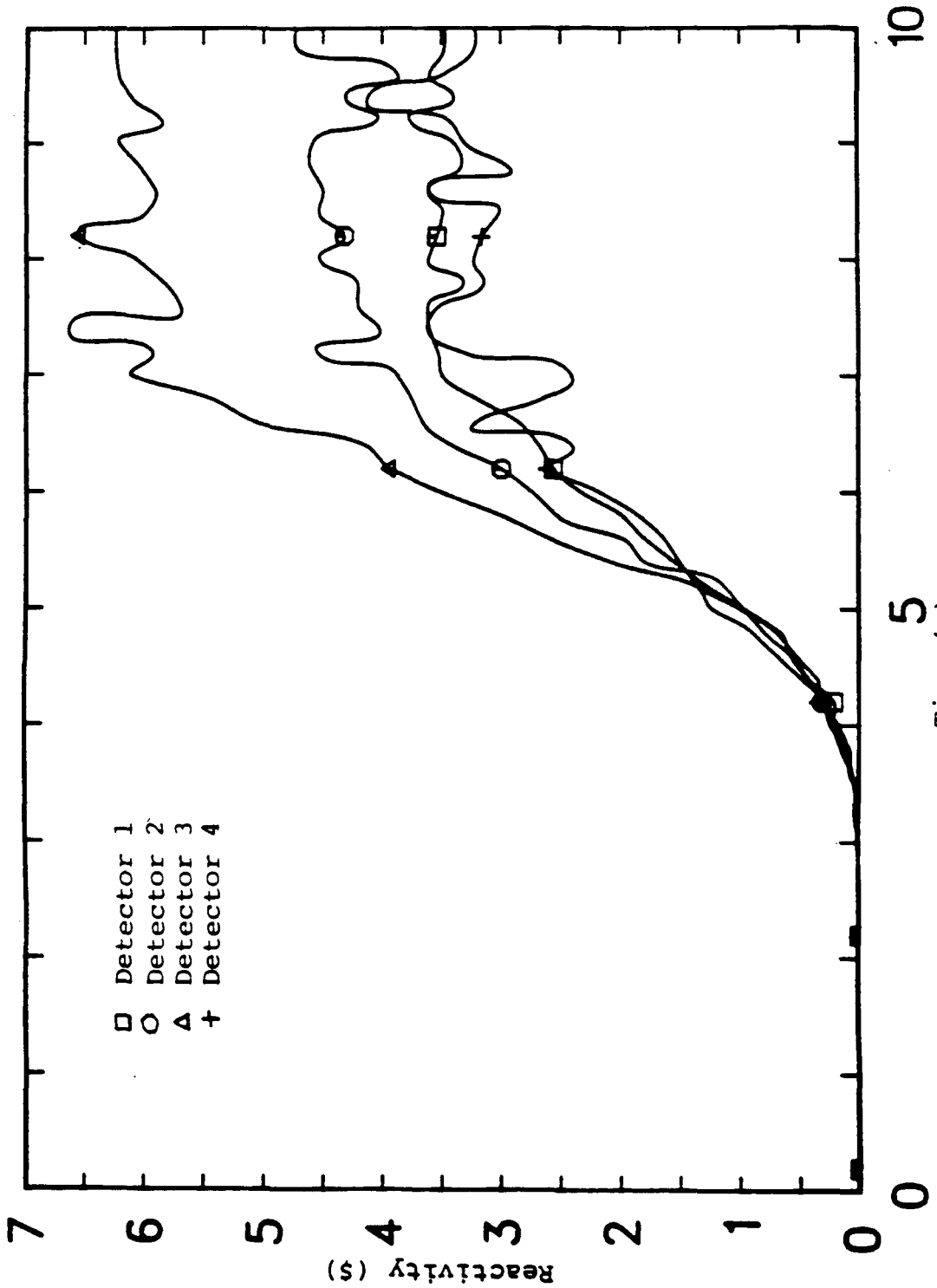

Figure 5.4 Integral rod worths vs. time without space-time correction.

the top part of the core, near the vicinity of the rod motion.. Taking advantage of this fact, we considered only the top half of the KAHTER facility in the calculation of the local function for twelve intermediate rod positions. In Figs. 5.5 through 5.8 are shown the local function for t = 0 s, 1 s, 2 s, and 3 s, respectively, calculated with the CITATION code in six energy groups and r-z-θ geometry. The rather localized effect of the rod withdrawal is illustrated clearly by the peaks in the distributions.

The detector correction factors obtained with the modal-local method are presented in Fig. 5.9. It can be seen in this figure that the shape function tilted to the bottom of the core as the rods were inserted. The detectors at the top of the core have correction factors smaller than 1 and those at the bottom, greater than 1, in accordance with the tilting. In the middle of the core there may be a surface where the shape function does not change appreciably and, therefore, yields correction factors $\simeq$ 1. This surface is the best location for in-core detectors, and may be near the nodal line of the first harmonic. The corrected integral rod worths are presented in Fig. 5.10 and Table 5.2. They clearly indicate that we are able to eliminate, to all practical purposes, the detector position dependence from the reactivity data. These results are in substantial agreement with the space-time corrected results, in particular, with the time-averaged reactivity of 3.91\$ $\pm$ 3% obtained through adiabatic calculations in Ref. 31.

First (Fast) Group

Sixth (Thermal) Group

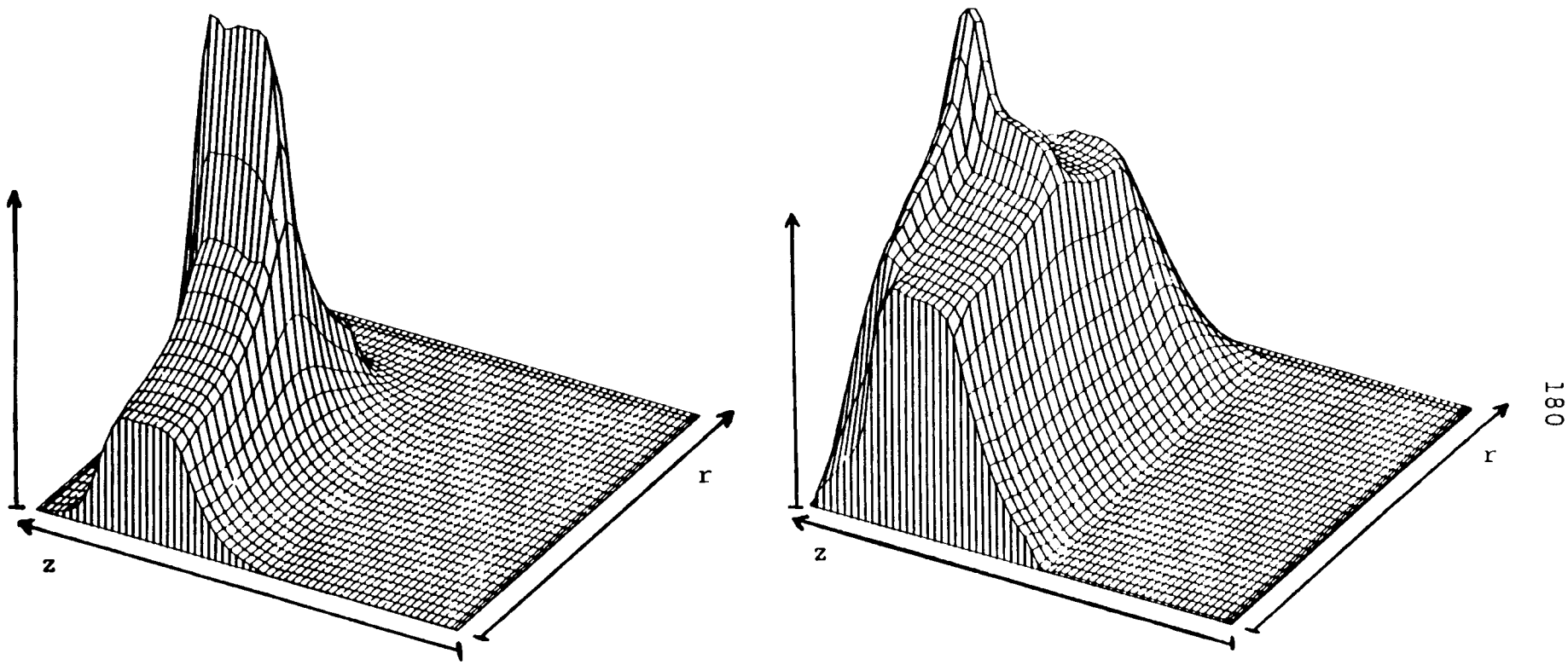

Figure 5.5 Local Function for Rod-Drop Experiment, Rods Withdrawn, t = 0 s.

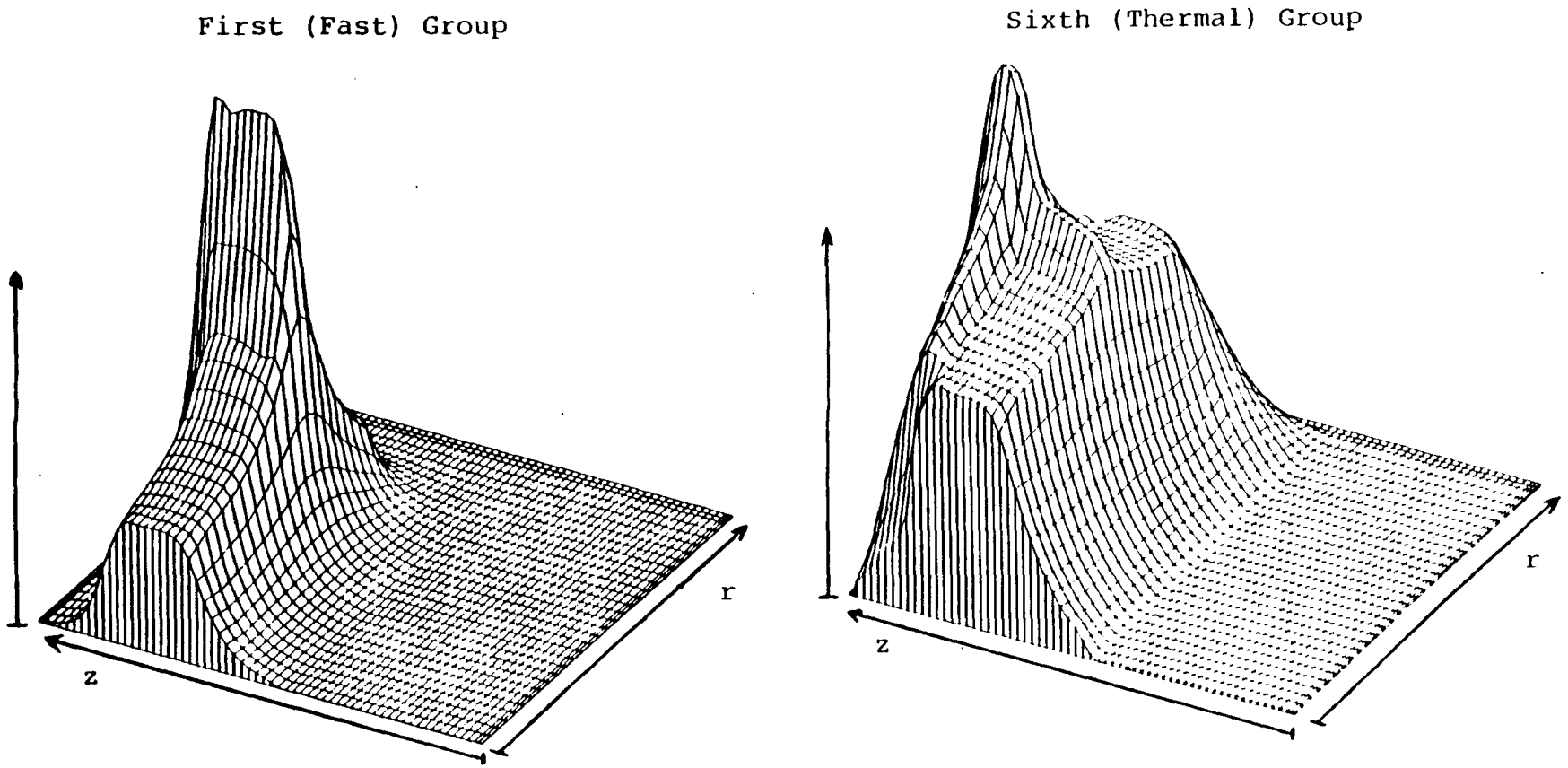

Figure 5.6 Local Function for Rod-Drop Experiment, t = 1 s into the transient.

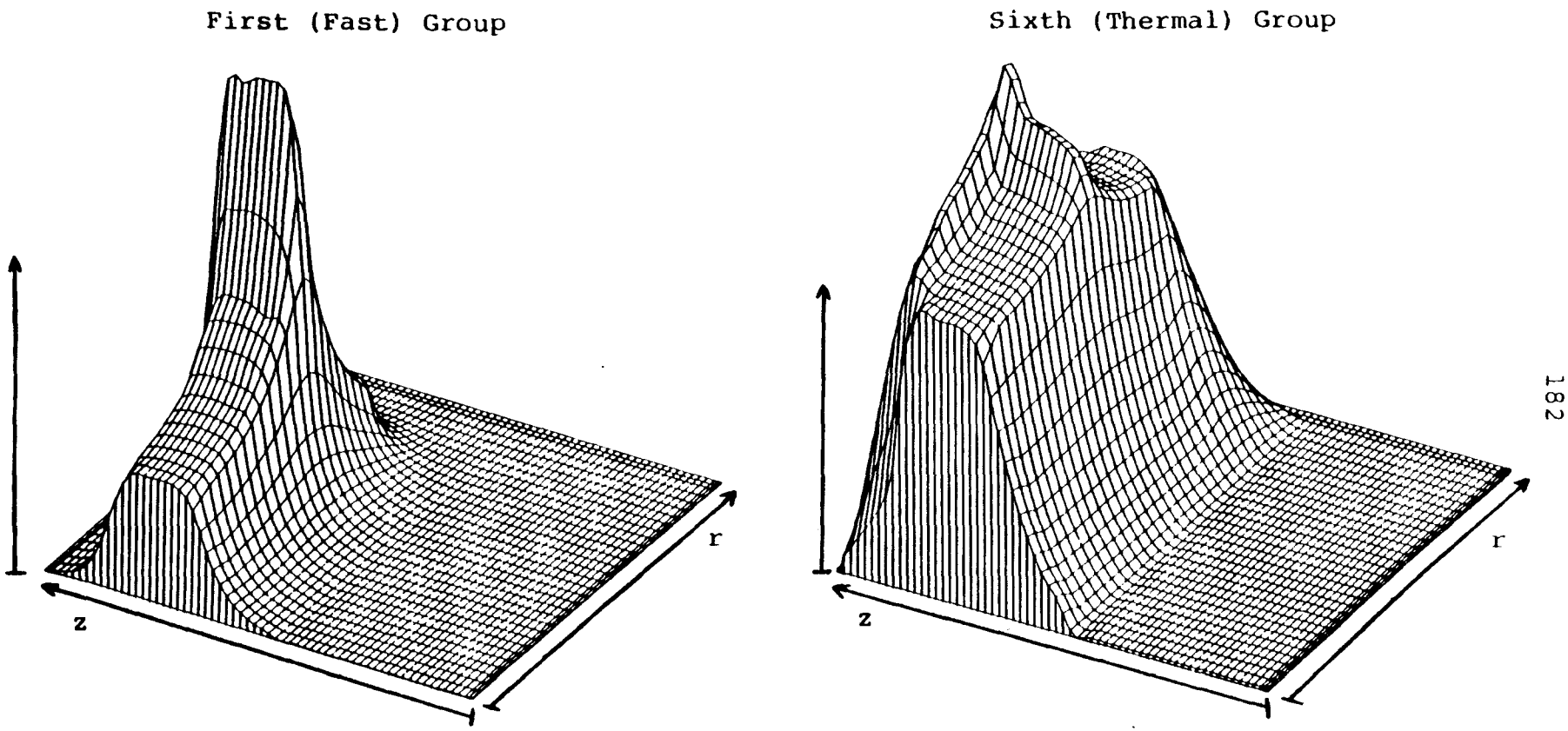

Figure 5.7 Local Function for Rod-Drop Experiment, t = 2 s into the transient.

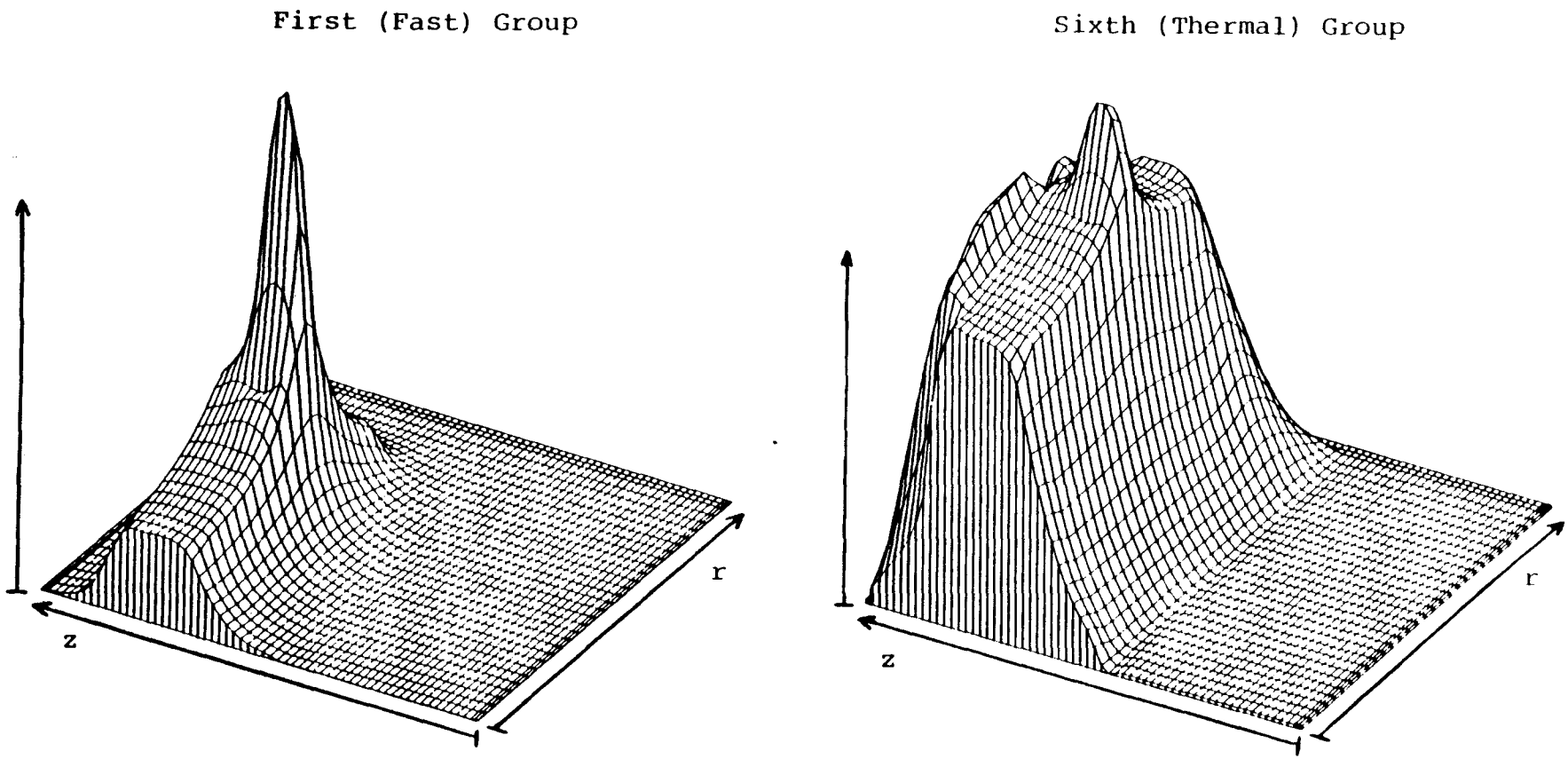

Figure 5.8 Local Function for Rod-Drop Experiment
t = 3 s into the transient.

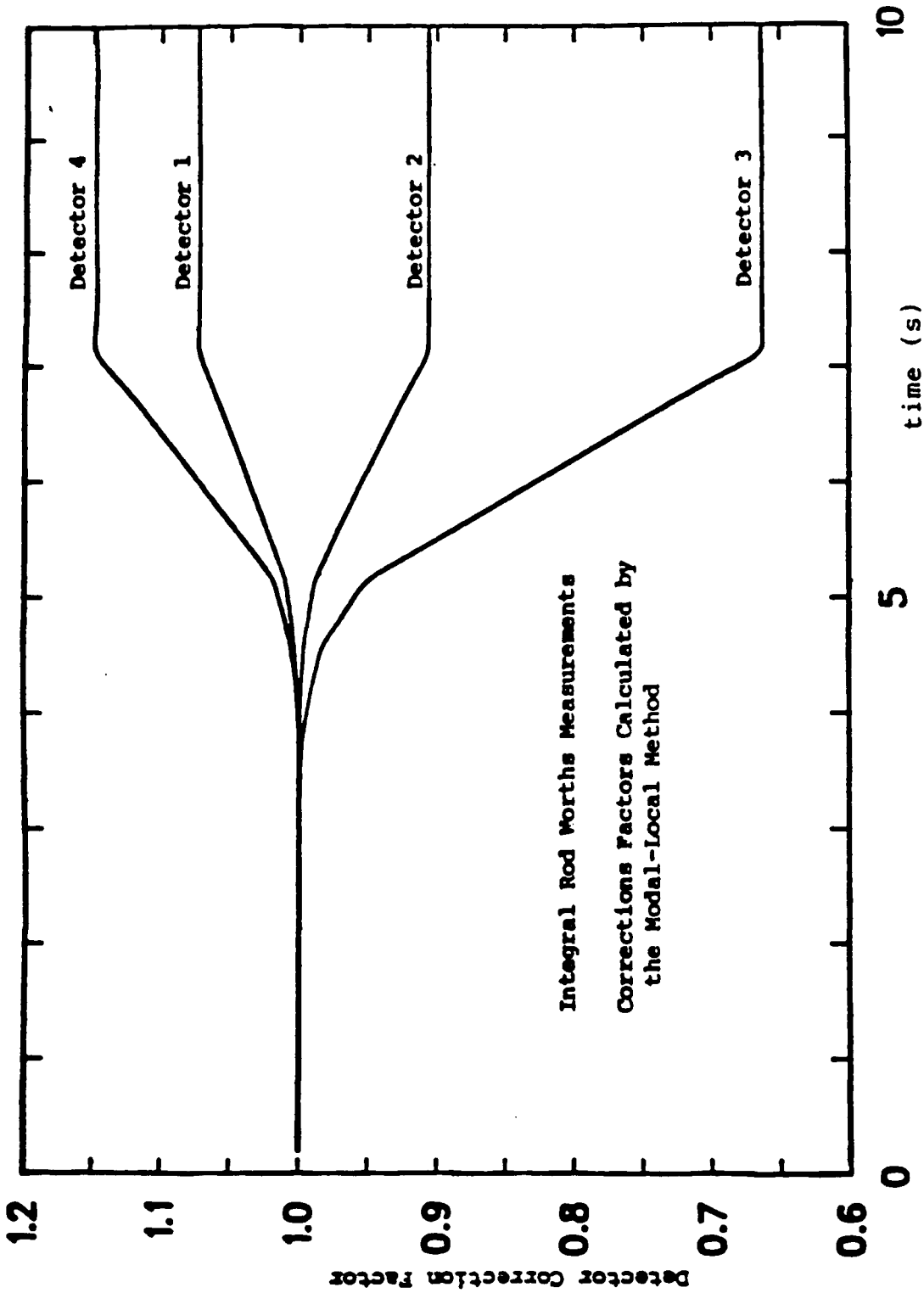

Figure 5.9 Correction factors vs. time

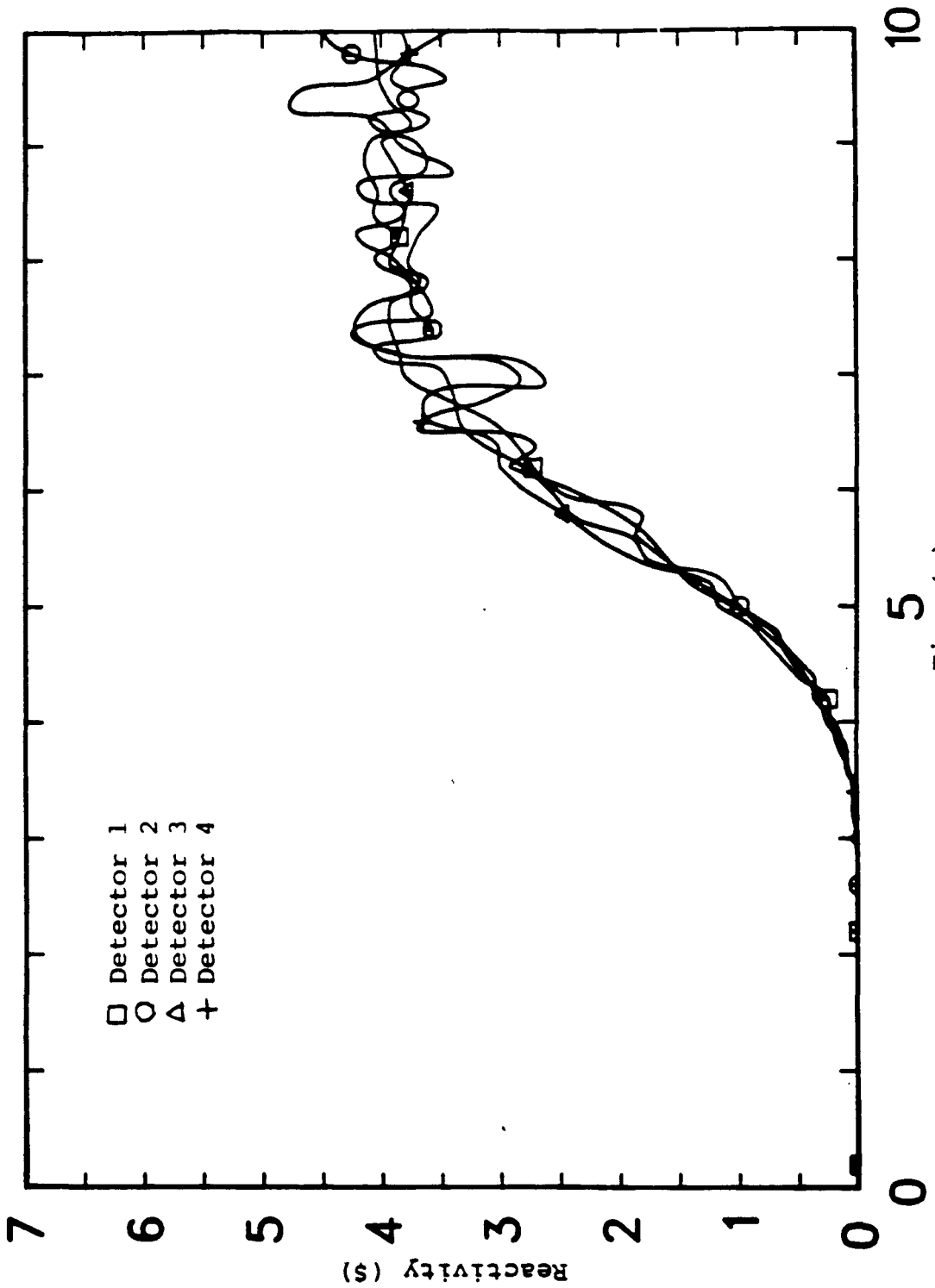

Figure 5.10 Integral rod worths vs. time obtained by the modal-local method.

Table 5.2

Integral rod worths with space-time correction obtained through the modal-local method.

Axial Detector Location (m)	Reactivity ($) ± Standard Deviation ($)			
	Channel A4	Channel A6	Channel A7	Channel A8
0.4	3.964 ± 0.260	3.816 ± 0.320	3.861 ± 0.271	3.872 ± 0.448
1.2	3.764 ± 0.142	3.834 ± 0.135	3.833 ± 0.119	3.918 ± 0.167
1.8	3.933 ± 0.187	3.889 ± 0.125	3.894 ± 0.103	3.777 ± 0.225
2.4	3.841 ± 0.223	3.611 ± 0.152	3.840 ± 0.196	3.893 ± 0.139

For the partially inserted rod worth measurements we analyzed the data collected at detector positions shown in Fig. 5.2. In our analysis, we considered the insertion of the top-reflector bank of absorber rods down to 0.285 m, 0.538 m, 0.782 m, and 1.0 m from the top of the top reflector. The uncorrected, time-averaged differential worths of the rods are given in Table 5.3 and Fig. 5.11, with the corrected reactivity worths presented in Table 5.4 and Fig. 5.12. The comparisons between Figs. 5.11 and 5.12, and between Tables 5.3 and 5.4 clearly indicate once again the applicability our space-time correction technique to eliminate the detector position dependence from rod reactivity worth data.

C. Errors and Uncertainties in the Rod Worth Measurements

There are undoubtedly several sources of errors or uncertainties in our space-time analysis of the KAHTER reactivity data. The most obvious source of uncertainties, especially in the integral rod worth measurements, is due the statistical fluctuations in the detector countrates obtained after complete insertion of the rods. The second important source of errors is due to the inaccuracy in predicting, with our modal-local method, changes in the shape function during the transient, or the correction factors to apply to the detector signals.

Table 5.3

Differential rod worths without space-time correction

Rod Insertion (m)	Reactivity ($) ± Standard Deviation ($)			
	Channel A4 Height = 1.2m	Channel A6 Height = 1.8m	Channel A7 Height = 2.4m	Channel A8 Height = 0.4m
0.285	0.164 ± 0.026	0.167 ± 0.012	0.185 ± 0.067	0.165 ± 0.022
0.538	1.090 ± 0.039	1.137 ± 0.043	1.266 ± 0.072	1.049 ± 0.076
0.782	2.492 ± 0.149	2.913 ± 0.177	3.705 ± 0.177	2.405 ± 0.150
1.0	3.510 ± 0.144	4.334 ± 0.241	6.042 ± 0.229	3.355 ± 0.332

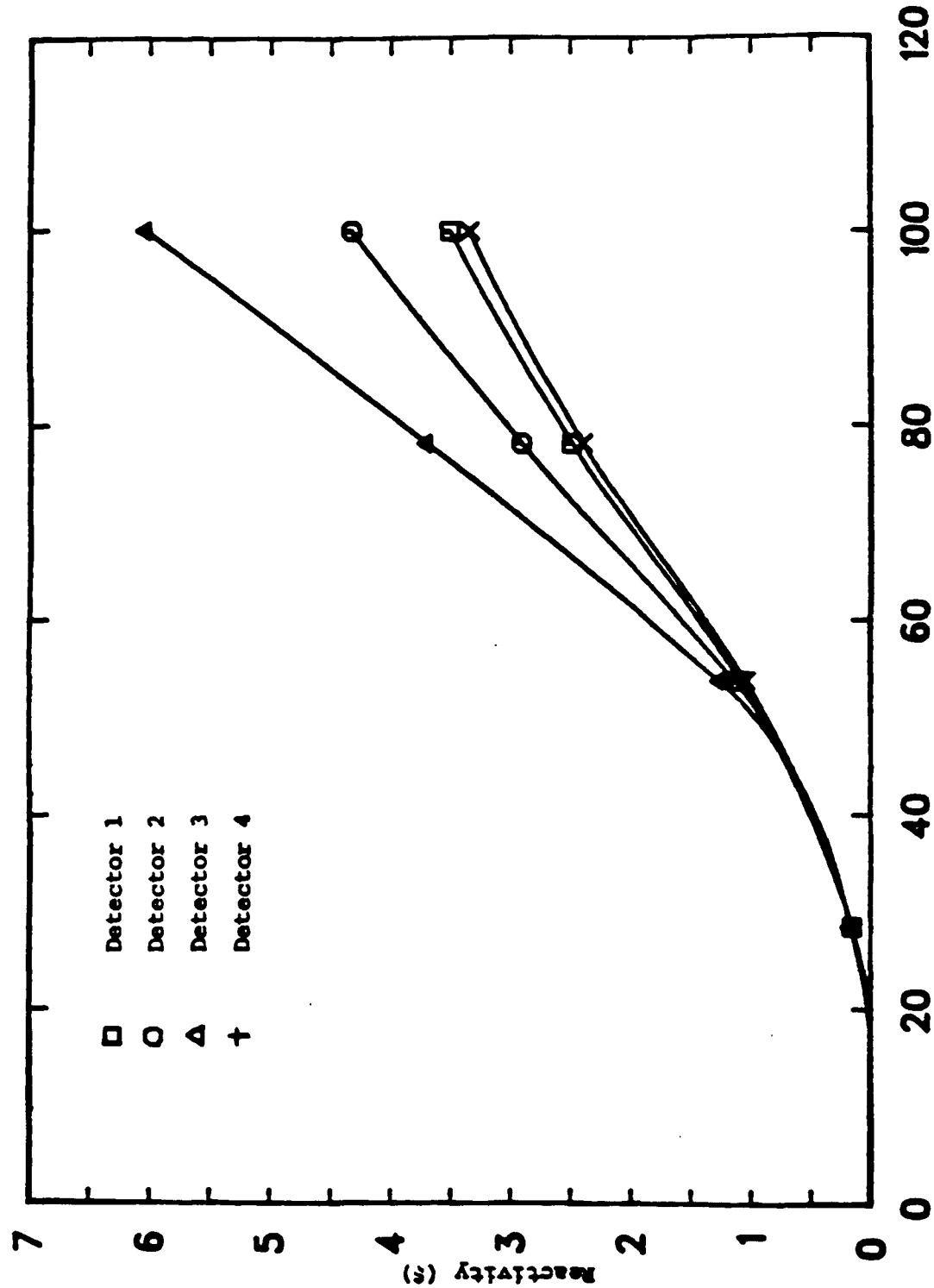

Figure 5.11 Differential rod worths without space-time correction.

Table 5.4

Differential rod worths with space-time correction obtained through the modal-local method.

rod insertion (m)	reactivity ($) ± standard deviation ($)			
	channel A4 height=1.2 m	channel A6 height=1.8 m	channel A7 height=2.4 m	channel A8 height=0.4 m
0.285	0.165 ± 0.027	0.166 ± 0.013	0.177 ± 0.069	0.170 ± 0.022
0.538	1.111 ± 0.039	1.107 ± 0.043	1.135 ± 0.069	1.111 ± 0.078
0.782	2.625 ± 0.156	2.714 ± 0.169	2.799 ± 0.139	2.687 ± 0.158
1.0	3.826 ± 0.153	3.884 ± 0.219	3.871 ± 0.169	3.918 ± 0.369

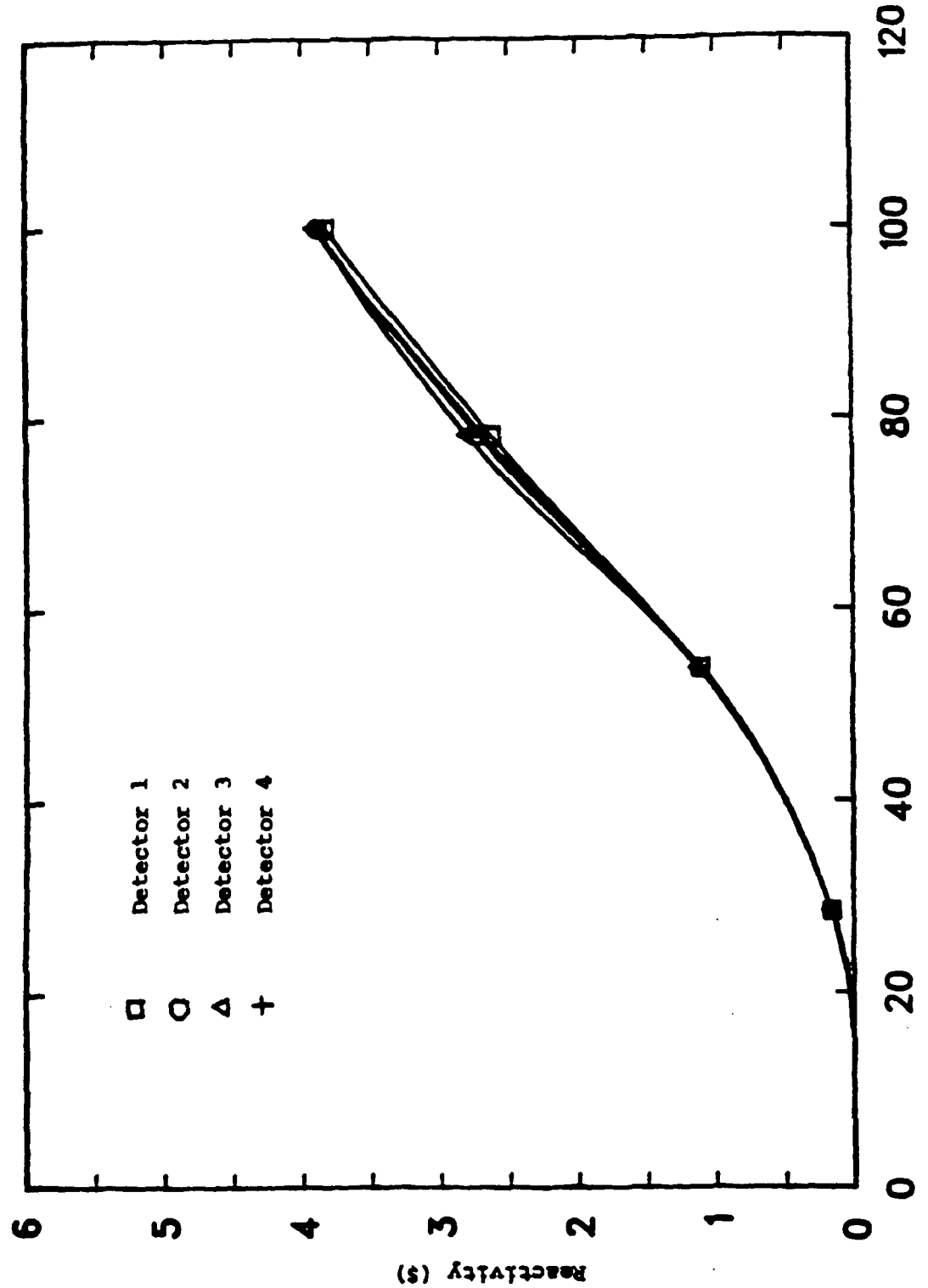

Figure 5.12 Differential rod worths obtained by the nodal-local method.

Statistical fluctuations in the detector signal contributes a large uncertainty to the calculated reactivity worths. In Tables 5.1 through 5.4 are shown, in addition to time-averaged reactivity values, standard deviations associated with the fluctuations in the calculated reactivity values. These fluctuations can be as large as 10% but on the average stay around 4%.

The detector counts were accumulated over intervals of 20.016 ms in the KAHTER rod worth experiments. For channels A6 and A7 this interval was sufficient for accumulating enough counts to give good statistics. For channel A8, after the rods were inserted, the number of counts per time interval was as low as 25 which would imply a standard deviation of 20%. To improve the statistics we grouped counts over 10 consecutive intervals, reducing the corresponding standard deviation in channel A8 data to about 6%. Clearly these residual fluctuations in the regrouped experimental data are responsible for the 3 to 4% fluctuations in the final reactivity values, observed in figures of Sect. B. For power reactors, however, the countrates are usually much higher and, therefore, should provide better statistics.

In Table 5.5 are shown the errors in the ratio $\frac{n}{\Lambda}$ and average reactivities between the CITATION and modal-local method at the beginning of the transient. The CITATION results were obtained by using the kinetics parameters and

detector correction factors from static CITATION calculations in the inverse kinetics equation. The differences in $\frac{n}{\Lambda}$ are rather small except for the detector located in channel A8 at a height of 0.4 m. For this detector location the 1.7 % difference in the shape function yielded a reactivity difference of about 2.3 %. This shows how sensitive the reactivity calculation is to changes in the initial and final values of the shape function.

In the two-dimensional simulation with the FX2-TH code the detector 3 presented the greatest error in reactivity due to its proximity to the top-reflector rods. However, the actual location of detector 3 is 22.5^{o} apart from the top-reflector rods. Therefore, the detector was not so close to the perturbation location, and the three-dimensional modal-local analysis provided fairly accurate correction factors as a function of time for detector 3. Only a three-dimensional calculation could account for the actual location of the detector satisfactorily.

The results for the integral rod worth obtained with the modal-local method and the results in Ref. 31 do not agree with the calculations performed with the FX2-TH code and the CITATION code. The FX2-TH code and the CITATION code produce integral rod worths of 4.614 $ and 4.580 $, respectively, while the experiments produced integral rod worth of about 3.85 $. The reason for such a large discrepancy is in the cross section set used for the KAHTER

Table 5.5

Comparison between the modal-local and the CITATION results.

channel	axial detector location (m)	error in n/Λ at t=10 s (%)	error in $\rho(t)$ at t=10 s (%)
A4	1.2	0.93	0.73
A6	1.8	0.30	1.8
A7	2.4	0.42	0.03
A8	0.4	1.74	2.3

top-reflector rods which overpredicts the rod worth. However, the flux distribution obtained with this set of cross section is found to be in good agreement with flux profile data obtained at the KAHTER facility.[32] For this reason the detector correction factors produced by the modal-local method could accurately account for the spatial redistribution of the neutron flux during the transient. The errors due to the approximations and assumptions made in the shape function calculation were discussed in Sect. IV.E.

Analysis of the time-dependent countrate data indicated that the detector signals decay approximately at the same rate as the top-reflector rods are inserted, but they end at different asymptotic levels. This makes them suitable for an adiabatic treatment, since the shape function at the end of the transient can be approximated by a static flux calculation as was demonstrated in Table 4.3 in Chapter IV. This is why the correction factors obtained, in Ref. 31, could yield corrected reactivity worths comparable to our time-dependent treatment.

CHAPTER VI

SUMMARY AND CONCLUSIONS

The main objective of this research has been to develop an improved method for analyzing reactivity measurements accompanied by spatial redistribution of the neutron flux. With this purpose we have considered the inverse kinetics equation to provide the core reactivity as a function of time. To obtain the necessary amplitude function from detector signals, a new technique called modal-local method has been proposed. Our results indicate that the inverse kinetics equation coupled with the modal-local method provide accurate reactivity as a function of time. The modal-local method is simple enough to be used in real time calculations so that the coupled system can be implemented as an on-line reactivity meter.

The modal-local method is based on a quasi-static approximation to the time-dependent diffusion equation. The shape function is approximated in our formulation through a sum of a global and a local function. The local function is calculated in the framework of fixed source solution in standard diffusion theory codes, and represents the substantial flux perturbations in the vicinity of core

parameter changes. The global function is calculated through a time-dependent lambda mode expansion, and accounts for the overall perturbations in the flux distribution. The resulting ordinary differential equations for the modal expansion coefficients can readily be solved to yield an approximate expression for the time-dependent shape function. The method requires evaluation of lambda modes, several integrals involving the lambda modes, and the local function before the time-dependent equations can be solved. The actual solution of the time-dependent shape function, however, is rather simple and inexpensive so that the coupled modal-local method can be used for on-line reactivity analysis.

In the power reactor environment it is necessary to evaluate the temperature distribution across the reactor core as well as the cross section dependency on temperature. A single channel model which yields fuel and coolant temperatures has been considered in this study. The feedback model accounted for Doppler effect in the fuel and for density effects in the coolant.

To verify the accuracy of the modal-local method, several static and time-dependent problems have been considered. The intent of the static tests has been the assessment of the accuracy of the modal-local method in predicting strong perturbations in the neutron flux. The perturbation in the flux distributions due to insertion of

the top-reflector absorber rods at the KAHTER facility was simulated. The calculated flux distributions indicate good agreement with the three-dimensional CITATION results in the core region, although a substantial error in the modal-local calculation is noted in the top reflector, especially in the vicinity of the absorber rods, i.e., the location of the perturbation. The agreement in the flux distribution at the detector locations between the modal-local and CITATION results is generally quite good.

For assessing the accuracy of the modal-local method in determining reactivity as a function of time we have simulated the rod-drop experiments performed at the KAHTER facility. For the purpose of comparisons, the results from the two-dimensional FX2-TH calculation is taken as our reference. The overall accuracy in the time-dependent shape function is similar to that for static calculations discussed above. Away from the region of rod motion, the shape function prediction by the modal-local method is generally good. The average relative error in the shape function between the modal-local method and the FX2-TH code for the unrodded, perturbed, configuration of the KAHTER facility is 3.1 %.

The reactivity traces obtained with the modal-local method for detectors away from the perturbation are in very good agreement with the FX2-TH results, with errors on the order of a percent. For detector 3 close to the perturbed

region, the error is somewhat larger. The space-time analyses with both the FX2-TH code and the modal-local method have shown that the kinetics parameters can play an important role in the determination of reactivity. For transients with large neutron flux tilts, e.g., in the KAHTER rod-drop tests, failure to account for the change in the generation time can cause errors as large as 4 % in the final reactivity.

In the power reactor environment a simplified one-dimensional, two-group model of a PWR has been considered to test the modal-local method. A differential rod worth measurement has been simulated with explicit representation of thermal-hydraulic feedback effects. Although the transient involved a relatively small change in the neutron flux, the uncorrected reactivity traces have shown strong dependency on the detector location. The analysis with the modal-local method has produced very good results for the net reactivity, for the feedback reactivity, and for the external reactivity due to the rod motion. The space time analysis shows that the bulk of the spatial redistribution of the neutron flux is due to the rod motion. The thermal hydraulic feedback acts to reduce the effects of the external perturbation on the neutron flux.

The static and time-dependent tests of the modal-local method show that the first-order perturbation approximation in the calculation of the local function, and the limited

number of modes in the expansion of the modal function account for the bulk of the errors in the method. The first approximation is basically responsible for the poor results of the modal-local method near the perturbation locations. The increase in the number of modes improves the global estimation of the shape function, but as few as two harmonics can produce accurate results with the help of the local function.

The space-time analysis of the KAHTER rod worth measurements also indicates good agreement between our modal-local calculations and earlier Jülich results based on static CITATION calculations. In addition, this also indicates that the adiabatic approximation to the shape function calculation may be sufficiently accurate in many space-time analysis of detector signals. The proposed method also has been successfully applied, with no additional effort, to the analysis of partially inserted rod worth measurements obtained at the KAHTER facility.

Applicability of the modal-local method as an on-line reactivity meter has been demonstrated through the analysis of the KAHTER data as well as through comparison with the FX2-TH simulation of the test. Based on the results of a simulated PWR rod worth measurement, we believe that our method will prove equally useful in the power reactor environment, where thermal-hydraulic feedback effects have

to be accurately represented in the shape function calculation.

There are areas in which our modal-local method could be applied. Some of these possibilities we have already mentioned: determination of perturbed flux distributions based on reference calculations and estimation of core integral parameters, all in the framework of the perturbation theory. Two important points for further investigation are the inclusion of higher order terms in the calculation of the local function, and a more sophisticated thermal-hydraulic model in three-dimensional geometry. With a more accurate treatment of the local function, we would be able to improve substantially the modal-local method where it is least accurate. A possibility is to have precalculated local functions also for the several modes. In this way the first order approximation on the local function could be avoided by considering the shape function from previous time step. The second point is that for a more realistic thermal-hydraulic treatment would be necessary for actual application of the modal-local method to the operating power reactor environment.

APPENDIX

THE LAMBDA MODES

The lambda modes are the eigenfunctions of the steady-state neutron diffusion equation. The neutron diffusion equation, being an eigenvalue equation, has an infinite number of solutions, the eigenfunctions, and corresponding to each of them, an eigenvalue. For the energy-dependent multi-dimensional neutron diffusion equation, the eigenfunctions form a complete set so that any function can be expanded in terms of them. This property makes the lambda modes of interest in reactor analysis for their potential applicability in perturbation theory. The estimation of perturbed flux distribution can be easily obtained by means of an expansion in terms of lambda modes of some reference configuration. The expansion coefficients are usually obtained through perturbation formulas.

With the notation introduced in Sect. II.A, the equation for the n^{th} lambda mode can be written as:

$$L_o(\underline{r},E)\phi_n(\underline{r},E) = \frac{k_o}{k_n}M_o(\underline{r},E)\ \phi_n(\underline{r},E) \qquad (1)$$

where, as before, $L_o(\underline{r},E)$ is the destruction operator which includes the leakage, absorption and scattering terms, $M_o(\underline{r},E)$ is the production operator, and k_o and k_n are the eigenvalues corresponding to the lambda mode ϕ_o and ϕ_n, respectively. Let us assume for convenience that the eigenvalues k_n of Eq. (1) are ordered from the largest to the smallest:

$$k_o > k_1 > k_2 > \ \ldots \ > k_{n-1} > k_n > k_{n+1} > \ \ldots$$

The largest eigenvalue k_o and its corresponding eigenfunction ϕ_o has a special physical meaning: k_o is the effective multiplication factor for the reactor and ϕ_o is the scalar neutron flux distribution.

The adjoint of Eq. (1) is also an eigenvalue equation and its solution, the adjoint modes $\phi_n^\dagger(\underline{r},E)$, have the same eigenvalues k_n:

$$L_o^\dagger(\underline{r},E)\phi_n^\dagger(\underline{r},E) = \frac{k_o}{k_n} M_o^\dagger(\underline{r},E)\ \phi_n^\dagger(\underline{r},E) \qquad (2)$$

The modes ϕ_n and $\phi_n^\dagger$ satisfy the following orthonormality condition:

$$\langle \phi_m^\dagger(\underline{r},E),\ M_o(\underline{r},E)\ \phi_n(\underline{r},E) \rangle = \delta_{mn}.$$

The physical interpretation of the fundamental adjoint mode $\phi_o^\dagger$ has been that of an importance function. It quantifies the importance of a neutron of energy E in a given position $\underline{r}$ in the core to the chain reaction or criticality. With this interpretation, $\phi_m^\dagger$ is usually chosen as a weight function, especially in perturbation theory where it allows simple formulas for reactivity, free of first order errors.[11]

As an example of lambda modes we consider a homogeneous slab of thickness a with zero flux at the boundaries . For one-energy group, Eq. (1) becomes:

$$- D \frac{d^2\phi_n}{dx^2} + \Sigma_a \phi_n = \frac{\nu\Sigma_f \phi_n}{k_n} \qquad (3)$$

with boundary conditions $\phi_n(0) = \phi_n(a) = 0$. The above equation can be written as

$$\frac{d^2\phi_n}{dx^2} + B_n^2 \phi_n = 0, \text{ where } B_n^2 = \frac{\frac{\nu\Sigma_f}{k_n} - \Sigma_a}{D} ,$$

and has the solutions $\sin(B_n x)$, with the buckling $B_n^2=[(n+1)\frac{\pi}{a}]^2$ obtained by satisfying the boundary conditions. The eigenvalues can also be expressed in terms of the core

parameters and the buckling. The lambda modes and the corresponding eigenvalues will be:

$$\phi_n(x) = \frac{2k_o}{a\nu\Sigma_f} \sin[\frac{(n+1)\pi x}{a}],$$

$$k_n = \frac{\nu\Sigma_f}{\Sigma_a + D(\frac{\pi}{a})^2(n+1)^2}.$$

In Fig. A.1 are shown a few of these lambda modes. Each mode usually can be identified by the number of nodal points or times the distribution flips the sign. The eigenvalues are dependent primarily on the curvature of the modes, or buckling; the greater is the buckling, the smaller is the eigenvalue k_n. For small reactors where leakage is large (large buckling), we should expect to see a larger separation between the eigenvalues of the modes, and for large thermal reactors where leakage is very small, a small separation between the eigenvalues. These general considerations also hold for heterogeneous reactor configurations, but the multi-dimensional problems make higher harmonic modes harder to be identified and obtained.

Standard neutron diffusion theory codes yield the fundamental eigenfunction ϕ_o and the fundamental eigenvalue k_o. The methods[15,38-41] that have been suggested for obtaining the higher lambda modes are in principle

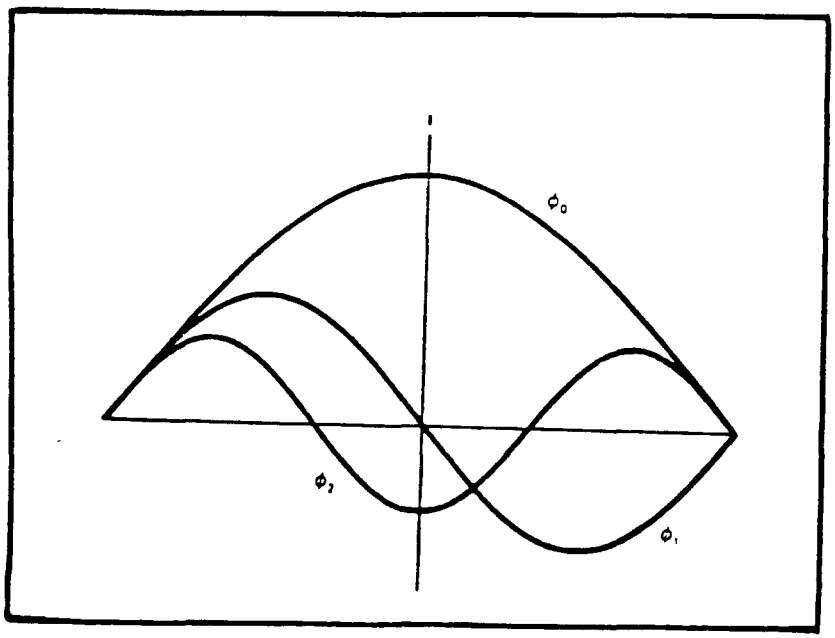

Figure A.1 Lambda modes for a slab reactor, first three modes.

applicable to the energy-dependent multi-dimensional problems. In practice, however, they work fine in one-energy group and one-dimensional problems but present difficulties in multi-group and multi-dimensional problems.

Calculation of Lambda Modes through the Power Method

Eq. (1) can be solved in a finite-difference framework by an iteration technique, called the inverse power method,[52,53] which yields both the eigenvalue k_o and the fundamental mode ϕ_o. The inverse power method consists of two steps: the outer iteration and the inner iteration. In the outer iteration a source the RHS of Eq. (1) is calculated, and in the inner iteration the flux distribution consistent with this source distribution is found. Calculation of higher harmonics through the inverse power method requires a modification of the source term in the outer iteration.

The outer iteration procedure works in the following way: An initial guess for the flux ϕ^o and eigenvalue k^o are given to obtain the source term in Eq. (1). Then the first outer iteration is performed,

$$\phi^1 = L_o^{-1} \frac{\chi P_o}{k^o} \phi^o,$$

where ϕ^1 is the flux distribution from the first iteration consistent with the initial source. The eigenvalue for the first iteration is calculated as:

$$k^1 = \frac{<\chi P_o \phi^1>}{<L_o \phi^1>} = k^o \frac{<\chi P_o \phi^1>}{<\chi P_o \phi^o>} .$$

With the flux and eigenvalue updated, the procedure is repeated for the next iteration. For the j^{th} outer iteration the solution of Eq. (1):

$$\phi^j = \left(\frac{1}{k^{j-1}} \cdots \frac{1}{k^o}\right) [L_o^{-1} \chi P_o]^j \phi^o. \qquad (4)$$

That the above expression converges to the fundamental mode is readily seen by expanding the initial flux guess ϕ_o in terms of the lambda modes:

$$\phi^o = \sum_{n=o}^{\infty} a_n \phi_n. \qquad (5)$$

Then substituting the above expansion in Eq. (4), and noting that

$$(L_o^{-1} \chi P_o) \phi_n = k_n \phi_n,$$

we obtain

$$\phi^j = \left(\frac{1}{k^{j-1}} \cdots \frac{1}{k^o}\right) \sum_{n=o}^{\infty} a_n [k_n]^j \phi_n. \qquad (6)$$

Since the eigenvalues are raised to the j^{th} power, this expression will eventually converge to the mode with the largest eigenvalue. Through this algorithm, therefore, ϕ^j converges to the fundamental mode ϕ_o for it has the largest eigenvalue.

Eq. (6), however, provides the clue to the calculation of higher harmonic modes. Consider the case where the initial guess ϕ^o did not have the fundamental mode component, that is, $a_o = 0$. Then the harmonic mode with the largest eigenvalue would be the first harmonic mode, and, thus, Eq. (6) would converge to it. This is the basis for the algorithms suggested in References 15, 38, 39, and 40. A given harmonic mode can be obtained through the power method by eliminating from the initial flux guess the components of lower harmonics.

The initial flux guess for obtaining the first harmonic mode should not contain any component of the fundamental mode

$$\phi^o - a_o\phi_o = \sum_{n=1}^{\infty} a_n \phi_n.$$

The coefficient a_o can be obtained by using the orthonormality condition for the lambda modes. Premultiplying Eq. (5) by $\phi_o^\dagger$ and the production operator divided by k_o, and integrating over volume and energy, we find

$$a_o = \langle \phi_o^\dagger(\underline{r},E),\ M_o(\underline{r},E)\ \phi^o(\underline{r},E) \rangle .$$

Since the fundamental modes $\phi_o^\dagger$ and ϕ_o are readily obtained from standard neutron diffusion theory codes, the coefficients a_o can be estimated, to yield the proper initial guess for the first harmonic. Thus, the first harmonic modes $\phi_1^\dagger$ and ϕ_1 can be obtained. In theory, the procedure can be repeated for obtaining higher harmonics by eliminating the lower harmonics already calculated. In practice, difficult convergence problems arise and special care should be taken for calculating higher harmonics.

If in the initial flux guess there is no component of the desired mode, the result obtained may be of no utility, or the iteration may never converge. Initial guesses close to the harmonic shape searched are desirable but if those are not possible, at least one should make sure that the guess contains the desired mode.

In many situations the nature of the harmonic tends to cause the fission source integrals to be zero. When this happens the calculation of the eigenvalue based on the ratio of successive iterates on the source integral may result in large errors since any small error in the iterates alters the ratio substantially. For this reason, in the implementation of the lambda mode capability in the CITATION code[42], the 2DBUM code[54], and the ONED code[55], the calculation of the eigenvalues was based on an absolute value of the source distribution. This approach has proved to work, and also required only small modifications in the codes.

From Eq. (6) it is easily seen that the convergence to a given mode will be faster if the separation between the eigenvalue of the mode and that of the next higher mode is greater. When the eigenvalues are only slightly different severe difficulties in convergence are encountered. The iterative process may go in the direction of one mode and then in the direction of another, alternating from time to time, without arriving anywhere. When different modes have similar eigenvalues, as in the case of a homogeneous cubic reactor, the iterative process will converge to a linear combination of these modes.

Near the nodal points of a mode, convergence criterion based on relative flux change may be too stringent for flux convergence. In our calculation we have used only a tight

convergence criterion on the relative eigenvalue error. For this reason, and for better elimination of lower harmonic contaminations, double precision arithmetic is advisable.

Harmonic contamination problems can be reduced if the number of inner iterations per outer iteration is increased. There are several symptoms to monitor regarding an increase in the lower mode contamination, including an increase in the relative flux change, increase in the relative eigenvalue change, cessation of acceleration, dominance ratios greater than unity, and eigenvalues that diverge toward the fundamental. When any of these symptoms is noticed one should stop and rethink how to continue the calculation from there on.

It may be possible to improve the rate of convergence of higher harmonic modes but results reported to date are not very encouraging. There is no single procedure that can insure fast convergence, in the contrary, sometimes it can cause undamped oscillations. Brittain[15] reports that a Chebychev acceleration of the outer iteration is essential to reduce running times. Vondy and Fowler[39] also report an extrapolation in the outer iteration helps reduce costs but that in certain conditions problems may arise. In our calculation of lambda modes with the ONED, 2DBUM and CITATION codes, we have not used any type of acceleration scheme and also eliminated coarse-mesh rebalancing which was found to create convergence problems. This procedure did

not allow fast convergence to higher harmonics but did decrease the chance of divergences.

REFERENCES

1. David L. Moses, "A Proposed Method for Inverse Reactivity Measurements in Large Nuclear Power Reactor Cores," Ph.D. Thesis, Nuclear Science and Engineering Division, Carnegie-Mellon University (1980).

2. A. J. Impink, Jr., J. R. Easter and W. D. Leggett, III, "Comparison of Predicted and Measured Nuclear Design Parameters at Begining of Life of Cycle 1 in the San Onofre Reactor," WCAP-3269-66, Westinghouse Electric Corporation (1968).

3. A. F. Henry, "The Application of Reactor Kinetics to the Analysis of Experiments," Nucl. Sci. Eng., 3, 52 (1958).

4. J. B. Yasinsky, M. Natelson and L. A, Hageman, "TWIGL - A Program to Solve the Two-Dimensional, Two-Group, Space-Time Neutron Diffusion Equations with Temperature Feedback," WAPD-TM-743 Bettis Atomic Power Laboratory (1968).

5. D. J. Diamond, Ed., "BNL-TWIGL, A program for calculating Rapid LWR Core Transients," BNL-NUREG-21925, Brookhaven National Laboratory (1976).

6. M. R. Buckner and J. W. Stewart, "Multidimensional Space-Time Nuclear-Reactor Kinetics Studies - Part I: Theoretical," Nucl. Sci. Eng., 59, 289 (1976).

7. R. W. Bowring et al., "MEKIN: MIT-EPRI Nuclear Reactor Core Kinectics Code," CCM-1, RP 228, Electric Power Research Institute (1975).

8. D. P. Griggs, M. S. Kazimi, and A. F. Henry, "TITAN: An Advanced Three-Dimensional Neutronics / Thermal-Hydraulics Code for Light Water Reactor Analysis," Proceedings of the Topical Meeting on Advances in Reactor Physics and Core Thermal Hydraulics, Kiamesha Lake, NY, 2, 766 (1982).

9. R. A. Shober, T. A. Daly, and D. R. Ferguson, "FX2-TH: A Two-Dimensional Nuclear Reactor Kinetics Code with Thermal-Hydraulic Feedback," ANL-78-97, Argonne National Laboratory (1978).

10. J. C. Luxat and G. M. Frescura, "Space-Time Neutronic Analysis of Postulated Loss of Coolant Accidents in CANDU Reactors", Nucl. Tech., 46, 507 (1979).

11. E. Greenspan, M. L. Williams, and J. H. Marable, "Time-Dependent Generalized Perturbation Theory for Coupled Neutron-Nuclide Problems," Nucl. Sci. Eng., 73, 210 (1980).

12. C. D. Kylstra and R. E. Uhrig, "Spatially Dependent Transfer Function for Nuclear Systems," Nucl. Sci. Eng., 22, 191 (1965).

13. A. R. Buhl, J. C. Robinson, and E. T. Tomlinson, "Intercomparison of Perturbing Techniques for Inferring the Reactivity of Fast Reactors," Nucl. Tech., 21, 67 (1974).

14. L. R. Foulke and E. P. Gyftopoulos, "Application of the Natural Mode Approximation to Space-Time Reactor Problems," Nucl. Sci. Eng., 30, 419 (1967).

15. I. Brittain, "Analysis of Rod Drop and Pulsed Source Measurements of Reactivity in the Winfrith SGHWR", AEEW-R-640, United Kingdom Atomic Energy Authority (1970).

16. B. E. Simons and J. S. King, "A Pulsed Neutron Technique for Reactvity Determination," Nucl. Sci. Eng., 3, 595 (1958).

17. T. Gozani, "Subcritical Reactivity Determinations-Comparison of Experimental Methods," Trans. Am. Nucl. Soc., 9, 236 (1966).

18. M. Becker, "Principles of, and Problems with, Pulsed-Neutron Reactivity Measurements," Trans. Am. Nucl. Soc., 9, 237 (1966).

19. E. Garelis and J. L. Russel, Jr., "Theory of Pulsed Neutron Source Measurements," Nucl. Sci. Eng., 16, 263 (1963).

20. C. A. Sastre, "The Measurement of Reactivity," Nucl. Sci. Eng., 8, 443 (1960).

21. R. L. Murray, C. R. Bingham, and C. F. Martin, "Reactor Kinetics Analysis by an Inverse Method," Nucl. Sci. Eng., 18, 481 (1964).

22. T. Gozani, "The Concept of Reactivity and its Application to Kinetic Measurements," Nukleonik, 5, 2, 55 (1963).

23. H. Gerwin and W. Scherer, "Ein Betrag zur Theoretischen Interpretation von Reaktivitats-Messungen", Jül-1177, Kernforschungsanlage Jülich (1975).

24. K. Ferguson, C. G. Poncelet, and A. J. Impink, "Development of Improved Data Analysis Methods for Reactivity Measurements in Large Thermal-Power Reactors," Nucl. Tech., 29, 37 (1976).

25. J. J. Woods and T. L. Wilson, "Comparison of Temperature Coefficient Calculations with Measurements in PWRs," Trans. Am. Nucl. Soc., 30, 712 (1978).

26. R. A. Kerr, T. R. Freeman, and D. M. Lucoff, "A Method for Measuring and Evaluating the Temperature Coefficient in the At-Power Conditionn," Trans. Am. Nucl. Soc., 30, 713 (1978).

27. A. R. R. Telford, "Measurements and Calculations of the Fuel Temperature Coeffcient of Reactivity for the Hinkley 'B' Advanced Gas-Cooled Reactor," Nucl. Tech., 56, 33 (1982).

28. R. Fuge and D. Ziegenbein, "Reactor Dynamic Perturbation Measurement," Nucl. Sci. Eng., 71, 309 (1979).

29. R. E. Kaiser et al., "Extrapolation of Small Sample Doppler Reactivity Measurements," Proceedings of the Topical Meeting on Advances in Reactor Physics and Core Thermal Hydraulic, Kiamesha Lake, New York (1982).

30. J. Moreira and J. C. Lee, "Space-Time Analysis of Reactor-Control-Rod-Worth Measurements," Nucl. Sci. Eng., 86, 91 (1984).

31. Kritisches Experiment KAHTER OTTO Statusbericht No. 6, Kernforschungsanlage Jülich (1980).

32. E. Pohlen, "Erprobung reaktorphysikalischer Rechenverfahren am kritischen Experiment zum HTR (KAHTER) im Hinblick auf die Güte der Berechenbarkeit des Einflusses des oberen Hohlraumes", Jül-1760, Kernforschungsanlage Jülich (1982).

33. K. O. Ott and D. A. Meneley, "Accuracy of the Quasi-Static Treatment of Spatial Reactor Kinetics", Nucl. Sci. Eng., 36, 402 (1969).

34. J. B. Yasinsky and A. F. Henry, "Some Numerical Experiments Concerning Space-Time Reactor Kinetics", Nucl. Sci. Eng., 22, 17 (1965).

35. J. B. Doshi and L. M. Grossman, "Space-Time Dynamics of a Fast Breeder Reactor for Localized Disturbances", Nucl. Sci. Eng., 65, 106 (1978).

36. B. I. Hauss and W. E. Kastenberg, "Introduction of the Quasi-Static Synthesis Method for Solution of Space-Time Reactor Kinetics Problems", Nucl. Sci. Eng., 69, 326 (1979).

37. M. J. Lineberry, "Estimation of Reactivity Worths by Local Calculation", Nucl. Sci. Eng., 54, 157 (1974).

38. C. H. Adams, "Calculations of Harmonics of the Multigroup, Diffusion-Theory, Finite-Difference Equations using DIF3D," FRA-TM-119, Argonne National Laboratory (1979).

39. D. R. Vondy and T. B. Fowler, "Solving the Uncommon Nuclear Reactor Core Neutronics Problems", Nucl. Sci. Eng., 83, 100 (1983).

40. R. Saito and S. Katsuragi, "Higher Order Perturbation Method in Reactor Calculation," Nucl. Sci. Tech., 6, 303 (1969).

41. A. Gandini, "On the Standard Perturbation Theory," Nucl. Sci. Eng., 79, 426 (1981).

42. T. B. Fowler, et al., "Nuclear Reactor Core Analysis Code: CITATION", ORNL-TM 2496, Rev. 2, Oak Ridge National Laboratory (1971).

43. M. W. Crump and J. C. Lee, "Calculation of Spatial Weighting Function for Ex-Core Neutron Detectors," Nucl. Tech., 41, 87 (1978).

44. J. E. Jones, "Evaluation of Subcriticality from a Modeled Asymmetric Rod-Drop for the Clinch River Breeder Reactor," Ph. D. Thesis, University of Tennessee (1980).

45. Z. A. Ackasu, G. S. Lellouche, and L. M. Shotkin, "Mathematical Methods in Nuclear Reactor Dynamics," Academic Press, Inc., New York (1971).

46. M. Bloser and H. R. Langohr, "Inverskinetischer Formalismus und Code IVKDT1 für IVK-Messungen", Interner Bericht IRE-20-73, Kernforschungsanlage Julich (1973).

47. J. M. Auerbach and S. G. Carpenter, "Microprocessor Controled Reactivity Meter for Real Time Monitoring of Reactors," Nucl. Power Syst. Symp., 9th, San Francisco, CA, 98 (1977).

48. S. Kaplan, "The Property of Finality and the Analysis of Problems in Reactor Space-Time Kinetics by Various Modal Expansions," Nucl. Sci. Eng., 9, 357 (1961).

49. W. D. Beckner and R. A. Rydin, "A Higher Order Relationship Between Static Power Tilts and Eigenvalue Separation in Nuclear Reactors," Nucl. Sci. Eng., 56, 131 (1975).

50. H. Mitani, "Higher Order Perturbation Method in Reactor Calculation," Nucl. Sci. Eng., 51, 180 (1973).

51. A. Gandini, "Implicit and Explicit Higher Order Perturbation Methods for Nuclear Reactor Analysis," Nucl. Sci. Eng., 67, 347 (1978).

52. E. Isaacson and H. B. Keller, "Analysis of Numerical Methods," Chapt. 4, John Wiley and Sons, New York (1966).

53. S. Nakamura, "Computation Methods in Engineering and Science," John Wiley and Sons, New York (1977).

54. 2DBUM code: a version of the 2DB code adapted to the Michigan Terminal System, MTS; W. W. Little, Jr. and R. W. Hardie, "2DB User's Manual - Revision I", BNWL-831 REV 1, Pacific Northwest Laboratory, Richland, Washington (1969).

55. J. C. Lee, "Finite-Difference Solution of One-Dimensional Neutron Diffusion Equation", Unpublished Lecture Note, University of Michigan, Nuclear Engineering Department (1974).

56. A. M. Weinberg and E. P. Wigner, "The Physical Theory of Neutron Chain Reactors," Chapter XXI, The University of Chicago Press, Chicago (1958).

57. K. F. Hansen, B. V. Koen and W. W. Little, Jr., "Stable Solutions of the Reactor Kinetics Equations," Nucl. Sci. Eng., 22, 51 (1965).